Soluble Catalysts for Aprotic

Li-O_2 Batteries



Xiangwen Gao

Trinity College

Department of Materials

University of Oxford

A thesis submitted for the degree of

Doctor of Philosophy

Michaelmas 2017

Declaration of Originality

I, Xiangwen Gao, hereby declare that this doctoral thesis, which is approximately 30,500 words in length, has been written by me that it is the record of work carried out by me. This thesis has not been submitted in any previous application for a higher degree.

Xiangwen Gao

Michaelmas 2017

Acknowledgements

First, I would like to thank my supervisor, Professor Peter G. Bruce for offering me the position in this group to work with talented colleagues and for his advice and strong support throughout my DPhil to make this thesis possible.

I am thankful to Dr. Yuhui Chen for his hand-by-hand teaching about various techniques and experiments and his advices and help on tackling down projects. I would like to thank Dr. Lee R. Johnson for his knowledge and his guidance on my projects and thesis revision.

I would also like to express my thanks and appreciation to all my group members, both past and present for the good times. Particularly, I would like to thank Dr. Chunmei Li and Dr. Fengjiao Yu for their advices and encouragement when I felt frustrated. I would like to thank Dr. Matthew Roberts and Ms. Zsofia Lazar for their useful help on science work and daily lab life. I would like to thank Dr. Andy Naylor for his discussion and help in SEM/PECS machine. I would like to thank Dr. Da Wang, Dr. Christian Kuss and Dr. Liyu Jin for their collaborations, discussions, and advices in various projects. I would like to thank Dr. Zarko Jovanov, Dr. Shanmu Dong, Dr. Euan McTurk, Mr. Lukas Lutz, Mr. Conrad Holc and Mr. Alexander Pateman for their discussions and effort in understanding metal oxygen batteries. Besides, I would like to thank Mr. Rong Hao and Mr. Niccolo Guerrini who have worked and fought together for this degree.

Finally, my special and sincere thanks to my parents Qilong Gao and Xiaoping Xu, my sisters Dongdi Gao, Xiaoyan Deng and Sulan Gao, my brothers-in-law, my nieces and nephews for their understanding, care and love to me. It is so important to have their support and company all the time. I could not have achieved this without them by my side.

Abstract

Aprotic lithium-air (O_2) batteries have attracted significant interest due to their high theoretical specific energy. In an aprotic Li-O_2 cell, O_2 is reduced to form Li_2O_2 on discharge and the process is reversed on charge. Li_2O_2 is an insulating and insoluble solid, leading ultimately to poor cycling rates, low capacities and early cell death if it formed on the electrode surface. This is exacerbated by formation of Li_2CO_3 due to the cathode degradation with the presence of Li_2O_2 surface film. It is therefore desirable to form Li_2O_2 particles in solution, typically in batteries with high donor number electrolyte solvents that can dissolve the LiO_2 intermediate. However, such solvents are more susceptible to nucleophilic attack by the reduced oxygen species, resulting in undesired side reactions.

This project focuses on tackling the dilemma by promoting solution phase formation of Li_2O_2 in relatively stable low donor number solvents. Phenol was investigated as a protic additive that acts as a phase-transfer catalyst, dissolving Li_2O_2, avoiding electrode passivation and forming large particles of Li_2O_2. Discharge mediators were studied to shift O_2 reduction to Li_2O_2 in solution via a new route that avoids the LiO_2 intermediate, so that it increases the discharge potential, suppresses the growth of the Li_2O_2 thin film on the cathode surface, and thus postpones the cell death, increases the discharge capacity 80-100 fold and permits high discharge capacities with relatively high rates.

However, Li_2O_2 particles growing via solution mechanism is disconnected from the electrode surface and therefore electronically isolated during charging, which requires redox mediators on charging. By combining discharge and charge mediators, the dual-mediator Li-O_2 cell in this project was able to sustain cycling with capacities of 2 mAh cm^{-2}_{areal} at a rate of 1 mA cm^{-2}_{areal} over 50 cycles. By forming/decomposing Li_2O_2 in solution and avoiding high charge potentials, the carbon instability is significantly mitigated.

Contents

Publication list **1**

Abbreviations **3**

Goals and targets **6**

Chapter 1. Introduction **7**

1.1 Background on energy storage 7

1.2 Introduction to Li-O_2 batteries 10

1.2.1 Aqueous Li-O_2 batteries 10

1.2.2 Aprotic Li-O_2 batteries 11

1.3 Electrochemical reactions in aprotic Li-O_2 batteries 13

1.3.1 Oxygen reduction reactions (ORRs) 13

1.3.2 Oxygen evolution reactions (OERs) 19

1.4 Components of an aprotic Li-O_2 battery 23

1.4.1 Electrolyte solutions 24

1.4.1.1 Organic carbonate solutions 25

1.4.1.2 DMSO-based solutions 26

1.4.1.3 Ether-based solutions 27

1.4.1.4 Other solutions 29

1.4.2 Electrolyte salts 30

1.4.3 Electrodes 32

1.4.3.1 Carbon cathode.....32

1.4.3.2 Lithium anode 35

1.5 Challenges and perspectives in aprotic Li-O_2 batteries.....36

1.6 References 37

Chapter 2. Experimental Section 52

2.1 Construction of Electrodes and Cell Assembly.....52

2.1.1 Preparation of electrodes and electrolytes 52

2.1.1.1 Cathodes preparation.....52

2.1.1.2 Anodes preparation 52

2.1.1.3 Electrolyte solutions preparation.....53

2.1.2 Cell Designs.....54

2.1.2.1 Swagelok-type cells 54

2.1.2.2 Three-electrode cells for electrochemical measurements 55

2.1.2.3 In situ differential electrochemical mass spectrometry cells 56

2.2 Characterisation techniques.....57

2.2.1 Cyclic voltammetry (CV) 57

2.2.2 Galvanostatic cycling with potential limitation (GCPL).....59

2.2.3 Powder X-ray diffraction (PXRD).....60

2.2.4 Fourier transform infrared spectroscopy (FTIR spectroscopy) 62

2.2.5 Raman Spectroscopy.....64

2.2.6 Nuclear Magnetic Resonance Spectroscopy (NMR Spectroscopy) 66

2.2.7 Ultraviolet-Visible Spectroscopy (UV-Vis Spectroscopy) 67

2.2.8 Scanning Electron Microscopy (SEM) 69

2.2.9 Differential Electrochemical Mass Spectrometry (DEMS) 70

2.3 References 72

Chapter 3. Phenol as a phase transfer catalyst in aprotic Li-O_2 batteries 73

3.1 Background of protic additives 73

3.2 Electrochemistry performance with phenol 74

3.3 Discharge studies with phenol in Li-O_2 cells 77

3.4 Discharge product characterisations 80

3.4.1 SEM analysis 80

3.4.2 PXRD and FTIR analysis 81

3.4.3 DEMS analysis 83

3.4.4 Yield measurements 85

3.4.5 Summary of characterisations 85

3.5 Discharge studies with perchloric acid in Li-O_2 cells 86

3.6 Mechanism of catalytic effect of acid additives 88

3.6.1 The effect of proton activity 88

3.6.2 The effect of conjugate bases 90

3.7 Conclusions 91

3.8 References 92

Chapter 4. Redox mediator promoting solution phase discharge in aprotic Li-O_2 batteries containing weakly solvating electrolyte solutions 97

4.1 Selection criteria for the discharge mediator.....98

4.2 Electrochemistry studies with DBBQ 100

4.3 Enhancing the cell performance of Li-O_2 cells with DBBQ.....101

4.3.1 Discharge performance with DBBQ.....101

4.3.2 Charge performance with DBBQ 103

4.4 Discharge product characterisations.....104

4.4.1 SEM analysis 104

4.4.2 PXRD, FTIR and Raman characterisations 106

4.4.3 NMR analysis 107

4.4.4 *In situ* DEMS analysis 108

4.4.5 Yield measurements.....110

4.5 Mechanism of O_2 reduction with DBBQ 111

4.5.1 Comparisons of several discharge electrocatalysts.....111

4.5.2 Mechanism.....113

4.5.3 Kinetics of the catalytic reactions.....115

4.6 Conclusions 118

4.7 References 119

Chapter 5. A rechargeable aprotic Li-O_2 battery with dual mediators stabilizing the carbon electrode.....124

5.1 Selection criteria for the charge mediator 125

5.2 Electrochemistry performance with dual mediators 125

5.3 Enhancing the cell performance with dual mediators 126

5.3.1 Cell design 126

5.3.2 Optimising cycling conditions 127

5.3.3 Cell performance analysis 129

5.4 Characterisations 131

5.4.1 Product analysis 131

5.4.2 Pressure cell and DEMS analysis 135

5.5 Rate capability of the dual-mediator cell 138

5.6 Stability 141

5.6.1 Carbon electrode stability 141

5.6.2 Electrolyte solution stability 144

5.7 Practical dual-mediator cell with Li metal as the anode 146

5.8 Mechanism 147

5.9 Conclusions 149

5.10 References 151

Chapter 6. Perspectives and future work 157

Publication list

[1] Chen, Y.†, Gao, X.†, Johnson, L. R. & Bruce, P. G. Kinetics of lithium peroxide oxidation by redox mediators and consequences for the lithium-oxygen cell. *Nat. Commun.* **9**, 767 (2018).

I and Y.C. contributed equally to this work. I, Y.C. and L.R.J. designed the experiments and analysed the data. I and Y.C. performanced electrochemical measurements and characterizations. P.G.B. wrote the first draft of the manuscript. All authors edited and finalised the manuscript.

[2] Wang, D.†, Gao, X.†, Chen Y., Jin L., Christian K. & Bruce, P. G. Plating and stripping calcium in an organic electrolyte. *Nat. Mater.* **17**, 16-20 (2018).

I and D.W. contributed equally to this work. I, together with D.W. designed the experiments and performanced electrochemical studies and characterizations. I and other co-workers analysed and interpreted the data. P.G.B. wrote the first draft of the manuscript. All authors edited and finalised the manuscript.

[3] Gao, X.†, Chen, Y.†, Johnson, L. R., Jovanov Z. P. & Bruce, P. G. A rechargeable lithium-oxygen battery with dual mediators stablizing the carbon cathode. *Nat. Energy* **2**, 17118 (2017).

I and Y.C. contributed equally to this work. We two designed the experiments and analysed the data. I performanced electrochemical performance tests and characterizations during cycling. P.G.B. wrote the first draft of the manuscript. All authors edited and finalised the manuscript.

[4] Gao, X., Jovanov, Z. P., Chen, Y., Johnson, L. R. & Bruce, P. G. Phenol-catalyzed discharge in the aprotic lithium-oxygen battery. *Angew. Chem. Int. Ed.* **56**, 6539-6543 (2017).

I designed the experiments with the help of Z.P.J. I performanced electrochemical performance tests and characterizations of discharge products. I and co-workers analysed and interpreted the data. P.G.B. wrote the first draft of the manuscript. All authors edited and finalised the manuscript.

[5] Gao, X.†, Chen, Y.†, Johnson, L. & Bruce, P. G. Promoting solution phase discharge in Li-O_2 batteries containing weakly solvating electrolyte solutions. *Nat. Mater.* **15**, 882–888 (2016).

I and Y.C. contributed equally to this work. We two designed the experiments and analysed the data. I performanced electrochemical performance studies and characterizations of discharge products. P.G.B. wrote the first draft of the manuscript. All authors edited and finalised the manuscript.

Abbreviations

BTU	- British thermal units
CE	- Counter Electrode
CV	- Cyclic Voltammetry
DBBQ	- 2,5-Di-tert-Butyl-1,4-Benzoquinone
DEGDME	- Diethylene Glycol Dimethyl Ether
DEMS	- Differential Electrochemical Mass Spectrometry
DMA	- *N*,*N*-Dimethylacetamide
DMC	- Dimethyl Carbonate
DMDMB	- 2,3-Dimethyl-2,3-dimethoxybutane
DME	- 1,2-Dimethoxyethane
DMSO	- Dimethyl Sulfoxide
$DMSO_2$	- Dimethyl Sulfone
DMPZ	- 5,10-Dimethylphenazine
DN	- Donor Number
EC	- Ethylene Carbonate
FC	- Ferrocene
FEG	- Field Emission Gun
FePc	- Iron Phthalocyanine
FTIR	- Fourier Transform Infrared
GCPL	- Galvanostatic Cycling with Potential Limitation
GDL	- Gas Diffusion Layer
HOMO	- Highest Occupied Molecular Orbital
ICP-MS	- Inductive Coupled Plasma Mass Spectroscopy

IL	- Ionic Liquid
LFP	- Lithium Iron Phosphate
LiPON	- Lithium Phosphorous Oxy-Nitride
LISICON	- Lithium Super Ionic CONductor
$LiSO_3CF_3$	- Lithium Triflate
LiTFSI	- Lithium Bis(trifluoromethane)slufonimide
Ni-MH	- Nickel-metal hydride
NMR	- Nuclear Magnetic Resonance
NPG	- Nanoporous Gold
OER	- Oxygen Evolution Reaction
ORR	- Oxygen Reduction Reaction
PAN	- Polyacrylonitrile
PC	- Propylene Carbonate
PTFE	- Polytetrafluoroethylene
rGO	- reduced Graphene Oxide
RE	- Reference Electrode
RM	- Redox Mediator
SEI	- Solid-Electrolyte Interphase
SEM	- Scanning Electron Microscopy
SERS	- Surface Enhanced Raman Spectroscopy
SS	- Stainless Steel
TBA	- Tetrabutylammonium
TDPA	- Tris(4-(diethyl amino)phenyl)amine
TEGDME	- Tetraethylene Glycol Dimethyl Ether
TEMPO	- 2,2,6,6-Tetramethyl-1-piperidinyloxy

THF	- Tetrahydrofuran
TMS	- Tetramethylsilane
TTF	- Tetrathiafulvalene
UV-Vis	- Ultraviolet-Visible
VACNT	- Vertically Aligned Carbon Nanotube
WE	- Working Electrode

Goals and targets

Studies in this field have demonstrated the necessity and benefits of Li_2O_2 growing from solution phase in aprotic lithium-oxygen batteries, which enables the battery to achieve large capacities and sustain relatively high cycling rates. Solvents with high polarity have strong solvation strength, solubilise the intermediate, and therefore are known to promote solution phase formation of Li_2O_2. However, such electrolyte solutions are also known to be susceptible to nucleophilic attack or proton abstraction by the reactive superoxide radicals, resulting in undesired side reactions. On the other hand, solvents with low polarity are relatively stable, but they favour the formation of Li_2O_2 on the electrode surface, leading to low capacities, low rates and early cell death. Little research has been carried out to deal with the dilemma.

Therefore, my goals in this thesis are making lithium-oxygen batteries with large capacities, high rates and meanwhile sustaining long-term stabilities. Weakly-solvating solvents are relatively stable against the reactive intermediate, so they are considered as the electrolyte solutions in this thesis. In order to have large capacities, Li_2O_2 has to form from solution and therefore efforts need to be made to make the intermediate soluble in the electrolytes. After reaching the target of realise large capacities and long-term stabilities in an aprotic lithium-oxygen batteries, I will try to fundamentally understand the mechanisms to optimise the approaches in the future. In all, the ultimate target is to have a practical cell with 500-600 Wh kg^{-1} with much faster rates, but this will be beyond the discussion in this thesis.

Chapter 1. Introduction

1.1 Background on energy storage

Fossil fuels are and will be the dominant source of energy worldwide for decades to come, and the burning of fossil fuels is contributing to the changing environment. It has been reported that the CO_2 in the atmosphere today has reached over 400 ppm compared to 278 pm at the beginning of the industrial revolution, and the total amount of other significant greenhouse gases such as CH_4, N_2O and SO_2 has reached over 480 ppm[1,2]. It also brings with it other severe pollutions such as acid rain. Moreover, the energy consumption in 2012 was 549 quadrillion British thermal units (quad BTUs, where 1 quad BTU equals to 293 TWh), and it is projected to rise to 629 quad BTUs by 2020[1]. With such an expanding market and electrification of transportation, it is desirable to replace the current gasoline-dependent consumption with more efficient energy storage systems, which should minimise the pollution at the same time. This is one of the biggest and most important challenges in the 21st century.

Renewable energy storage systems, such as electrochemical energy storage is one of the possible solutions. One of the benefits of renewable energy systems is that it can power the transport in cities and meanwhile brings non-localised gas emissions, which makes it easier to cope with the gas pollution. Among all the electrochemical energy storage systems including fuel cells, supercapacitors, batteries, *etc.*, rechargeable batteries have attracted huge interest and focus worldwide. A rechargeable battery is known as a “secondary cell”, which can be charged and discharged many times, storing and releasing the electrical energy. Nickel-metal hydride (Ni-MH) batteries have been used for decades[6,7], however, such systems have a relatively low specific energy, around 40 Wh kg^{-1}, which limits its use.

Lithium ion (Li-ion) batteries first came on the market in 1990s and since then it has become one of the most widely used rechargeable batteries in portable electronic devices due to its high energy density and specific energy, energy per unit volume and mass and absence of a memory effect compared with lead-acid batteries and Ni-MH ones[8-10]. A Li-ion battery typically consists of an insertion anode like graphite and a lithium transition-metal oxide cathode such as $LiCoO_2$, $LiNi_{1/3}Mn_{1/3}Co_{1/3}O_2$ (NMC333) and layered nickel manganese cobalt oxides with reduced nickel and cobalt content with significantly higher specific energy and energy density (MRNMC) separated by a carbonate-based electrolyte solution. Lithium ions move from the anode, through the electrolyte to the cathode on discharge and moves back on charge[9]. Li-ion batteries based on the $LiNi_{1/3}Mn_{1/3}Co_{1/3}O_2$ cathode can reach a specific energy of 200-220 Wh kg^{-1}, resulting in its application in electronic transportation[3,9,10].

As shown in Fig. 1-1, transition metals like cobalt are critical to store charge in cathodes in Li-ion batteries, which normally have toxicity and little natural abundancy, leading to high costs and environmental issues. Together with the fact that cathode material like $LiCoO_2$ has limited energy density (theoretically 350-400 Wh kg^{-1}), the Li-ion battery system can barely meet the expanding market for the electronic vehicles. New electrochemical energy storage systems providing higher energy densities are proposed in the recent years and have attracted large interests in the community, such as lithium-sulphur(Li-S) batteries, lithium-oxygen ($Li-O_2$) batteries, *etc.* A comparison of the system-level energy density and specific energy for lithium-ion batteries and lithium-oxygen batteries is concluded by Gallagher *et al.* and shown in Fig. 1-1[10]. Specific energy is defined as the energy per unit mass and energy density is defined as the energy per volume so that it is reasonable to compare the energy released among different systems. A $Li-O_2$ battery has the highest specific energy of ~ 3500 Wh kg^{-1} and a high energy density of ~ 3500 Wh L^{-1}, which is several times higher than that

of a Li-ion battery[3,11]. Therefore, the Li-O_2 battery theoretically is the best rechargeable battery possible. In a practical battery system, Li-O_2 batteries demonstrate promising usable specific energy of 400-550 Wh kg^{-1}, still much higher than Li-ion batteries. However, if you compare the usable energy density of Li-O_2 batteries (300-450 Wh L^{-1}) with some advanced Li-ion batteries like Li/MRNMC, it becomes less attractive due to the demand for O_2 gases or gas filter equipment to avoid the contamination of CO_2 and water, which requires some battery volume.

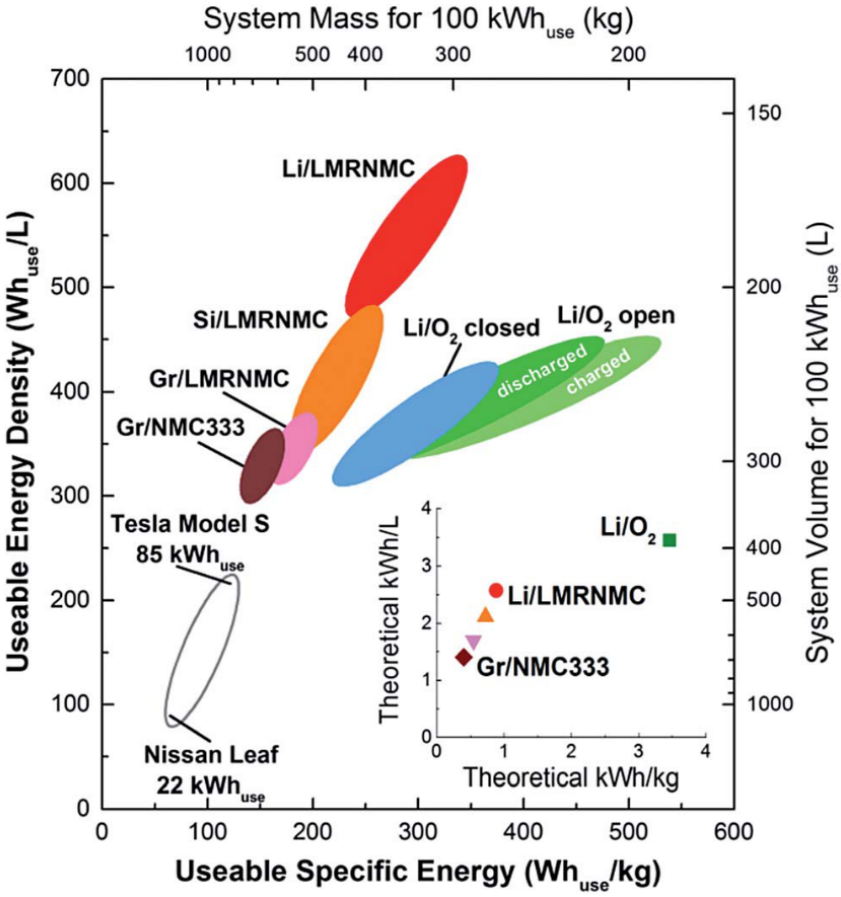


Figure 1-1 Calculated systems-level energy density and specific energy for 100 kWh of usable energy and 80 kW of net power at a nominal voltage of 360 V. Insert shows the theoretical specific energy and energy density considering both anode and cathode active materials[10].

Besides, realising a Li-O_2 in practice is a significant challenge as it combines a Li metal anode and an O_2 cathode, two of the most challenging electrode reactions known.

1.2 Introduction to Li-O_2 batteries

A Li-O_2 battery consists of an anode, such as lithium metal and Li-rich material (Li_xSi, Li_xSn) and a cathode, such as carbon and metal carbide, separated by an electrolyte solution. Based on the different nature of electrolyte solutions, two types of Li-O_2 batteries are distinguished and termed as aqueous Li-O_2 batteries and non-aqueous (aprotic) Li-O_2 batteries.

1.2.1 Aqueous Li-O_2 batteries

A typical aqueous Li-O_2 battery consists of Li serving as the anode, porous carbon serving as the cathode and an aqueous solution with varying ranges of pH values serving as the electrolyte solution. A lithium superionic conducting film is applied to the lithium electrode to avoid vigorous reactions between lithium and water. Depending on the pH of the aqueous solutions, the oxygen reduction reaction varies[12-14]. In an acidic electrolyte solution such as LiCl-NH_4Cl in H_2O, Li reacts with O_2 in the solution, combining with Cl^- to form LiCl as the discharge product[12]. The reaction is shown as:

$$2\ Li + ½\ O_2 + 2\ NH_4Cl \rightarrow 2\ LiCl + 2\ NH_3 + H_2O \qquad (1.1)$$

The formation of LiCl is at the cost of NH_4Cl, and therefore after a long-time discharge, the acidic or neutral solution will eventually become alkaline solution. More importantly, the specific energy of the aqueous Li-O_2 batteries in acidic solutions is much lower than that in basic solutions. In a basic solution such as LiOH-LiCl in H_2O, at the cathode, O_2 is reduced involving H_2O to form LiOH as the discharge product (E^0 = 3.2 V *vs.* Li^+/Li), with the reaction shown as:

$$2\ Li + ½\ O_2 + H_2O \rightarrow 2\ LiOH \qquad (1.2)$$

When LiOH reaches its solubility in H_2O (12.8 g/ 100 g of H_2O at room temperature), it will precipitate as $LiOH{\cdot}H_2O$, clogging the pores of the cathode, blocking the O_2 mass transport and therefore leading to the end of discharge[13]. LiOH is oxidised on charge or mechanically removed from the cell. It is vital to find practical and efficient electrocatalysts for oxygen reduction and evolution reactions in aqueous Li-O_2 batteries. Another big challenge is to prevent the corrosion of lithium metal by H_2O, requiring further effort in this field[12].

1.2.2 Aprotic Li-O_2 batteries

The aprotic Li-O_2 battery was first reported by Jiang *et al.* in 1996, where polyacrylonitrile (PAN) as a polymer electrolyte was used[15]. The Li/PAN-based polymer electrolyte/oxygen cell exhibited a capacity of 1400 mAh g^{-1}_{carbon} at a current density of 0.1 mA cm^{-2}. However, such Li-O_2 cells had poor cycleability and a short lifetime and did not attract large attention. In 2006, Bruce *et al.* demonstrated Li_2O_2 could be oxidised on charge, showing that a rechargeable Li-O_2 battery could be possible[28]. In 2012, Bruce and co-workers described a high-rate Li-O_2 battery albeit with relatively low capacities using nanoporous gold (NPG) as the cathode and lithium perchlorate in dimethyl sulfoxide ($LiClO_4$-DMSO) as the aprotic electrolyte solution[16], with the results are shown in Fig. 1-2.

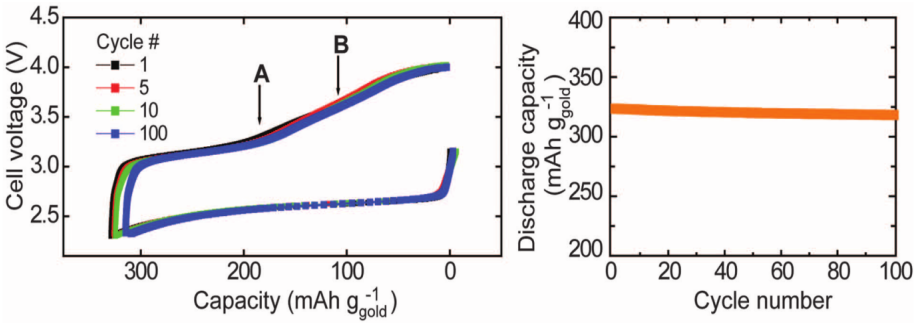


Figure 1-2 Discharge/charge curves (left) and cycling profile (right) for a Li-O_2 cell with NPG as the air electrode and 0.1 M $LiClO_4$-DMSO electrolyte, at a current density of 500 mA g^{-1} (based on the mass of Au)[16].

An initial discharge capacity of ~ 320 mAh g^{-1}_{gold} was achieved. After 100 cycles, the capacity was still over ~ 300 mAh g^{-1}_{gold}, demonstrating 95 % capacity retention. On charge, a flat plateau ending at A and a rising plateau B to the end is seen in Fig. 1-2, indicating complicated charge process that requires further understanding of such system. Since then, significant progress has been made.

The composition of an aprotic Li-O_2 battery, shown in Fig. 1-3, is similar to the aqueous system except that the electrolyte solutions are organic solutions. In an aprotic Li-O_2 battery, on discharge, O_2 is reduced to Li_2O_2 (E^0 = 2.96 V *vs.* Li^+/Li), exhibiting theoretically a specific energy of 3505 Wh kg^{-1}, based on the mass of Li_2O_2, with the desired reaction shown as:

$$2\ Li + O_2 \rightarrow Li_2O_2 \qquad (1.3)$$

On charge, Li_2O_2 is oxidised to Li^+ and O_2[3].

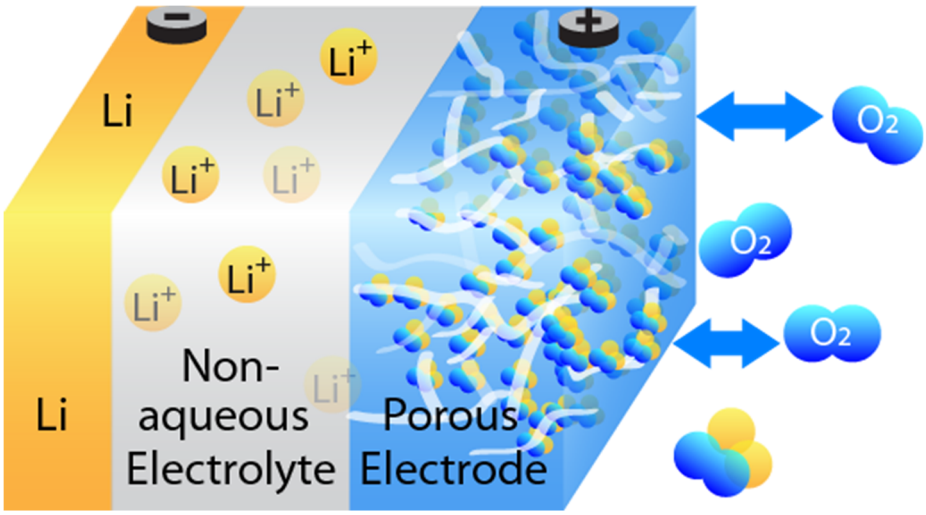


Figure 1-3 Schematic of the composition of an aprotic Li-O_2 battery. Li metal as the negative electrode, porous positive O_2 electrode and the non-aqueous electrolyte in between.

Besides Li_2O_2, other types of Li-O_2 batteries based on different discharge products were investigated as well. Grey and co-workers reported a highly efficient, rechargeable Li-O_2

battery with reduced graphene oxide (rGO) as the cathode and lithium iodide (LiI) in 1,2-dimethoxyethane (DME)-based solution with large amounts of H_2O as the electrolyte[18]. LiOH was formed and decomposed during cycling, exhibiting extremely large capacities and excellent cycling performance. Lithium superoxide (LiO_2) is known to be stable only at < 50 K[19], but Amine and co-workers claimed a Li-O_2 cell based on LiO_2 as the discharge product, which was adsorbed on an iridium-based electrode to be stabilised[20]. The cells showed much better reversibility and cycleability, comparing to cells based on O_2/Li_2O_2 redox pairs, although at the expense of specific energy (1 e^-/O_2 for LiO_2 instead of 2 e^-/O_2 for Li_2O_2). However, these systems are still at the early stage and the mechanisms remained unclear[21-27]. In this thesis, I focus on aprotic Li-O_2 batteries with Li_2O_2 as the desired discharge products.

1.3 Electrochemical reactions in aprotic Li-O_2 batteries

Early work on aprotic Li-O_2 batteries focused on organic carbonate-based electrolyte solutions like $LiPF_6$ in propylene carbonate (PC), ethylene carbonate (EC) and dimethyl carbonate (DMC)[28-33], which are commonly used in Li-ion batteries. However, after several years of investigation, such cells turned out to suffer irreversible decomposition, forming undesired products such as lithium carbonate (Li_2CO_3), lithium formate (HCO_2Li), lithium acetate (CH_3CO_2Li), *etc*[34-38]. With the revealing of the electrolyte instability, the community has realized the importance of understanding the mechanisms of Li-O_2 batteries on oxygen reduction and evolution reactions.

1.3.1 Oxygen reduction reactions (ORRs)

On discharge, O_2 is reduced to form Li_2O_2 in aprotic Li-O_2 batteries. In the past decade, several groups studied the discharge performances in Li-O_2 batteries, and different results

were shown in different electrolyte systems: Abraham and Mukerjee claimed large particles of Li_2O_2 with the doughnut shape[39], while Luntz and McCloskey exhibited a thin film of Li_2O_2 on the electrode surface[40-42]. The differences highlighted the importance of understanding O_2 reduction reactions in the presence of Li^+ in different electrolyte solutions.

A number of groups have now elucidated the mechanism of O_2 reduction to Li_2O_2[43-47], and the whole route of ORR is similar in various aprotic electrolytes, as shown in the following steps: O_2 is first reduced to O_2^-, which binds Li^+ to form LiO_2, Reaction 1.4. LiO_2 can be further reduced to Li_2O_2, Reaction 1.5 a, and meanwhile due to its thermodynamic instability, it can spontaneously disproportionate to Li_2O_2 and O_2, Reaction 1.5 b.

$$O_2 + Li^+ + e^- \rightarrow LiO_2 \qquad (1.4)$$

$$LiO_2 + Li^+ + e^- \rightarrow Li_2O_2 \qquad (1.5\ a)$$

$$2\ LiO_2 \rightarrow Li_2O_2 + O_2 \qquad (1.5\ b)$$

The E^0 for LiO_2 formation (reaction 1.4) is 2.7 V, which, according to Johnson *et al.*, is the potential determining step of the entire discharge process[43]. The 0.3 eV thermodynamic energy barrier has to be overcome to form the discharge product Li_2O_2. It was confirmed by Luntz and co-workers[48], who discharged the planar electrode at different current densities, and even at a modest current density (1 μA cm^{-2}), the discharge plateau was still at 2.7 V, excluding the possibility of kinetic issues to induce the overpotential[48]. In order to minimise the discharge overpotential, the discharge reaction mechanism needs to be changed. It is suggested to increase the E^0 for reaction 1.4 by surface adsorption or chemically stabilising LiO_2 to lower its free energy[43,49].

The electrochemical reduction reaction (1.5 a) and the chemical disproportionation reaction (1.5 b) are competitive reactions, which leads to different discharge routes. Bruce's group

recently has shown that if LiO_2 remains on the electrode surface and favours the electrochemical reduction, it will form as a thin film, Fig. 1-4[43], termed as surface mechanism. The ionic and electronic conductivity of Li_2O_2, according to Gerbig *et al.*, is 10^{-10}-10^{-9} S cm^{-1} and 10^{-12}-10^{-11} S cm^{-1} at 100 ^oC[50]. Considering the low conductivity, the Li_2O_2 film on the electrode surface will be limited to 7 nm at room temperature, leading to low capacities, low rates and early cell death[43,48]. Operating Li-O_2 batteries at higher temperatures can increase the conductivity and enhance the charge transport and hence improve the discharge performance, but it may induce greater side reactions and unexpected by-products[51]. However, if LiO_2 can dissolve in the solution and form large Li_2O_2 particles by the chemical disproportionation reactions, Li_2O_2 then grows as large particles with toroid shape, keeping Li_2O_2 away from the electrode surface, termed as solution mechanism, which results in large capacities and high rates, Fig. 1-4[43]. It is therefore important and beneficial to have the solution mechanism during discharge. The key factor that determines which pathway the cell operates is the solubility of the intermediate LiO_2, which depends on the free energy of the reaction 1.6:

$$LiO_2^{*} \leftrightarrow O_2^{\bullet-}{}_{(sol)} + Li^{+}{}_{(sol)} \qquad (1.6)$$

Bruce *et al.* have elucidated the effect of electrolyte solutions in controlling the discharge pathways[43]. Donor number (DN) is a quantitative measure of the strength of solvents as Lewis bases to solvate cations. In low DN solvents like acetonitrile (CH_3CN, DN= 14), the reaction 1.6 has a positive free energy change (ΔG^0 = + 36 kJ mol^{-1}). Li^+ solvation is too weak and LiO_2 remains on the electrode surface to be further reduced. However, in high DN solvents like dimethyl sulfoxide (DMSO, DN= 30), the negative free energy change (ΔG^0 = - 20 kJ mol^{-1}) leads to strong Li^+ solvation, with LiO_2 dissolved and $O_2^{\bullet-}$ stabilized in solutions, which favours the reaction 1.5 b with large particles of Li_2O_2 formation[43].

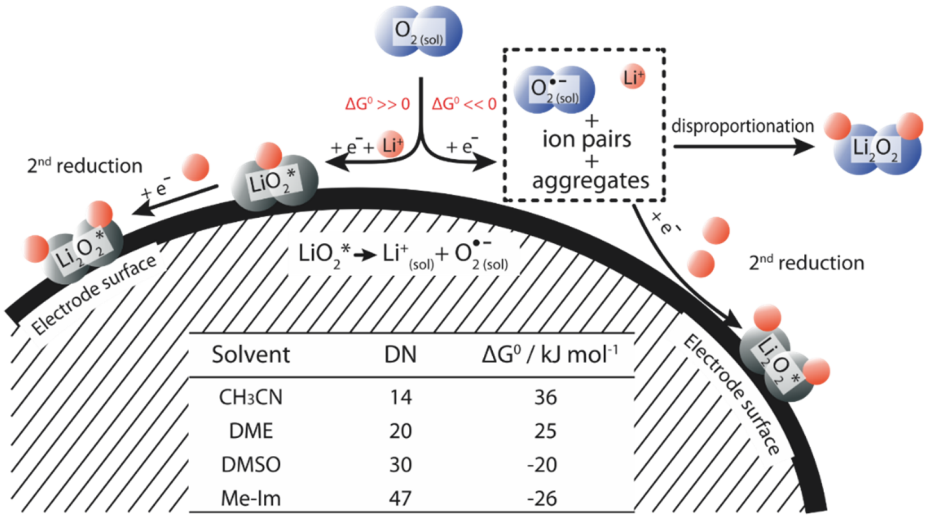


Figure 1-4 Schematic of the O_2 reduction mechanism in different aprotic solvents containing Li^+. Surface pathway is favoured when $\Delta G^0 >> 0$ (low DN), while solution pathway is favoured when $\Delta G^0 << 0$ (high DN). The table inserted shows the estimated ΔG^0 for reaction 1.6 in solvents with different DNs[43].

Besides electrolyte solvents, many groups have studied the effect of electrolyte salts in aprotic Li-O_2 batteries on the discharge performances[52-54]. Burke *et al.* examined the discharge capacity with different ratio of lithium bis(trifluoromethane)slufonimide (LiTFSI) and lithium nitrate ($LiNO_3$). The result is shown in Fig. 1-5 (a), where higher ratio of $LiNO_3$: LiTFSI led to higher discharge capacities. They also demonstrated that nodular morphologies appeared on the electrode surface in the low $LiNO_3$ ratio electrolyte, while large toroid particles indicating solution growth of Li_2O_2 were found in the high $LiNO_3$ ratio electrolyte, Fig. 1-5 (b), (c)[53].

Sharon *et al.* measured the discharge capacities in Li^+-based electrolyte with different anions and the capacity could be enhanced 8 times by using a different lithium salt such as $LiNO_3$ rather than LiTFSI, Fig. 1-6[54]. All these results suggest that in low DN solvents, although Li^+ has a poor coordination with the solvent, some anions like NO_3^- are able to coordinate strongly with Li^+. It is analogous to the solvated Li^+ ions in high DN solvents, where the

reduced superoxide species are stabilised with lower free energy to disproportionate in solution, leading to toroid shapes of Li_2O_2, optimizing the cell capacity and sustaining a longer cell life[55].

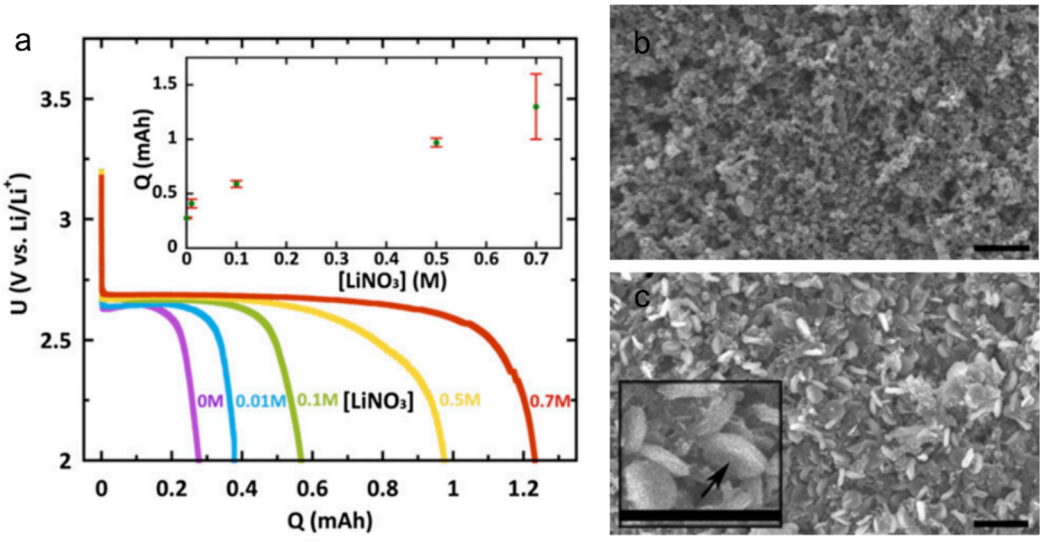


Figure 1-5 (a) Representative galvanostatic discharge profiles of Li-O_2 cells (450 uA/cm^2 under 1.5 atm O_2 to a 2 V cut-off). Insert shows the capacity dependence on $LiNO_3$ concentration. (b), (c) SEM images of the cathodes discharged at 45 uA/cm^2 using 1 M total Li^+ concentration, with (b) 0.01 M $LiNO_3$, and (c) 0.7 M $LiNO_3$. Scale bars, 1 μm[53].

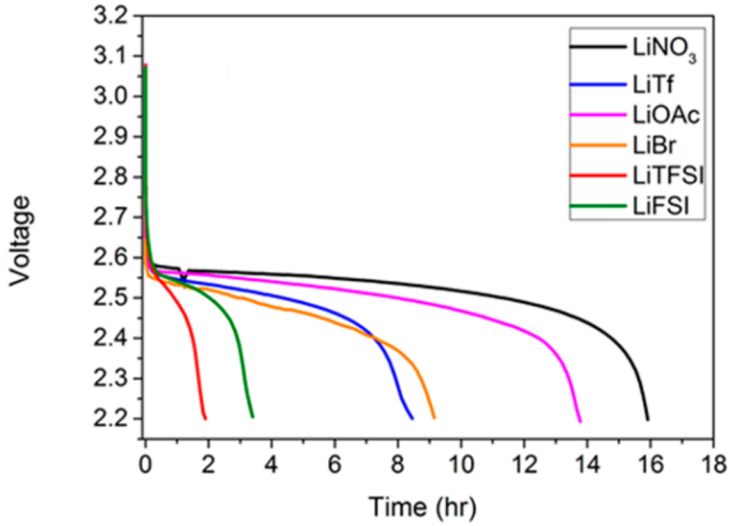


Figure 1-6 Galvanostatic discharge curves (3 uA/cm^2) of 1 M LiX in diglyme with various lithium salts using sputtered gold cathodes[54].

Aprotic additives to the electrolyte solutions, such as H_2O can also influence the LiO_2 solubility to achieve the solution mechanism through solvation of lithium cation or superoxide anion[44,56-59]. Gasteiger and co-workers studied the effect of H_2O as an impurity on the Li_2O_2 growth and the cell performance by adding different amounts of H_2O in the electrolyte solution. As shown in Fig. 1-7, the discharge capacity with 1000 ppm H_2O could be 10 times higher than that without H_2O and large discharge current with high discharge capacity is achievable with the presence of H_2O. They also claimed that the addition of H_2O contributed to the toroid shape of Li_2O_2 in low DN solvents[56,57]. Luntz *et al.* also found that trace amount of water can enhance the discharge capacities[44]. However, contrary to Gasteiger's work[56], they claimed that the addition of water led to more parasitic chemistry[44]. The controversy results of the addition of protic addtives needs further explorations and highlights the importance of stability issues when introducing additives into the cell systems.

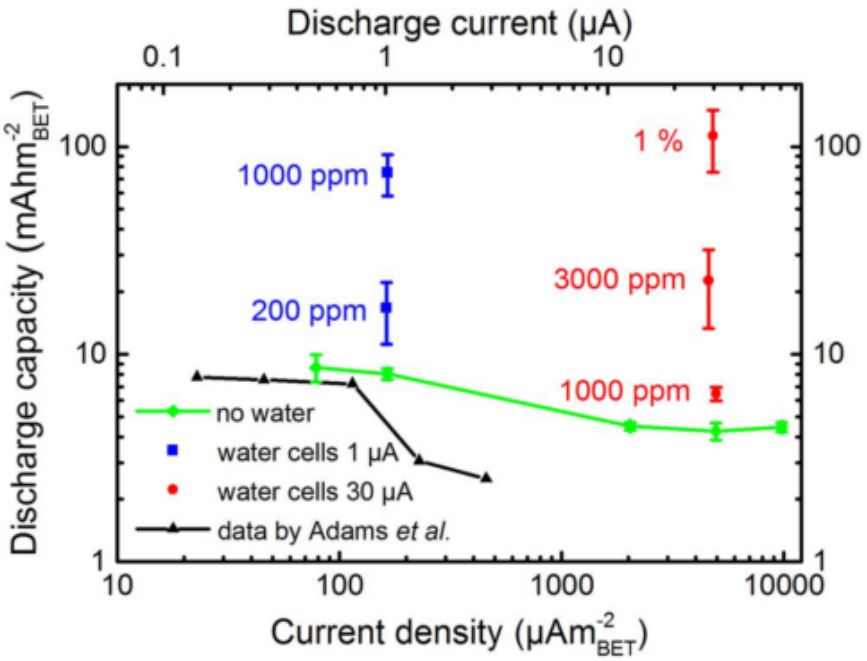


Figure 1-7 First discharge capacity as a function of discharge current and current density in the cells with low-surface-area carbon paper cathodes and 0.5 M LiTFSI in diglyme as electrolyte with various amount of water[56].

Soluble catalysts and redox shuttles were also studied to catalyse oxygen reduction reactions[60-64]. Owen and co-workers proposed ethyl viologen redox couple, $EtV^{2+}/EtV^{\cdot+}$ as the discharge redox shuttle and the mechanism is shown in Fig. 1-8.

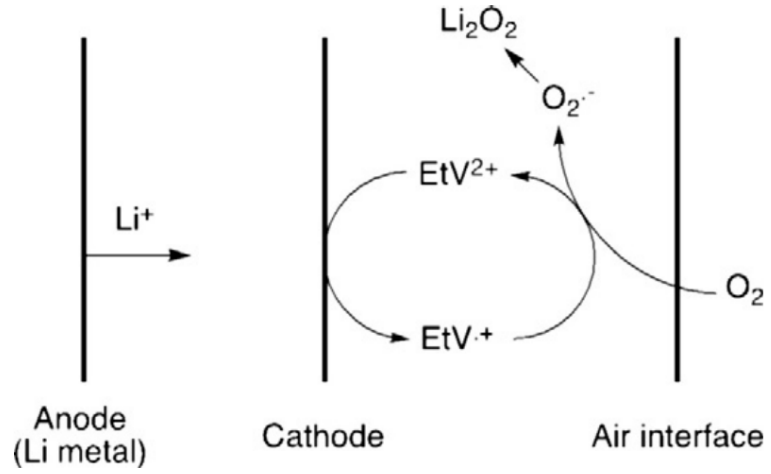


Figure 1-8 Schematic showing $EtV^{2+}/EtV^{\cdot+}$ redox shuttle transferring the ORR site away from the electrode surface to solution[60].

EtV^{2+} can be reduced at the electrode surface and the reduced form, $EtV^{\cdot+}$, then diffuses to the air interface to be reoxidised by oxygen to form lithium superoxide or peroxide[60]. Owen claimed that it was preferable to form the discharge product at the gas interface to avoid the solid discharge product blocking further access to the electrode surface so that a higher capacity could be achieved.

1.3.2 Oxygen evolution reactions (OERs)

Many OER mechanisms have been proposed to describe the charge process in aprotic Li-O_2 batteries, but it is still under debate whether the charge goes by 1-e^- transfer (similar to ORR) or a 2-e^- transfer without the formation of LiO_2 as the charge intermediate[55,65-67]. It is difficult to elucidate the charge mechanism because the morphology of the discharge product Li_2O_2 may vary depending on many factors like electrolyte solutions and discharge

current densities[48,56]. Oxidation of large Li_2O_2 particles grown from solution compared to the thin Li_2O_2 film on the electrode surface is more challenging[43,49,68]. In addition, the reactive Li_2O_2 reacts with the electrolytes on discharge and charge, forming insulating side products on the Li_2O_2 surface, which adds difficulty to predict the charge process.

In 2006, Ogasawara *et al.* tried to oxidise Li_2O_2 in ethylene carbonate/dimethyl carbonate (EC:DMC = 1:1 v/v), and the evolution of O_2 was observed by mass spectrometry[28]. If LiO_2 was present as the charge intermediate, it would react with the carbonate electrolyte to induce solvent decomposition rather than being further oxidised to evolve O_2. Therefore, the charge process was proposed as the reaction 1.7:

$$Li_2O_2 \rightarrow O_2 + 2\,Li^+ + 2\,e^- \qquad (1.7)$$

Shao-Horn and co-workers divided the charge process into three stages by probing the kinetics of the redox processes in the discharged Li_2O_2, shown in Fig. 1-9[67]. The first stage is a slope from 3 V to 3.4 V, corresponding to 25 % of the whole charge process, which is attributed to the lithium deintercalation process via a solid solution route from the outer part of Li_2O_2 to form LiO_2-like species on the surface ($Li_2O_2 \rightarrow LiO_2 + Li^+ + e^-$). The LiO_2-like species disproportionate to form Li_2O_2 and evolve O_2 ($2\,LiO_2 \rightarrow O_2 + Li_2O_2$), yielding an overall 2-e^- reaction 1.7. It is consistent with the 2 e^-/O_2 OER process observed by McCloskey and co-workers who measured the Li_2O_2 oxidation in DME solvent during the sloping charging step[69]. According to Luntz *et al.*, this process requires relatively small overpotential (< 0.2 V) even at high current densities and no catalyst is required at this stage[45]. Shao-Horn *et al.* observed that the decomposition of Li_2O_2 only took place at the contacts between Li_2O_2 and the electrode by the *in situ* TEM technique. During the charge process, the contact spots might be lost, which leads to a considerable ohmic polarisation to reach the second stage[70].

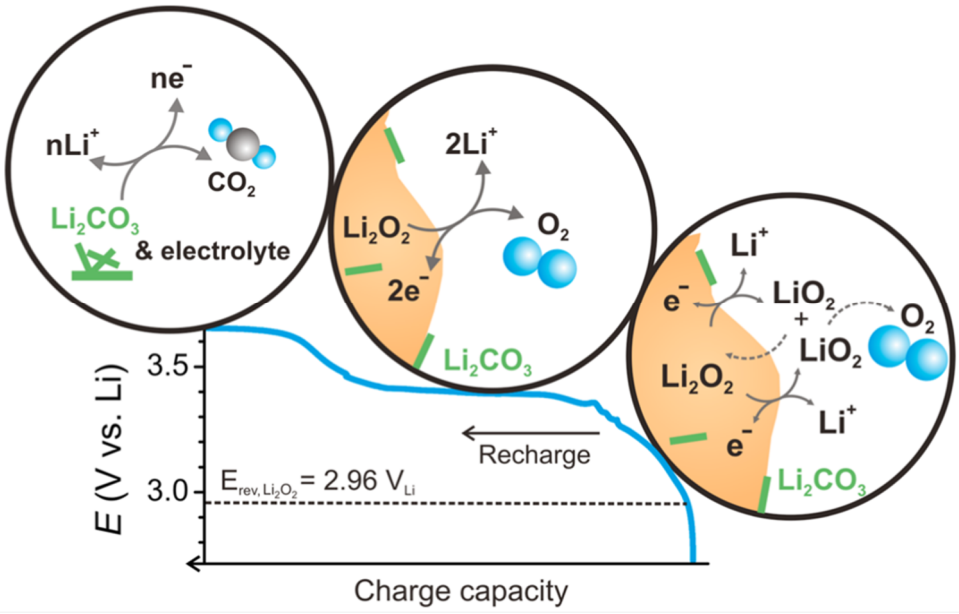


Figure 1-9 Proposed reaction mechanism of Li-O_2 recharge with three different stages. Stage 1 is a deintercalation process from the outer part of Li_2O_2 to form LiO_2-like species, which disproportionate to evolve O_2. Stage 2 is the oxidation of bulk Li_2O_2 particles via a two-phase transition. Stage 3 is the decomposition of carbonate-type by-products and electrolyte[67].

The second stage is a flat plateau at ~ 3.4 V, which covers half of the whole charge capacity. The bulk Li_2O_2 is oxidised at this stage to evolve O_2[67]. A considerable overpotential can be observed at this stage, where OER catalysts like metal oxides start to play their roles to minimise the overpotential[71-73]. The third stage is a rising plateau at the end of the charge process, which is assigned to the oxidation of the by-products accumulated during the discharge and charge process and the decomposition of the electrolyte.

Nazar and co-workers analysed the charge reactions for electrochemically formed Li_2O_2 (E-Li_2O_2) and commercial Li_2O_2 (C-Li_2O_2) and they observed different oxidation processes for these two different types of Li_2O_2[66]. For E-Li_2O_2, a two-stage oxidation process was proposed. The amorphous lithium components comprising of noncrystalline Li_2O_2 and side products arising from degradation of electrolyte such as lithium formate is oxidised first, and at the higher potential, the crystalline peroxide is oxidised via a Li-deficient solid

solution phase. While for C-Li_2O_2, a one-stage mechanism was proposed that a Li-deficient component ($Li_{2-x}O_2$) is formed and the crystallite Li_2O_2 is gradually decomposed.

Besides experimental analysis, density functional theory calculations have been performed to gain a better understanding of the charge process[74,75]. Ceder and co-workers studied the Li_2O_2 oxidation potential on different crystal facets and found that a lower overpotential is required to oxidise Li_2O_2 on some crystal facets, which supported the experimental observations of O_2 evolution and Li_2O_2 decomposition at the early charge stage. They also suggested the most energetically favourable pathway as $Li_{n+4}O_{n+4}$ → $Li_{n+3}O_{n+4}$ → $Li_{n+2}O_{n+4}$ → $Li_{n+2}O_{n+2}$ → $Li_{n+1}O_{n+2}$ → $Li_{n+1}O_n$ → Li_nO_n.

Although the mechanism of OER in Li-O_2 batteries is still unclear, it is likely that during the charge process, Li-deficient $Li_{2-x}O_2$ is formed on the Li_2O_2 surface, which will immediately disproportionate to evolve O_2. As mentioned above, catalysts in the oxygen evolution reaction in fuel cells were also used in Li-O_2 batteries to minimise the charge overpotential. However, it was found that some of these catalysts favoured the decomposition of electrolyte solutions[76,77]. Moreover, the limited active sites at the solid-solid contact on the cathode surface leads to low catalyst activities[77]. In addition, large Li_2O_2 particles growing from solution mechanisms on discharge are remote from the electrode surface and therefore electronically isolated during charging[5,78]. To address these problems, soluble catalysts or redox mediators (RMs) are used. Charge redox mediators are molecules dissolved in the electrolyte that are oxidised at a potential higher than the equilibrium potential of Li_2O_2 formation. The schematic is shown in Fig. 1-10. On charge, mediators are oxidised at the electrode surface to the oxidised forms, which diffuse into solution and oxidise Li_2O_2. The soluble catalysts have wet contact with the solid Li_2O_2, even if the Li_2O_2 is poorly attached to the cathode, thus maximising the interaction areas for the catalysis.

Therefore, Li_2O_2 particles are oxidised and O_2 is evolved, with the mediator molecular being reduced and regenerated back to the electrode surface for the cycle to be repeated.

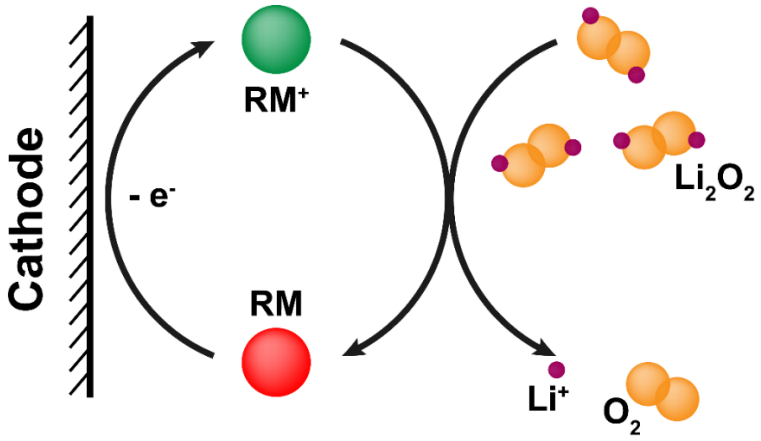


Figure 1-10 Schematic showing redox mediators catalysing oxygen evolution reactions during charging in aprotic Li-O_2 cells.

Chen *et al.* first reported tetrathiafulvalene (TTF) as an efficient charge mediator, where high charge current (1 mA cm^{-2}) is achievable which is impossible without charge mediators[17]. Since then, more charge mediators have been explored with potentials closer to that for Li_2O_2 oxidation, including tris(4-(diethyl amino)phenyl)amine (TDPA), iron phthalocyanine (FePc), 5,10-dimethylphenazine (DMPZ), LiI, LiBr, 2,2,6,6-tetramethyl-1-piperidinyloxy (TEMPO) and other redox-active molecules[77,79-85]. Kang *et al.* proposed some design principal for finding a catalyst based on the ionization energy. Some calculations suggested that soluble catalysts should have suitable highest occupied molecular orbital (HOMO) energy levels of the pristine and oxidised forms considering the Li_2O_2 decomposition energy and oxidation potential of the electrolyte solvent[77].

1.4 Components of an aprotic Li-O_2 battery

In an aprotic Li-O_2 battery, reduced oxide species such as superoxide and peroxide are present and recently singlet oxygen was reported in aprotic Li-O_2 batteries as well, which

are likely to attack the inactive components in the battery including electrolyte solutions, electrolyte salts and electrodes, leading to the depletion of these components. The undesired decomposition products are generally insulating and they passivate the electrode surface, resulting in early cell death and poor cycling performance. It is important to understand the decomposition pathways and find truly stable components for aprotic Li-O_2 batteries.

1.4.1 Electrolyte solutions

Many electrolytes have been studied and used in Li-ion batteries in the past few decades, and several requirements are proposed. Similar to a Li-ion battery, a good electrolyte should be good electronic insulator and ionic conductor, where ion transport is facilitated and meanwhile the possibility of self-discharge is kept to a minimum. It should have a wide electrochemical window and good thermal stability[86,87]. Moreover, in an aprotic Li-O_2 cell with the presence of reduced oxygen species, the chemical stability of the electrolyte solutions is even more challenging. Recently, the highly reactive singlet oxygen ($^1O_2$) was reported in Li-O_2 cells and it was claimed to contribute to the majority of parasitic reactions[31,34]. Wandt *et al.* first presented experimental investigation of singlet oxygen formation during charge. They used a spin trap to capture $^1O_2$ and form a stable radical that could be detected by electron paramagnetic resonance spectroscopy. Singlet oxygen was shown to be evolved during Li_2O_2 oxidation at potentials above 3.55 V[34]. Freunberger and co-workers further reported the direct observation of singlet oxygen formation during discharge or from the onset of charging. The amount of $^1O_2$ increased during discharge or during the early charging stages or charging at higher voltages, and it was enhanced by the presence of trace amount of H_2O. The addition of $^1O_2$ traps and quenchers could effectively minimise parasitic reactions on discharge and charge[31]. Significant attempts have been made by Bruce[16,43,88-90], Shao-Horn[91-93], Luntz[94-96], Nazar[97-99], Zhou[100-102], Aurbach[103,104] and

many other groups to search for stable electrolyte solutions, but no satisfactory electrolyte has been found. The long-term stability of the electrolyte solutions is probably one of the biggest challenges in aprotic Li-O_2 batteries.

1.4.1.1 Organic carbonate solutions

Early studies on Li-O_2 cells focused on organic carbonate-based electrolyte solutions, as they are widely used in Li-ion batteries with advantages like low volatility, compatibility with Li metal and wide electrochemical windows. Bruce and co-workers, in 2011, investigated the discharge and charge performance in PC-based Li-O_2 cells[34]. They found that the discharge process was dominated by undesired decomposition reactions and there was no evidence of reversible oxygen reduction to Li_2O_2. The decomposition products like $C_3H_6(OCO_2Li)_2$, Li_2CO_3, CH_3CO_2Li and HCO_2Li formed on discharge were partially oxidised on charge. They proposed the intermediate superoxide was responsible for the decomposition, shown in Fig. 1-11.

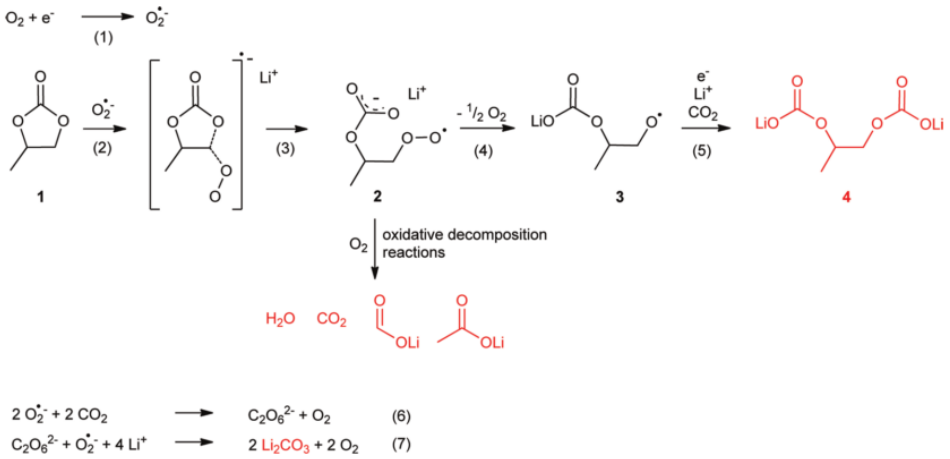


Figure 1-11 Proposed reaction mechanism on discharge in carbonate solutions showing the decomposition routes. For example, PC decomposes in the presence of superoxide[34].

Since then, numerous researches proved that the primary discharge products for carbonate solutions are various carbonate species due to nucleophilic attack by O_2^- at the ethereal

carbon atom[33,35,105]. The cycling performance depends entirely on back-to-back irreversible side reactions and at the same time, it consumes the electrolyte solutions.

The consumption of electrolyte solutions and the accumulation of insulating side products resulted in capacity fading and eventually caused the cell failure. It also brings into question the validity of most results before 2012, where organic carbonate solvents were widely used. The failure of carbonate solutions as suitable electrolytes motivated research into other solvents, including ethers, amides, DMSO and ionic liquids (ILs).

1.4.1.2 DMSO-based solutions

DMSO has a high DN of 29.8. It favours the solution mechanism during discharge in Li-O_2 batteries and leads to a larger discharge capacity compared to other lower DN solvents[43], which make it commonly used in Li-O_2 batteries[16,17,106,107].

Xu *et al.* first investigated DMSO as an electrolyte solution for Li-O_2 batteries showing high discharge capacity, low charge potential and good rate performances[108]. Bruce *et al.* later reported Li-O_2 cells based on $LiClO_4$/DMSO as the electrolyte with NPG and TiC as the air electrode, which showed 100 cycles with little capacity decay and better stability against Li_2O_2[16,106]. Aurbach and co-workers also demonstrated reversible behaviour for ORR and OER in DMSO on gold electrodes, however, when carbon electrode was used, large amounts of side products were found during the ORR process[104]. The instability of DMSO was confirmed by other groups: long time exposure of DMSO to KO_2 solution led to the formation of dimethyl sulfone ($DMSO_2$)[109], and LiOH was also found through the reaction between Li_2O_2 and DMSO[93]. The decomposition mechanism is shown in Fig. 1-12 where reduced oxygen species are involved[104].

The decomposition reaction is time-dependent and longer exposure time of DMSO to superoxide and peroxide led to more decomposition, which indicates that DMSO is not suitable as the electrolyte for long-time cycling. Further studies proved that high DN solvents are more readily to suffer attack from reduced oxygen species compared to low DN solvents and the search for stable electrolyte solutions should focus on low DN solvents[43,49].

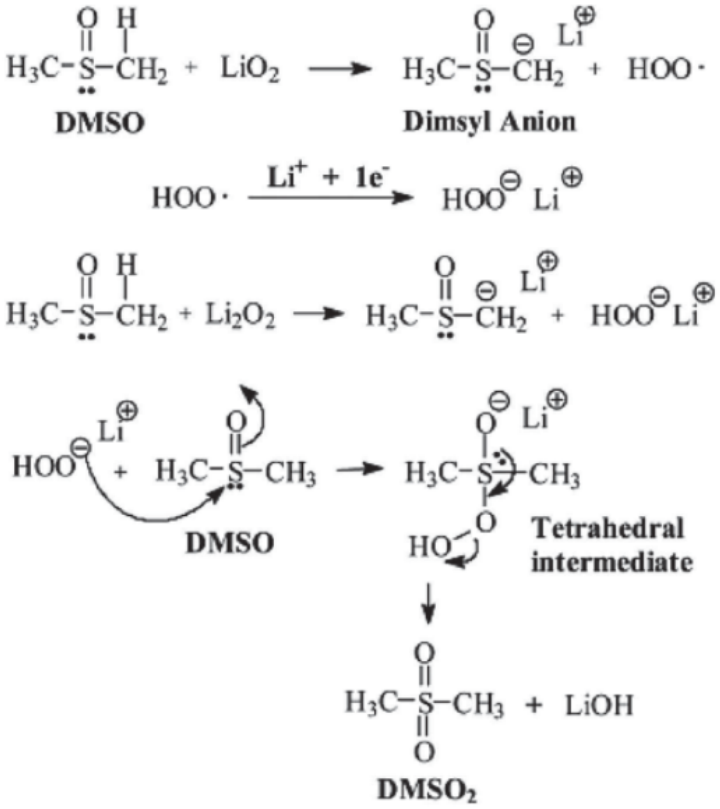


Figure 1-12 Proposed degradation mechanism of DMSO on discharge in aprotic Li-O_2 cells. In the presence of Li^+ during ORR, DMSO was decomposed to form $DMSO_2$ and LiOH by reduced oxygen species[104].

1.4.1.3 Ether-based solutions

Ethers such as 1,2-dimethoxyethane (DME) and tetraethylene glycol dimethyl ether (TEGDME) with an intermediate DN have been intensively studied in Li-O_2 cells due to their compatibility with Li metal and high electrochemistry window (> 4.5 V versus Li^+/Li)

[36]. More importantly, they are expected to shower greater stability against reduced O_2 species compared to organic carbonates and high DN solvents[36]. Read *et al.* first reported an ether-based Li-O_2 cell, exhibiting good stability and excellent rate capability[110]. Later on, Luntz *et al.* compared the discharge performance from the DME-based electrolyte and carbonate-based electrolyte and confirmed Li_2O_2 as the main discharge product in ether-based electrolyte[36,76]. McCloskey *et al.* showed the highest Li_2O_2 yield among cells employing aprotic electrolytes without additives in the P50/LiTFSI/DME-based cell. Due to the high volatility of DME, researches also focus on glycol ethers with higher molecular weights[49,111]. Sharon and co-workers compared different glycol ethers and they found that diethylene glycol dimethyl ether (DEGDME) exhibited the best cycling performance[111].

Unfortunately, although ether solvents are more stable than carbonate solvents, researchers found that glycol ethers are unstable on discharge and they still suffer decomposition reactions[36,69,76,88,103]. Freunberger *et al.* proposed that the glycol ethers in Li-O_2 cells could undergo hydrogen abstraction from the CH_2 group near the O atom in the ethers by superoxide radicals[88]. Considering superoxide is a poor base and cannot abstract these hydrogen atoms, Sharon *et al.* proposed a nucleophilic attack by Li_2O_2, shown in Fig. 1-13. Li_2O_2 in its solid state is unreactive with the ether solvents, however, before the solid precipitation, the peroxide species is highly active, which can attack the solvent molecules via its α-H and β-H near O , especially in the presence of the highly electrophilic Li ions, forming lithium acetate, formate, carbonate, *etc*[103].

Efforts were made to improve the performance of the relatively stable ether-based electrolyte solutions. Cecchetto *et al.* mixed TEGDME with N-methyl-(n-butyl) pyrrolidinium bis(trifluoromethanesulfonyl)imide, which showed a higher conductivity and larger electrochemical oxidation window[112]. Mixture of glycol ethers was used to balance the stability and volatility to improve the cycling performance. However, these methods did

not fundamentally solve the problem of nucleophilic attack. Since the reduced O_2 species are likely to attack the hydrogen atom near the O atom, both Nazar and Aurbach proposed the modification of ether molecules by replacing the hydrogen atoms with more bulky groups or stable atoms[98,103]. Nazar and co-workers substituted the reactive hydrogen in DME with methyl group to form 2,3-dimethyl-2,3-dimethoxybutane (DMDMB) as a new electrolyte solution. The DMDMB-based Li-O_2 battery exhibited less decomposition and much better cycling performance, which provided an approach to prevent the decomposition of solvent molecules[98].

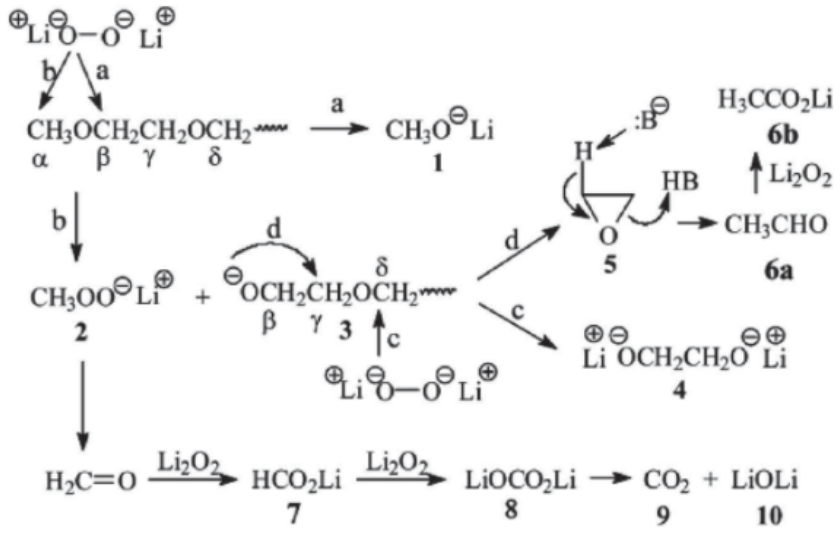


Figure 1-13 Proposed degradation mechanism of glycol ethers on discharge in aprotic Li-O_2 cells by Li_2O_2. Before the solid precipitation of Li_2O_2, glycol ethers are proposed to suffer from nucleophilic attack[103].

1.4.1.4 Other solutions

Ionic liquids (ILs) are widely used in studying oxygen reduction reactions and some are applied as electrolyte solutions or as electrolyte mixtures in Li-O_2 batteries to improve the conductivity and stability[113-115]. However, it is difficult to purify the ILs and the remaining impurities can possibly induce unknown side reactions[116]. Amide-based solutions have also

been used as electrolyte solutions. Walker *et al.* exhibited a rechargeable Li-O_2 battery with *N,N*-dimethylacetamide (DMA) as the electrolyte, which showed over 40 cycles with capacity limited to 1 mAh cm^{-2} with low overpotentials[117]. However, the amides are not stable against Li anode, resulting in a poor solid-electrolyte interphase (SEI) on the anode. According to Chen *et al.*, amides also suffer from the reaction with reduced oxide species, limiting its application in long-time cell[89]. Vincent *et al.* demonstrated a Li-O_2 battery with $LiNO_3$-KNO_3 molten salt electrolyte at 150 °C, where high capacity with low overpotential was obtained. However, the low O_2 solubility hinders the rate capability and the high temperature may cause more side reactions[118].

It appears that all commercial off-the-shelf electrolyte solutions examined to date exhibit instability to highly reactive environment in aprotic Li-O_2 batteries and it remains one of the biggest challenges to find a suitable electrolyte solution[55,87].

1.4.2 Electrolyte salts

The lithium salt in aprotic Li-O_2 batteries should meet basic requirements of high solubility, good conductivity, wide electrochemistry window and stability against the cell components[86]. Furthermore, similar to the solvent stability, the lithium salts need to be stable against reduced oxide species and singlet oxygen.

Lithium hexafluorophosphate ($LiPF_6$) was used as the electrolyte salt in Li-O_2 cells in early studies because it is one of the preferred lithium salts in Li-ion batteries[28,39]. However, further studies showed that it reacts with Li_2O_2. Oswald *et al.* presented direct formation of LiF when Li_2O_2 was exposed to the $LiPF_6$-based electrolyte[119]. Salts like lithium tetrafluoroborate ($LiBF_4$) and lithium bis(oxalato)borate (LiBOB) were also found to undergo decomposition by reduced O_2 species, where they are decomposed to form lithium

triborate (LiB_3O_5), lithium oxalate (LiC_2O_4), LiF, *etc*[120-122]. These lithium salts are therefore unsuitable for aprotic Li-O_2 cells.

Zhang and co-workers found lithium perchlorate ($LiClO_4$) had the best stability during discharge, which is in accord with Veith's work[121,122]. However, some conflicting results were reported about $LiClO_4$. Shao *et al.* found that $LiClO_4$ was unstable in the O_2 rich environment[123] and Edstrom and co-workers showed the presence of LiCl on the electrode surface with XPS, suggesting some decomposition of $LiClO_4$[124]. LiTFSI and lithium triflate ($LiSO_3CF_3$) were explored and found to have minor signs of decomposition to LiF, which raises safety concerns[121]. It was shown that $LiSO_3CF_3$ would corrode the Al current collector, therefore Al should be avoided with such salts. $LiNO_3$ is commonly used as the electrolyte salt combining with DMA as the electrolyte solution[117,125-128]. Kang *et al.* found that $LiNO_3$ as the electrolyte salt can eliminate CO_2 evolution[126] and Walker *et al.* showed good cycling performance with $LiNO_3$ as the electrolyte salt. Amides are unstable against Li anode, but the presence of $LiNO_3$ helps form a protective SEI layer, improving the cell performance[117,128]. Halides such as lithium iodide (LiI) and lithium bromide (LiBr) are proposed as suitable electrolyte salts and additives due to their active redox couples that can readily oxidise Li_2O_2, but such salts have safety issues and they are known to attack the cell compounds[80,84,129]. It should be noted that the slight decomposition of these salts is not the main sources of side products in Li-O_2 cells, comparing to the decomposition of electrolyte solutions.

Researches have shown that anions in the salts have significant effects in determining the cell performance by changing the solubility of the intermediate to form Li_2O_2. Thus, there is a trade-off between enhancement of the discharge capacity and the long-term stability of the cell, and cares should be paid during selection of the electrolyte salts for Li-O_2 cells[53,54].

1.4.3 Electrodes

1.4.3.1 Carbon cathode

Besides the selection of stable and optimised electrolyte, the search of a practical air electrode is also of paramount importance[12,55]. The ultimate goal of the air electrodes is to achieve high specific capacity and power capability of Li-O_2 cells yet achieve a long cycle life. Cheap materials, good electronic and ionic conductivity and optimised air electrode structure for fast oxygen diffusion are required for a suitable air electrode[31,130]. Among all the candidates, porous carbon materials have been widely studied as the air electrodes in aprotic Li-O_2 cells because they can provide sufficient charge transfer for the electrochemical reactions and at the same time have space for housing the discharge products. However, researchers have found that carbon substrate contributes to the side reactions and suffered severe decomposition during cycling[94,107].

McCloskey *et al.* used isotope-labelled carbon to distinguish the electrode decomposition from the electrolyte decomposition, where they found that the carbon was unstable on both discharge and charge. On discharge, Li_2O_2 in contact with C forms a few monolayers of Li_2CO_3 on the C-Li_2O_2 interface, reaction 1.8 and 1.9.

$$Li_2O_2 + C + ½\ O_2 \rightarrow Li_2CO_3 \qquad (1.8)$$

$$2\ Li_2O_2 + C \rightarrow Li_2O + Li_2CO_3 \qquad (1.9)$$

The insulating Li_2CO_3 film led to a large overpotential on charge and the highly oxidizing environment in turn promoted further carbon decomposition[94]. McCloskey *et al.* also found that the amount of by-products did not vary with different types of carbon, indicating that the side reactions were not sensitive to the carbon types[69].

Thotiyl *et al.* also used carbon isotopes (^{13}C carbon) to study the stability of carbon in $LiClO_4$/DMSO and $LiPF_6$/TEGDME based Li-O_2 cells and confirmed the evolution of $^{13}CO_2$ on charge in both systems. After discharge and charge, acid treatment was employed to detect the $^{12}CO_2$ and $^{13}CO_2$ evolution resulting from the electrolyte decomposition and carbon electrode decomposition, respectively. Phosphoric acid (H_3PO_4) was first used to analyse inorganic carbonate and Fenton's reagent (a solution of hydrogen peroxide with ferrous ions) was then used to detect organic carbonate. They found in Fig. 1-14 that carbon was relatively stable during discharge and the decomposition began above 3.5 V on charge in the presence of Li_2O_2, oxidatively decomposing to form Li_2CO_3[107].

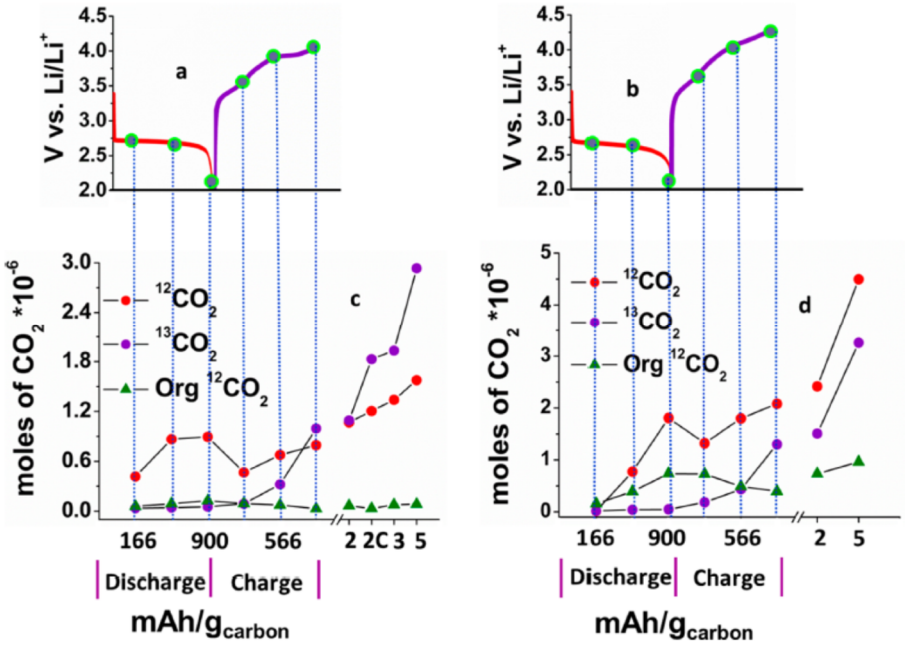


Figure 1-14 Different types of CO_2 evolution showing the carbon electrode and electrolyte decomposition at various points during cycling in various electrolytes. (a,b) Discharge-charge curves on the first cycle for DMSO- and TEGDME-based electrolytes, respectively, at a carbon electrode. (c,d) Moles of CO_2 evolved from the carbon electrodes at different stages of discharge and charge treated with acids. The values (166 *etc.*) on the x-axis do not represent a scale but indicate the states-of-charge at which the cathodes were sampled[107].

Bruce and co-workers also measured the direct chemical reaction of carbon with Li_2O_2 and found that the Li_2O_2/C reaction is dependent on the carbon surface composition, where a more hydrophilic and defective carbon surface leads to faster carbon degradation[107]. It was confirmed by Iktis *et al.* who reported that the superoxide species generated on discharge would react with carbon with activated double bonds to form epoxy groups and carbonates from their XPS studies[131].

Shao-Horn and co-workers observed considerable chemical and morphological changes of products during cycling in a DME-based Li-O_2 cell with vertically aligned carbon nanotube (VACNT) as the air electrode. They showed direct evidence of Li_2CO_3-like species at the VACNTs-Li_2O_2 interface but not significantly on the Li_2O_2 surfaces exposed to the electrolyte, which is in accord with McCloskey's studies, where they claimed that the carbonate was difficult to remove during cycling, leading to the irreversibility of the cell[132].

As shown from the various research studies above, the carbon decomposition is complex in an aprotic Li-O_2 cell. It not only depends on the carbon surface composition but also depends on the potential-dependent decomposition and electrolyte decomposition promoted by the carbon surface. The net effect emphasizes that the stability of the electrode and electrolyte cannot be considered separately[55]. Since the carbon electrode is unstable above 3.5 V on charge in the presence of Li_2O_2 and seems not to be a good choice as the air electrode, some non-carbon materials like NPG, TiC and TiO_x were studied, which showed good cycling performance in aprotic Li-O_2 batteries[16,106,133,134]. Electrochemical deposition methods to modify the carbon surface and heterogeneous catalysts have been investigated to protect the carbon electrode[135-138]. However, the low mass of the carbon-based electrode has the highest specific capacity, making the alternative materials less attractive. It would be an encouraging target for me to stabilise carbon and make it as the air electrode in a Li-O2 cell with minor decomposition.

1.4.3.2 Lithium anode

Metallic lithium is widely used as the anode for Li-ion batteries and aprotic Li-O_2 batteries, but some stability and safety challenges remain to be solved. In Li-ion batteries where organic carbonate solvents serve as the electrolyte solutions, a stable SEI layer is formed which protects the anode from further decomposition. However, in aprotic Li-O_2 cells, carbonate solvents are unsuitable and therefore the SEI layer loses its effect and large amount of decomposition is observed on the anode. In 2011, Abraham and co-workers studied cycling performance in $LiPF_6$-TEGDME and they observed severe morphology change in the Li anode, where the surface was covered with brown precipitate, possibly due to the reaction between the electrolyte and lithium. Besides, the crossover of O_2 from the cathode to anode results in undesired decomposition of the lithium anode. Amine and co-workers studied the possible degradation on the Li anode in a TEGDME-based electrolyte, with the presence of O_2. LiOH and some carbonates were observed after a few cycles. LiOH is neither an electron conductor nor a Li^+ ion conductor, and therefore the accumulation of such insoluble products will block Li^+ migration, leading to poor cell performance[139].

In order to form a stable SEI layer to avoid further decomposition, Walker *et al.* used $LiNO_3$ as the electrolyte salt in DMA and demonstrated excellent cell cycling performance[117]. The effect of $LiNO_3$ forming a protective layer between the Li metal and the electrolyte was proposed and mentioned above[127,128]. Lithium ion conducting membranes, such as lithium super ionic conductor (LISICON) and lithium phosphorous oxy-nitride (LiPON), were applied in aprotic and aqueous Li-O_2 batteries to protect Li from reactions with additives in the bulk electrolytes[68,140]. A similar idea was proposed by Truong *et al.* who fabricated single-crystal silicon membranes that are capable of conducting Li^+ through the lattices. However, the Li-ion conductivity in the membrane is quite low, 3-4 orders lower than

LISICON[141]. Scrosati and co-workers used a pre-lithiated silicon electrode (Li_xSi) as a negative electrode and exhibited 15 cycles with a limited capacity of 1000 mAh g^{-1}_{carbon}[142].

1.5 Challenges and perspectives in aprotic Li-O_2 batteries

With the high theoretical specific energy of 3500 Wh kg^{-1}, aprotic Li-O_2 cells have gained great attention worldwide. Significant progress has been achieved, but such technology is still at the early stage of development and many challenges need to be solved before coming onto the market. Firstly, a dilemma of achieving high capacity and long-time stability remains one of the most challenging issues. The solution route in high DN solvent is preferred to reach high capacity with high rates, but such solvents are unstable against the reduced oxygen species. The relatively stable low DN solvents lead to surface route, which has limited capacity with low rates due to the formation of insulating Li_2O_2 films on the electrode. Secondly, it seems that all commercial electrolytes examined to date exhibit instability to highly reactive environment in the cell. Design of a robust strategy for effectively screening the electrolyte stability is essential to the development of aprotic Li-O_2 batteries. Furthermore, both the air electrode and Li anode suffer from instability against cell components and great effort is required to optimise the electrodes for practical application.

This project will focus on solving the capacity and stability issues by soluble catalysts. To increase the capacity, several additives and mediators are investigated to promote solution phase formation of Li_2O_2 in low DN solvents, which show a considerable increase in the discharge capacity compared to that without additives. The mechanisms are studied to provide some idea on tackling the dilemma of achieving high capacity and long-time stability. In Chapter 5, charge mediators are explored to oxidise the large Li_2O_2 particles growing from solution in Chapter 4. By combining two redox mediators that shuttle

electrons between the electrode surface and the Li_2O_2 in solution, discharge and charge processes are fast, reversible and sustainable on cycling, with high capacities to store energy and low charging voltages. These studies also provide some insight in rendering the carbon electrode stable.

1.6 References

1 Chu, S., Cui, Y. & Liu, N. The path towards sustainable energy. *Nat. Mater.* **16**, 16-22 (2016).

2 Butler, J. H. & Montzka, S. A. The NOAA annual greenhouse gas index. (National Oceanic & Atmospheric Administration, 2016).

3 Bruce, P. G., Freunberger, S. A., Hardwick, L. J. & Tarascon, J.-M. Li-O_2 and Li-S batteries with high energy storage. *Nat. Mater.* **11**, 19-29 (2012).

4 Bruce, P. G., Hardwick, L. J. & Abraham, K. M. Lithium-air and lithium-sulfur batteries. *MRS Bull.* **36**, 506-512 (2011).

5 Aurbach, D., McCloskey, B. D., Nazar, L. F. & Bruce, P. G. Advances in understanding mechanisms underpinning lithium–air batteries. *Nat. Energy* **1**, 16128 (2016).

6 Bergstrom, S. Nickel-Cadmium Batteries-Pocket type. *J. Electrochem. Soc.* **99**, 248C-250C (1952).

7 Linden, D. & Reddy, T. B. *Handbook of batteries*. 3 edn, (McGraw-Hill Professional, 2002).

8 Nagaura, T. & Tozawa, K. Lithium ion rechargeable battery. *Prog. Batteries Sol. Cells* **9**, 209-217 (1990).

9 Tarascon, J. M. & Armand, M. Issues and challenges facing rechargeable lithium batteries. *Nature* **414**, 359-367 (2001).

10 Gallagher, K. G. *et al.* Quantifying the promise of lithium–air batteries for electric vehicles. *Energy Environ. Sci.* **7**, 1555 (2014).

11 Su, Y. S., Fu, Y., Cochell, T. & Manthiram, A. A strategic approach to recharging lithium-sulphur batteries for long cycle life. *Nat. Commun.* **4**, 2985 (2013).

12 Lu, J. *et al.* Aprotic and aqueous Li-O_2 batteries. *Chem. Rev.* **114**, 5611-5640 (2014).

13 Zhang, J. G., Wang, D. Y., Xu, W., Xiao, J. & Williford, R. E. Ambient operation of Li/Air batteries. *J. Power Sources* **195**, 4332-4337 (2010).

14 Imanishi, N., Luntz, A. C. & Bruce, P. G. *The lithium air battery: fundamentals*. (Springer, 2014).

15 Abraham, K. M. & Jiang, Z. A polymer electrolyte-based rechargeable lithium/oxygen battery. *J. Electrochem. Soc.* **143**, 1-5 (1996).

16 Peng, Z., Freunberger, S. A., Chen, Y. & Bruce, P. G. A reversible and higher-rate Li-O_2 battery. *Science* **337**, 563-566 (2012).

17 Chen, Y., Freunberger, S. A., Peng, Z., Fontaine, O. & Bruce, P. G. Charging a Li–O_2 battery using a redox mediator. *Nat. Chem.* **5**, 489–494 (2013).

18 Liu, T. *et al.* Cycling Li-O_2 batteries via LiOH formation and decomposition. *Science* **350**, 530-533 (2015).

19 Bryantsev, V. S., Blanco, M. & Faglioni, F. Stability of lithium superoxide LiO_2 in the gas phase: computational study of dimerization and disproportionation reactions. *J. Phys. Chem. A* **114**, 8165-8169 (2010).

20 Lu, J. *et al.* A lithium-oxygen battery based on lithium superoxide. *Nature* **529**, 377-382 (2016).

21 Burke, C. M. *et al.* Implications of 4 e⁻oxygen reduction via iodide redox mediation in Li–O_2 batteries. *ACS Energy Lett.* **1**, 747-756 (2016).

22 Papp, J. K. *et al.* Poly(vinylidene fluoride) (PVDF) binder degradation in Li-O_2 batteries: a consideration for the characterization of lithium superoxide. *J. Phys. Chem. Lett.* **8**, 1169-1174 (2017).

23 Viswanathan, V. *et al.* Comment on "Cycling Li-O_2 batteries via LiOH formation and decomposition". *Science* **352**, 667-667 (2016).

24 Shen, Y., Zhang, W., Chou, S.-L. & Dou, S.-X. Comment on "Cycling Li-O_2 batteries via LiOH formation and decomposition". *Science* **352**, 667-667 (2016).

25 Liu, T., Kim, G., Carretero-González, J., Castillo-Martínez, E. & Grey, C. P. Response to Comment on "Cycling Li-O_2 batteries via LiOH formation and decomposition". *Science* **352**, 667-667 (2016).

26 Liu, T. *et al.* Response to Comment on "Cycling Li-O_2 batteries via LiOH formation and decomposition". *Science* **352**, 667-667 (2016).

27 Tan, P., Ni, M., Shao, Z., Chen, B. & Kong, W. Numerical investigation of a non-aqueous lithium-oxygen battery based on lithium superoxide as the discharge product. *Appl. Energy* **203**, 254-266 (2017).

28 Ogasawara, T., Debart, A., Holzapfel, M., Novak, P. & Bruce, P. G. Rechargeable Li_2O_2 electrode for lithium batteries. *J. Am. Chem. Soc.* **128**, 1390-1393 (2006).

29 Beattie, S. D., Manolescu, D. M. & Blair, S. L. High-capacity lithium–air cathodes. *J. Electrochem. Soc.* **156**, A44-A47 (2009).

30 Debart, A., Paterson, A. J., Bao, J. & Bruce, P. G. Alpha-MnO_2 nanowires: a catalyst for the O_2 electrode in rechargeable lithium batteries. *Angew. Chem. Int. Ed.* **47**, 4521-4524 (2008).

31 Xiao, J. *et al.* Optimization of air electrode for Li/air batteries. *J. Electrochem. Soc.* **157**, A487-A492 (2010).

32 Lu, Y.-C., Gasteiger, H. A., Parent, M. C., Chiloyan, V. & Shao-Horn, Y. The influence of catalysts on discharge and charge voltages of rechargeable Li–oxygen batteries. *Electrochem. Solid-State Lett.* **13**, A69-A72 (2010).

33 Xu, W. *et al.* Investigation on the charging process of Li_2O_2-based air electrodes in Li–O_2 batteries with organic carbonate electrolytes. *J. Power Sources* **196**, 3894-3899 (2011).

34 Freunberger, S. A. *et al.* Reactions in the rechargeable lithium-O_2 battery with alkyl carbonate electrolytes. *J. Am. Chem. Soc.* **133**, 8040-8047 (2011).

35 Bryantsev, V. S. *et al.* Predicting solvent stability in aprotic electrolyte Li–air batteries: nucleophilic substitution by the superoxide anion radical ($O_2^{\bullet -}$). *J. Phys. Chem. A* **115**, 12399-12409 (2011).

36 McCloskey, B. D., Bethune, D. S., Shelby, R. M., Girishkumar, G. & Luntz, A. C. Solvents' critical role in nonaqueous lithium–oxygen battery electrochemistry. *J. Phys. Chem. Lett.* **2**, 1161-1166 (2011).

37 Xiao, J. *et al.* Investigation of the rechargeability of Li–O_2 batteries in non-aqueous electrolyte. *J. Power Sources* **196**, 5674-5678 (2011).

38 Veith, G. M., Dudney, N. J., Howe, J. & Nanda, J. Spectroscopic characterization of solid discharge products in Li–air cells with aprotic carbonate electrolytes. *J. Phys. Chem. C* **115**, 14325-14333 (2011).

39 Laoire, C., Mukerjee, S., Plichta, E. J., Hendrickson, M. A. & Abraham, K. M. Rechargeable Lithium/TEGDME-$LiPF_6$/O_2 battery. *J. Electrochem. Soc.* **158**, A302-A308 (2011).

40 Albertus, P. *et al.* Identifying capacity limitations in the Li/oxygen battery using experiments and modeling. *J. Electrochem. Soc.* **158**, A343-A351 (2011).

41 Viswanathan, V. *et al.* Electrical conductivity in Li_2O_2 and its role in determining capacity limitations in non-aqueous Li-O_2 batteries. *J. Chem. Phys.* **135**, 214704 (2011).

42 McCloskey, B. D., Scheffler, R., Speidel, A., Girishkumar, G. & Luntz, A. C. On the mechanism of nonaqueous Li–O_2 electrochemistry on C and its kinetic overpotentials: Some implications for Li–air batteries. *J. Phys. Chem. C* **116**, 23897-23905 (2012).

43 Johnson, L. *et al.* The role of LiO_2 solubility in O_2 reduction in aprotic solvents and its consequences for Li–O_2 batteries. *Nat. Chem.* **6**, 1091-1099 (2014).

44 Aetukuri, N. B. *et al.* Solvating additives drive solution-mediated electrochemistry and enhance toroid growth in non-aqueous Li-O_2 batteries. *Nat. Chem.* **7**, 50-56 (2015).

45 Hummelshoj, J. S., Luntz, A. C. & Norskov, J. K. Theoretical evidence for low kinetic overpotentials in Li-O_2 electrochemistry. *J. Chem. Phys.* **138**, 034703 (2013).

46 Laoire, C. O., Mukerjee, S., Abraham, K. M., Plichta, E. J. & Hendrickson, M. A. Influence of nonaqueous solvents on the electrochemistry of oxygen in the rechargeable lithium−air battery. *J. Phys. Chem. C* **114**, 9178-9186 (2010).

47 Adams, B. D. *et al.* Current density dependence of peroxide formation in the Li-O_2 battery and its effect on charge. *Energy Environ. Sci.* **6**, 1772-1778 (2013).

48 Luntz, A. C. *et al.* Tunneling and polaron charge transport through Li_2O_2 in Li–O_2 batteries. *J. Phys. Chem. Lett.* **4**, 3494-3499 (2013).

49 Gao, X., Chen, Y., Johnson, L. & Bruce, P. G. Promoting solution phase discharge in Li-O_2 batteries containing weakly solvating electrolyte solutions. *Nat. Mater.* **15**, 882–888 (2016).

50 Gerbig, O., Merkle, R. & Maier, J. Electron and ion transport in Li_2O_2. *Adv. Mater.* **25**, 3129-3133 (2013).

51 Li, L. & Manthiram, A. Dual-electrolyte lithium-air batteries: influence of catalyst, temperature, and solid-electrolyte conductivity on the efficiency and power density. *J. Mater. Chem. A* **1**, 5121-5127 (2013).

52 Gunasekara, I., Mukerjee, S., Plichta, E. J., Hendrickson, M. A. & Abraham, K. M. A study of the influence of lithium salt anions on oxygen reduction reactions in Li-air batteries. *J. Electrochem. Soc.* **162**, A1055-A1066 (2015).

53 Burke, C. M., Pande, V., Khetan, A., Viswanathan, V. & McCloskey, B. D. Enhancing electrochemical intermediate solvation through electrolyte anion selection to increase nonaqueous Li-O_2 battery capacity. *Proc. Natl. Acad. Sci. U. S. A.* **112**, 9293-9298 (2015).

54 Sharon, D. *et al.* Mechanistic role of Li^+ dissociation level in aprotic Li-O_2 battery. *ACS Appl. Mater. Interfaces* **8**, 5300-5307 (2016).

55 Aurbach, D., McCloskey, B. D., Nazar, L. F. & Bruce, P. G. Advances in understanding mechanisms underpinning lithium–air batteries. *Nat. Energy* **1**, 16128 (2016).

56 Schwenke, K. U., Metzger, M., Restle, T., Piana, M. & Gasteiger, H. A. The influence of water and protons on Li_2O_2 crystal growth in aprotic Li-O_2 cells. *J. Electrochem. Soc.* **162**, A573-A584 (2015).

57 Meini, S., Piana, M., Tsiouvaras, N., Garsuch, A. & Gasteiger, H. A. The effect of water on the discharge capacity of a non-catalyzed carbon cathode for Li-O_2 batteries. *Electrochem. Solid-State Lett.* **15**, A45-A48 (2012).

58 Xia, C. *et al.* Direct evidence of solution-mediated superoxide transport and organic radical formation in sodium-oxygen batteries. *J. Am. Chem. Soc.* **138**, 11219-11226 (2016).

59 Zhu, Y. G. *et al.* Proton enhanced dynamic battery chemistry for aprotic lithium-oxygen batteries. *Nat. Commun.* **8**, 14308 (2017).

60 Lacey, M. J., Frith, J. T. & Owen, J. R. A redox shuttle to facilitate oxygen reduction in the lithium air battery. *Electrochem. Commun.* **26**, 74-76 (2013).

61 Lodge, A. W., Lacey, M. J., Fitt, M., Garcia-Araez, N. & Owen, J. R. Critical appraisal on the role of catalysts for the oxygen reduction reaction in lithium-oxygen batteries. *Electrochim. Acta* (2014).

62 Yao, K. P. C. *et al.* Utilization of cobalt bis(terpyridine) metal complex as soluble redox mediator in Li–O_2 batteries. *J. Phys. Chem. C* **120**, 16290-16297 (2016).

63 Liu, J. *et al.* An Organic Catalyst for Li–O_2 batteries: dilithium quinone-1,4-dicarboxylate. *ChemSusChem* **8**, 2198-2203 (2015).

64 Matsuda, S., Hashimoto, K. & Nakanishi, S. Efficient Li_2O_2 formation via aprotic oxygen reduction reaction mediated by quinone derivatives. *J. Phys. Chem. C* **118**, 18397-18400 (2014).

65 Ganapathy, S. *et al.* Operando nano-beam diffraction to follow the decomposition of individual Li_2O_2 grains in a non-aqueous Li-O_2 battery. *J. Phys. Chem. Lett.*, 3388–3394 (2016).

66 Ganapathy, S. *et al.* Nature of Li_2O_2 oxidation in a Li-O_2 battery revealed by operando X-ray diffraction. *J. Am. Chem. Soc.* **136**, 16335-16344 (2014).

67 Lu, Y.-C. & Shao-Horn, Y. Probing the reaction kinetics of the charge reactions of nonaqueous Li–O_2 batteries. *J. Phys. Chem. Lett.* **4**, 93-99 (2012).

68 Gao, X., Jovanov, Z. P., Chen, Y., Johnson, L. R. & Bruce, P. G. Phenol-catalyzed discharge in the aprotic lithium-oxygen battery. *Angew. Chem. Int. Ed.* **56**, 6539-6543 (2017).

69 McCloskey, B. D. *et al.* Combining accurate O_2 and Li_2O_2 assays to separate discharge and charge stability limitations in nonaqueous Li–O_2 batteries. *J. Phys. Chem. Lett.* **4**, 2989-2993 (2013).

70 Zhong, L. *et al. In situ* transmission electron microscopy observations of electrochemical oxidation of Li_2O_2. *Nano Lett.* **13**, 2209-2214 (2013).

71 Shang, C. *et al.* Compatible interface design of CoO-based Li-O_2 battery cathodes with long-cycling stability. *Sci. Rep.* **5**, 8335 (2015).

72 Li, F. *et al.* Superior performance of a Li-O_2 battery with metallic RuO_2 hollow spheres as the carbon-free cathode. *Adv. Energy Mater.*, 1500294 (2015).

73 Park, J.-B. *et al.* Improvement of electrochemical properties of lithium–oxygen batteries using a silver electrode. *J. Phys. Chem. C* **119**, 15036-15040 (2015).

74 Kang, S., Mo, Y., Ong, S. P. & Ceder, G. A facile mechanism for recharging Li_2O_2 in Li–O_2 batteries. *Chem. Mater.* **25**, 3328-3336 (2013).

75 Mo, Y., Ong, S. P. & Ceder, G. First-principles study of the oxygen evolution reaction of lithium peroxide in the lithium-air battery. *Phys. Rev. B* **84**, 205446 (2011).

76 McCloskey, B. D. *et al.* On the efficacy of electrocatalysis in nonaqueous Li-O_2 batteries. *J. Am. Chem. Soc.* **133**, 18038-18041 (2011).

77 Lim, H.-D. *et al.* Rational design of redox mediators for advanced Li–O_2 batteries. *Nat. Energy* **1**, 16066 (2016).

78 Gao, X., Chen, Y., Johnson, L. R., Jovanov, Z. P. & Bruce, P. G. A rechargeable lithium–oxygen battery with dual mediators stabilizing the carbon cathode. *Nat. Energy* **2**, 17118 (2017).

79 Kundu, D., Black, R., Adams, B. & Nazar, L. F. A highly active low voltage redox mediator for enhanced rechargeability of Lithium–oxygen batteries. *ACS Cent. Sci.* **1**, 510-515 (2015).

80 Lim, H. D. *et al.* Superior rechargeability and efficiency of lithium-oxygen batteries: hierarchical air electrode architecture combined with a soluble catalyst. *Angew. Chem. Int. Ed.* **53**, 3926-3931 (2014).

81 Bergner, B. J. *et al.* How to improve capacity and cycling stability for next generation Li-O_2 batteries: approach with a solid electrolyte and elevated redox mediator concentrations. *ACS Appl. Mater. Interfaces* **8**, 7756-7765 (2016).

82 Bergner, B. J., Schurmann, A., Peppler, K., Garsuch, A. & Janek, J. TEMPO: a mobile catalyst for rechargeable Li-O_2 batteries. *J. Am. Chem. Soc.* **136**, 15054-15064 (2014).

83 Bergner, B. J. *et al.* Understanding the fundamentals of redox mediators in Li-O_2 batteries: a case study on nitroxides. *Phys. Chem. Chem. Phys.* **17**, 31769-31779 (2015).

84 Kwak, W.-J. *et al.* Li–O_2 cells with LiBr as an electrolyte and a redox mediator. *Energy Environ. Sci.* **9**, 2334-2345 (2016).

85 Sun, D. *et al.* A solution-phase bifunctional catalyst for lithium-oxygen batteries. *J. Am. Chem. Soc.* **136**, 8941-8946 (2014).

86 Xu, K. Nonaqueous liquid electrolytes for lithium-based rechargeable batteries. *Chem. Rev.* **104**, 4303-4418 (2004).

87 Li, Y., Wang, X., Dong, S., Chen, X. & Cui, G. Recent advances in non-aqueous electrolyte for rechargeable Li-O_2 batteries. *Adv. Energy Mater.* **6**, 1600751 (2016).

88 Freunberger, S. A. *et al.* The lithium-oxygen battery with ether-based electrolytes. *Angew. Chem. Int. Ed.* **50**, 8609-8613 (2011).

89 Chen, Y., Freunberger, S. A., Peng, Z., Barde, F. & Bruce, P. G. Li-O_2 battery with a dimethylformamide electrolyte. *J. Am. Chem. Soc.* **134**, 7952-7957 (2012).

90 Peng, Z. *et al.* Oxygen reactions in a non-aqueous Li^+ electrolyte. *Angew. Chem. Int. Ed.* **50**, 6351-6355 (2011).

91 Lu, Y. C. *et al.* Lithium-oxygen batteries: bridging mechanistic understanding and battery performance. *Energy Environ. Sci.* **6**, 750-768 (2013).

92 Amanchukwu, C. V., Harding, J. R., Shao-Horn, Y. & Hammond, P. T. Understanding the chemical stability of polymers for lithium–air batteries. *Chem. Mater.* **27**, 550-561 (2015).

93 Kwabi, D. G. *et al.* Chemical instability of dimethyl sulfoxide in lithium–air batteries. *J. Phys. Chem. Lett.* **5**, 2850-2856 (2014).

94 McCloskey, B. D. *et al.* Twin problems of interfacial carbonate formation in nonaqueous Li–O_2 batteries. *J. Phys. Chem. Lett.* **3**, 997-1001 (2012).

95 Luntz, A. C. & McCloskey, B. D. Nonaqueous Li-air batteries: a status report. *Chem. Rev.* **114**, 11721-11750 (2014).

96 Khetan, A., Luntz, A. & Viswanathan, V. Trade-offs in capacity and rechargeability in nonaqueous Li–O_2 batteries: Solution-driven growth versus nucleophilic stability. *J. Phys. Chem. Lett.* **6**, 1254-1259 (2015).

97 Black, R. *et al.* Screening for superoxide reactivity in Li-O_2 batteries: effect on Li_2O_2/LiOH crystallization. *J. Am. Chem. Soc.* **134**, 2902-2905 (2012).

98 Adams, B. D. *et al.* Towards a stable organic electrolyte for the Lithium oxygen battery. *Adv. Energy Mater.* **5**, 1400867 (2015).

99 Kundu, D. *et al.* Nanostructured metal carbides for aprotic Li–O_2 batteries: New insights into interfacial reactions and cathode stability. *J. Phys. Chem. Lett.* **6**, 2252-2258 (2015).

100 Kitaura, H. & Zhou, H. Reaction and degradation mechanism in all-solid-state lithium-air batteries. *Chem. Commun.* **51**, 17560-17563 (2015).

101 Zhang, T. & Zhou, H. A reversible long-life lithium-air battery in ambient air. *Nat. Commun.* **4**, 1817 (2013).

102 Song, Z. & Zhou, H. Towards sustainable and versatile energy storage devices: an overview of organic electrode materials. *Energy Environ. Sci.* **6**, 2280 (2013).

103 Sharon, D. *et al.* On the challenge of electrolyte solutions for Li–air batteries: monitoring oxygen reduction and related reactions in polyether solutions by spectroscopy and EQCM. *J. Phys. Chem. Lett.* **4**, 127-131 (2012).

104 Sharon, D. *et al.* Oxidation of dimethyl sulfoxide solutions by electrochemical reduction of oxygen. *J. Phys. Chem. Lett.* **4**, 3115-3119 (2013).

105 Laino, T. & Curioni, A. A new piece in the puzzle of lithium/air batteries: computational study on the chemical stability of propylene carbonate in the presence of lithium peroxide. *Chem. Eur. J.* **18**, 3510-3520 (2012).

106 Ottakam Thotiyl, M. M. *et al.* A stable cathode for the aprotic Li-O_2 battery. *Nat. Mater.* **12**, 1050-1056 (2013).

107 Ottakam Thotiyl, M. M., Freunberger, S. A., Peng, Z. & Bruce, P. G. The carbon electrode in nonaqueous Li-O_2 cells. *J. Am. Chem. Soc.* **135**, 494-500 (2013).

108 Xu, D., Wang, Z., Xu, J., Zhang, L. & Zhang, X. Novel DMSO-based electrolyte for high performance rechargeable Li-O_2 batteries. *Chem. Commun.* **48**, 6948-6950 (2012).

109 Mozhzhukhina, N., Méndez De Leo, L. P. & Calvo, E. J. Infrared spectroscopy studies on stability of dimethyl sulfoxide for application in a Li–air battery. *J. Phys. Chem. C* **117**, 18375-18380 (2013).

110 Read, J. Characterization of the lithium/oxygen organic electrolyte battery. *J. Electrochem. Soc.* **149**, A1190-A1195 (2002).

111 Sharon, D., Hirshberg, D., Afri, M., Frimer, A. A. & Aurbach, D. The importance of solvent selection in Li-O_2 cells. *Chem. Commun.* **53**, 3269-3272 (2017).

112 Cecchetto, L., Salomon, M., Scrosati, B. & Croce, F. Study of a Li-air battery having an electrolyte solution formed by a mixture of an ether-based aprotic solvent and an ionic liquid. *J. Power Sources* **213**, 233-238 (2012).

113 Monaco, S. *et al.* An electrochemical study of oxygen reduction in pyrrolidinium-based ionic liquids for lithium/oxygen batteries. *Electrochim. Acta* **83**, 94-104 (2012).

114 Kwon, H. M. *et al.* Stability of glyme solvate ionic liquid as an electrolyte for rechargeable Li-O_2 batteries. *ACS Appl. Mater. Interfaces* **9**, 6014-6021 (2017).

115 Wang, H. *et al.* A solvate ionic liquid as the anolyte for aqueous rechargeable Li-O_2 batteries. *ChemElectroChem* **2**, 1144-1151 (2015).

116 Das, S. *et al.* Instability of ionic liquid-based electrolytes in Li–O_2 batteries. *J. Phys. Chem. C* **119**, 18084-18090 (2015).

117 Walker, W. *et al.* A rechargeable Li-O_2 battery using a lithium nitrate/N,N-dimethylacetamide electrolyte. *J. Am. Chem. Soc.* **135**, 2076-2079 (2013).

118 Giordani, V. *et al.* A molten salt lithium-oxygen battery. *J. Am. Chem. Soc.* **138**, 2656-2663 (2016).

119 Oswald, S. *et al.* XPS investigations of electrolyte/electrode interactions for various Li-ion battery materials. *Anal. Bioanal. Chem.* **400**, 691-696 (2011).

120 Hyoung Oh, S., Yim, T., Ekaterina, P. & Nazar, L. F. Decomposition reaction of lithium bis(oxalato)borate in the rechargeable lithium-oxygen cell. *Electrochem. Solid-State Lett.* **14**, A185-A188 (2011).

121 Nasybulin, E. *et al.* Effects of electrolyte salts on the performance of Li–O_2 batteries. *J. Phys. Chem. C* **117**, 2635-2645 (2013).

122 Veith, G. M., Nanda, J., Delmau, L. H. & Dudney, N. J. Influence of lithium salts on the discharge chemistry of Li–air cells. *J. Phys. Chem. Lett.* **3**, 1242-1247 (2012).

123 Shao, Y. *et al.* Making Li-air batteries rechargeable: material challenges. *Adv. Funct. Mater.* **23**, 987-1004 (2013).

124 Younesi, R., Veith, G. M., Johansson, P., Edström, K. & Vegge, T. Lithium salts for advanced lithium batteries: Li–metal, Li–O_2, and Li–S. *Energy Environ. Sci.* **8**, 1905-1922 (2015).

125 Sharon, D. *et al.* Catalytic behavior of lithium nitrate in Li-O_2 cells. *ACS Appl. Mater. Interfaces* **7**, 16590-16600 (2015).

126 Kang, S. J., Mori, T., Narizuka, S., Wilcke, W. & Kim, H. C. Deactivation of carbon electrode for elimination of carbon dioxide evolution from rechargeable lithium-oxygen cells. *Nat. Commun.* **5**, 3937 (2014).

127 Giordani, V. *et al.* Synergistic effect of oxygen and $LiNO_3$ on the interfacial stability of lithium metal in a Li/O_2 battery. *J. Electrochem. Soc.* **160**, A1544-A1550 (2013).

128 Uddin, J. *et al.* Lithium nitrate as regenerable SEI stabilizing agent for rechargeable Li/O_2 batteries. *J. Phys. Chem. Lett.* **4**, 3760-3765 (2013).

129 Kwak, W.-J. *et al.* Understanding the behavior of Li-oxygen cells containing LiI. *J. Mater. Chem. A* **3**, 8855-8864 (2015).

130 Zhang, S. S., Foster, D. & Read, J. Discharge characteristic of a non-aqueous electrolyte Li/O_2 battery. *J. Power Sources* **195**, 1235-1240 (2010).

131 Itkis, D. M. *et al.* Reactivity of carbon in lithium-oxygen battery positive electrodes. *Nano Lett.* **13**, 4697-4701 (2013).

132 Gallant, B. M. *et al.* Chemical and morphological changes of Li–O_2 battery electrodes upon cycling. *J. Phys. Chem. C* **116**, 20800-20805 (2012).

133 Kundu, D., Black, R., Berg, E. J. & Nazar, L. F. A highly active nanostructured metallic oxide cathode for aprotic Li–O_2 batteries. *Energy Environ. Sci.* **8**, 1292-1298 (2015).

134 Qiu, F. *et al.* Ordered mesoporous TiC-C composites as cathode materials for Li-O_2 batteries. *Chem. Commun.* **52**, 2713-2716 (2016).

135 Jian, Z. *et al.* Core–Shell-Structured CNT@RuO_2 composite as a high-performance cathode catalyst for rechargeable Li–O_2 batteries. *Angew. Chem. Int. Ed.* **53**, 442-446 (2014).

136 Wu, F. *et al.* Facile synthesis of boron-doped rGO as cathode material for high energy Li-O_2 batteries. *ACS Appl. Mater. Interfaces* **8**, 23635-23645 (2016).

137 Xue, H. *et al.* Hierarchical porous nickel cobaltate nanoneedle arrays as flexible carbon-protected cathodes for high-performance lithium-oxygen batteries. *ACS Appl. Mater. Interfaces* **8**, 8427-8435 (2016).

138 Li, G. *et al.* Pomegranate-inspired design of highly active and durable bifunctional electrocatalysts for rechargeable metal-air batteries. *Angew. Chem. Int. Ed.* **55**, 1-7 (2016).

139 Assary, R. S. *et al.* The effect of oxygen crossover on the anode of a Li–O_2 battery using an ether-based solvent: insights from experimental and computational studies. *ChemSusChem* **6**, 51-55 (2013).

140 Guo, Z., Li, C., Liu, J., Wang, Y. & Xia, Y. A long-life lithium-air battery in ambient air with a polymer electrolyte containing a redox mediator. *Angew. Chem. Int. Ed.* **56**, 7505-7509 (2017).

141 Truong, T. T. *et al.* Single-crystal silicon membranes with high lithium conductivity and application in lithium-air batteries. *Adv. Mater.* **23**, 4947-4952 (2011).

142 Hassoun, J. *et al.* A metal-free, lithium-ion oxygen battery: a step forward to safety in lithium-air batteries. *Nano Lett.* **12**, 5775-5779 (2012).

Chapter 2. Experimental Section

2.1 Construction of Electrodes and Cell Assembly

2.1.1 Preparation of electrodes and electrolytes

2.1.1.1 Cathodes preparation

For carbon paper electrodes, binder-free gas diffusion layers (GDL, H2315, Quintech) served as the O_2 electrode in the Swagelok cells. The porosity of the GDL is ~ 80 %. The roughness factor (total surface area: areal area) is 90 and the Brunauer-Emmett-Teller surface area is below 1 m^2 g^{-1}. GDLs were heated under an Ar: H_2 (95: 5 v/v) atmosphere at 900 °C for three hours before transferring into an Ar-filled glovebox prior to use.

For carbon/PTFE composite electrodes, carbon powder, either super P carbon black (Csp, Timcal) or ^{13}C-carbon (Aldrich), and polytetrafluoroethylene (PTFE) with weight ratio of 9: 1 were mixed with isopropanol, stirred for 10 mins, and then sprayed onto a stainless steel (SS) mesh (100 mesh, Advent-RM). The mesh was then punched into half-inch diameter disks for use. Each electrode contained 2~3 mg of carbon material. To remove the surfactants, the electrodes were washed with ethanol and water 3 times, and dried under vacuum at 120 °C overnight before transferring into the glovebox.

2.1.1.2 Anodes preparation

In a practical cell, Li metal (Aldrich) serves as the anode. However, lithium is incompatible with some electrolytes like amides. Furthermore, when soluble additives are present in the electrolyte, a solid electrolyte membrane is required to protect the lithium to avoid reactions of any catalysts that diffuses to the anode. For example, a piece of lithium super ionic

conductor (LISICON, Ohara, 0.8 mm thickness) disk was used in this project to separate the anode from the cathode. For fundamental researches on cathodes, $LiFePO_4$ (LFP) electrodes are sometimes used to replace the reactive lithium metal as the anode to avoid unwanted side reactions.

The preparation procedure was similar to that of carbon/PTFE composite electrodes, where LFP, Super P and PTFE with weight ratio of 8:1:1 were mixed with isopropanol, compressed to a thin film and cut into half-inch diameter disks to use. To ensure a stable and constant potential as a reference electrode (RE), LFP composite electrodes were chemically pre-oxidised 20 % of total capacity to Li_xFePO_4 ($x< 1$) in a solvent containing 1.5 ml of acetic acid (Aldrich), 3.6 ml of 30 % H_2O_2 (Aldrich), and 250 ml of H_2O to reach the flat plateau at 3.45 V vs. Li^+/Li. To ensure sufficient capacity during cycling and minimize the polarization on the anode, the total capacity of LFP electrode was 5 times greater than that of the cathode. The LFP electrode was washed with ethanol and water 3 times, dried under vacuum at 120 °C overnight, and then transferred into the glovebox.

2.1.1.3 Electrolyte solutions preparation

All electrolyte solvents were dried over 4 Å molecular sieves (Aldrich) for several days before distillation. Solvents, including tetraethylene glycol dimethyl ether (TEGDME, Aldrich), diethylene glycol dimethyl ether (DEGDME, Aldrich) and dimethyl sulfoxide (DMSO, Aldrich) were distilled over CaH_2 (Aldrich) under vacuum. Some volatile solvents, *e.g.* 1,2-dimethoxyethane (DME, Aldrich), acetonitrile (MeCN, Aldrich) and tetrahydrofuran (THF, Aldrich) were distilled under Ar (BOC)[1]. All solvents were further dried for several days over freshly activated 4 Å molecular sieves before use. The final water content was < 4 ppm (determined by Karl Fischer titration).

All electrolyte salts including tetrabutylammonium bis(trifluoromethane)sulfonimide (TBATFSI, 99.0 %, Aldrich), lithium bis(trifluoromethane)sulfonimide (LiTFSI, 99.95 %, Aldrich), Tetrabutylammonium perchlorate ($TBAClO_4$, electrochemical analysis grade, Aldrich), and Lithium perchlorate ($LiClO_4$, battery grade, Aldrich) were stored in an Ar-filled glovebox. TBATFSI and LiTFSI were dried at 70 ^oC under vacuum and $TBAClO_4$ and $LiClO_4$ were dried at 140 ^oC under vacuum over several days prior to use. Salts including thymoquinone (Aldrich), 3,5-di-tert-butyl-o-benzoquinone (Aldrich), 2,5-di-tert-butyl-1,4-benzoquinone (DBBQ, Aldrich), 2,2,6,6-Tetramethyl-1-piperidinyloxy (TEMPO, purified by sublimation, 99%, Aldrich) and Phenol (Aldrich) were used as received.

2.1.2 Cell Designs

2.1.2.1 Swagelok-type cells

Lab cells were designed based on Swagelok tube fittings (Swagelok) and normally a cell consists of a body, two nuts (half-inch diameter), two stainless steel pistons as current collectors, a piece of PTFE film (0.125 mm thickness) and two sets of Nylon ferrules insulating the body and pistons. A Swagelok cell was constructed from bottom to top by the following sequence: an anode SS piston, anode (LFP), two pieces of glass fibre separators (Whatman) wetted with electrolyte (0.1 ~ 0.2 ml), cathode and cathode SS piston, with the schematic shown in Fig. 2-1. All cell components were dried at 90 °C under vacuum prior to use. For cells with Li metal as the anode, LISICON was used to avoid unwanted side reactions. The assembled cells were filled with O_2 (N6 grade, BOC) and tested in the glovebox. O_2 gas was dried by a moisture trap filled with activated 3 Å molecular sieves.

For pressure cells, the cell assembly was the same as described above. A pressure sensor (Omega Engineering Ltd.) was connected to the headspace of the cell to monitor the change

of pressure during cell cycling. The headspace of the cell was 4.95 (± 0.03) ml. The cell was assembled inside the glovebox and filled with dried O_2 before cycling. The cell was cycled in an temperature-controlled oil bath (Julabo) at 20 ^oC to avoid pressure change caused by temperature fluctuation[2].

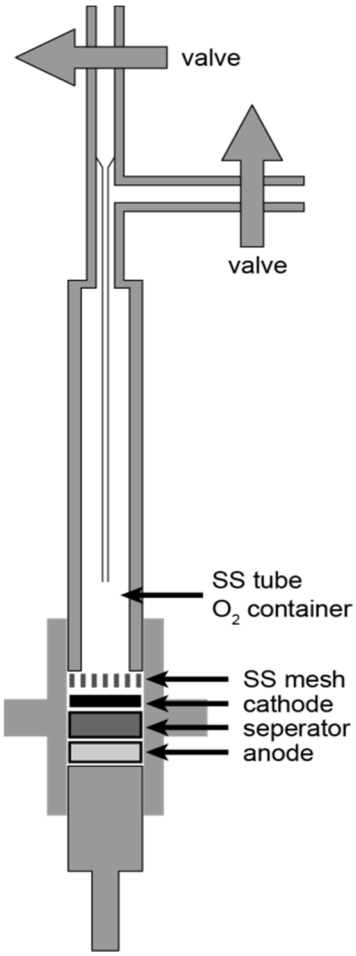


Figure 2-1. Schematic of a Swagelok-type Li-O_2 cell. An assembled cell with components of a Swagelok-type cell from bottom to top by: an anode SS piston, anode, glass fibre separators wetted with electrolyte, cathode and a cathode SS piston.

2.1.2.2 Three-electrode cells for electrochemical measurements

Electrochemical measurements were performed in a five-neck, airtight glass cell with valves to control the gas inlet and outlet, Fig. 2-2. Polycrystalline gold disks (Au, 3 mm diameter, BAS Inc.) and glassy carbon disks (GC, 3 mm diameter, BAS Inc.) were used as the working

electrodes (WEs). WEs were polished with 0.05 μm alumina slurry, rinsed with deionised water and then dried under vacuum before use. A platinum wire separated by a sintered glass frit from the bulk electrolyte served as the counter electrode (CE). A commercial non-aqueous silver electrode (BAS Inc.) was used as the reference electrode (RE), where a silver wire was immersed in 10 mM silver nitrate ($AgNO_3$) in MeCN and 1 M $TBAClO_4$ as the supporting electrolyte and a Vycor porous glass frit separated them from the bulk electrolyte solution. The RE was calibrated using ferrocenium/ferrocene (FC^+/FC) redox couple. Another homemade RE was based on $LiFePO_4$, which was pre-oxidised to Li_xFePO_4 as mentioned before. This was then placed in 0.1 M $LiClO_4$ in DMSO separated from the bulk electrolyte with a porous frit, providing a fixed potential.

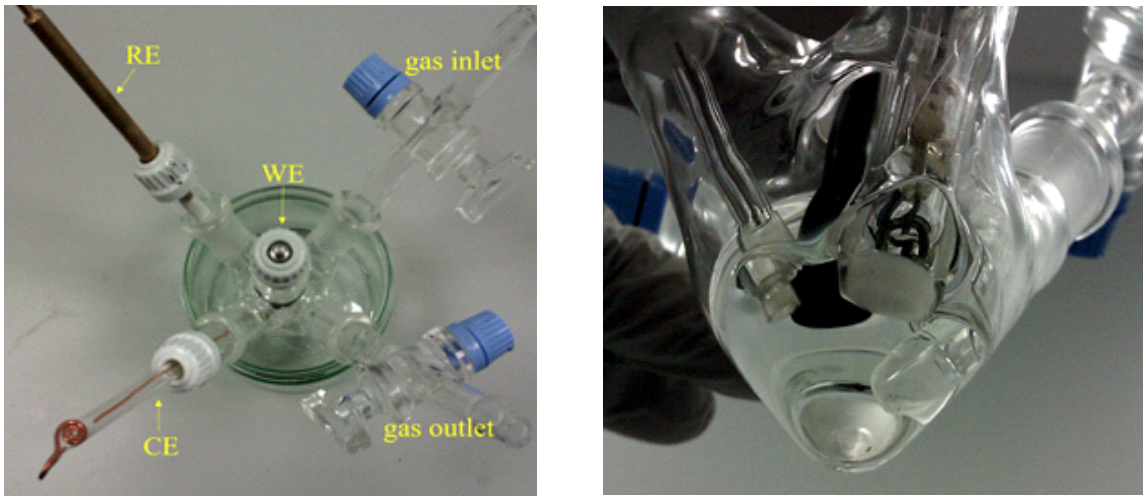


Figure 2-2. Design of a three-electrode flask cell. A constructed five-neck cell with WE, CE, RE, gas inlet and outlet.

2.1.2.3 *In situ* differential electrochemical mass spectrometry cells

In situ DEMS cells were designed previously by a group member for an electrode with bigger geometric surface area, around 4 cm diameter to ensure enough gas consumption and evolution for detection. The schematic is shown in Fig. 2-3. The construction from bottom up was similar to that in Swagelok cells: a stainless steel sheet as the current collector, LFP

electrodes as the anode, Ag wire or a piece of precharged LFP as the reference, glass fibre separators soaked in electrolyte saturated with O_2, various types of carbon electrodes as the positive electrode, a stainless steel mesh as the current collector and a spring on the top to ensure the tightness. The gas inlet and outlet are on the cathode side. After assembling the cell in an Ar-filled glovebox, it was connected to a mass spectrometer (Thermofisher) to analyse the gases consumed and evolved and at the same time carry out the electrochemistry performance.

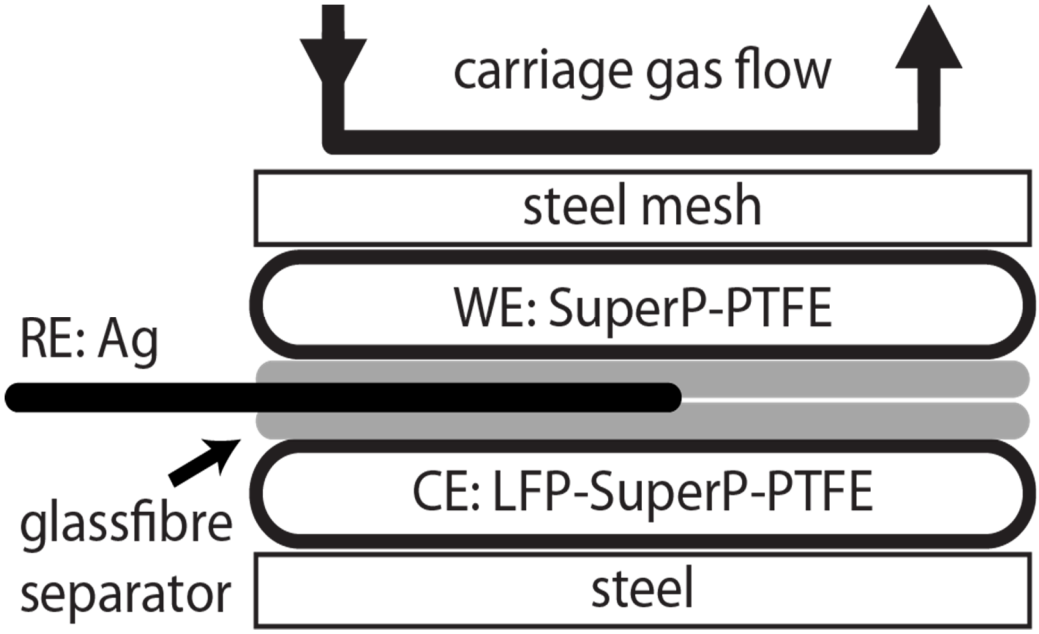


Figure 2-3. Schematic of an *in situ* DEMS cell. Example of an *in situ* DEMS cell with Super P as the WE, LFP as the CE, and Ag as the RE.

2.2 Characterisation techniques

2.2.1 Cyclic voltammetry (CV)

Cyclic voltammetry is a widely used technique for acquiring qualitative information about electrochemical reactions. It provides information such as the standard potential of a redox couple, chemical reversibility of a redox reaction, electron transfer kinetics and so on[3].

A typical voltammogram for oxygen reduction in an aprotic solvent is shown in Fig. 2-4. The measurements were carried out on a VMP 3 potentiostat (Biologic Science Instrument). Here, 0.5 M TBATFSI in O_2-saturated TEGDME served as the electrolyte, Au planar electrode as WE, Pt wire as CE and Ag as RE. The potential (*E*) is swept linearly at a scan rate of 100 mV s^{-1} from 2.5 V to 2.1 V (*vs.* Li^+/Li), where O_2 is reduced to O_2^-. The potential is then swept back at the same scan rate from 2.1 V to 3.7 V (*vs.* Li^+/Li), where O_2^- is oxidised back to O_2. During the potential swept process, the current (*i*) is recorded. In order to compare the planar electrodes with different surface areas, current density (*j*) is plotted versus *E* in Fig. 2-4.

From a CV curve, one is easily able to gather such information as knowing the reversibility of the redox couple by comparing the reduction and oxidation peak current and knowing the diffusion coefficient by comparing the peak current with different scan rates.

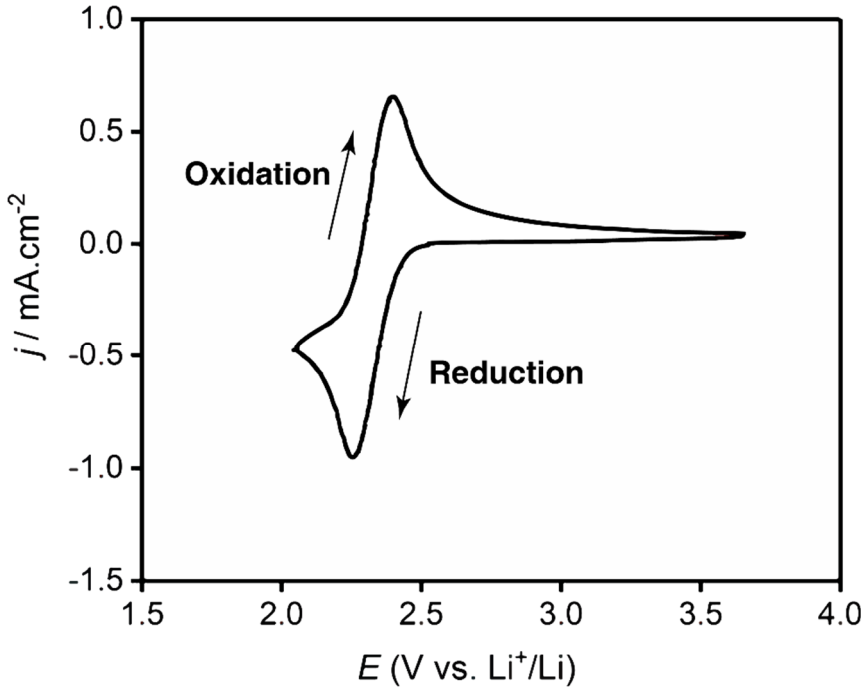


Figure 2-4. A typical CV curve for oxygen reduction and oxidation in aprotic solvents. A CV curve recorded in 0.5 M TBATFSI in O_2 saturated TEGDME at Au electrode at a scan rate of 100 mV s^{-1}.

Sometimes, CV measurements were also applied in Swagelok-type cells with porous electrodes for electrochemistry studies in the cell. As the air electrode structure is different from planar Au electrode used in the flask cell measurements, slow scan rate CV measurements should be employed, where the scan rate is reduced to 0.5 mV s^{-1}.

2.2.2 Galvanostatic cycling with potential limitation (GCPL)

GCPL is the main technique for testing cell performances, and therefore is heavily used in Li-ion and Li-O_2 battery characterisations. In this project, GCPL experiments were carried out on VMP 3 (Biologic), Maccor Battery Test System (Maccor) and Autolab Potentiostat & Galvonostat. A typical load curve for an aprotic Li-O_2 cell is shown in Fig. 2-5 with the potential cut-off. A cell was discharged and charged at a constant current, *e.g.* 0.1 mA cm^{-2}, and the potential was recorded as a function of time (t). The capacity was plotted against the potential demonstrating several important parameters of this Li-O_2 cell.

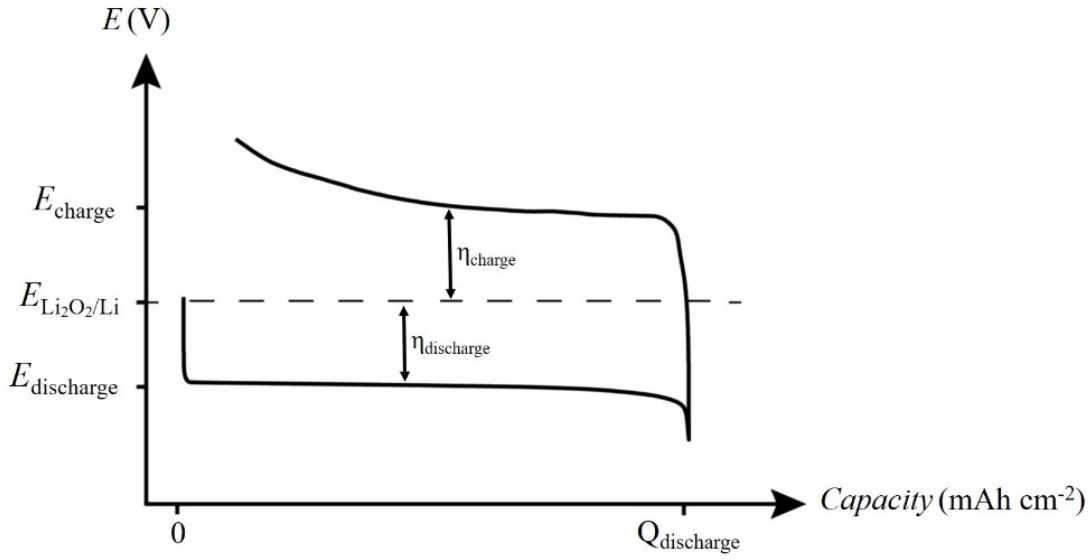


Figure 2-5. Typical load curve of an aprotic Li-O_2 cell with potential cut-off method applied.

The total amount of the charge passed per unit area (A) of electrode is given by: Q = it / A, where A represents the geometric area of the electrode. The flat plateau seen in Fig. 2-5 on

most of the discharge and charge process are assigned as the discharge potential ($E_{discharge}$) and the charge potential (E_{charge}), respectively. The potential difference between the discharge/charge potential and the standard potential, 2.96 V (vs. Li^+/Li), for Li_2O_2/Li is termed as the overpotential, shown as $\eta_{discharge}$ and η_{charge} in Fig. 2-5. In a typical Li-O_2 cell, the discharge potential is ~ 2.6 V with a sudden death at the end of discharge, and the charge potential is above 4 V with some capacity loss.

During the measurements, one way to stop the cell is to limit the potential, as seen in Fig. 2-5, where the cell is discharged to the low cut-off potential and charged to the high cut-off potential. The other method widely used in aprotic Li-O_2 cells is capacity-limited cycling measurement: once the discharge process reaches a set and certain capacity, it will automatically enter the charge process to continue the cycling. Capacity-limited method can avoid surface passivation, ensure mass transport and therefore achieve better performance.

The GCPL experiments can be stopped at any point during the cycling, *e.g.* at a certain potential or at a certain capacity. The cells are then dissembled and the cathodes are rinsed with solvents several times, dried under vacuum prior to further analysis.

2.2.3 Powder X-ray diffraction (PXRD)

PXRD is one of the most widely used techniques for structural characterisation of powders. The technique is mainly used for phase identification, lattice parameter calculation, particle size analysis and so on.

In crystallography studies, X-rays with wavelengths ranging from 0.05 nm to 0.25 nm are generated by synchronic radiation or bombarding a metal target, *e.g.* Cu or Fe with electrons. When X-rays go through a substance, as they are in the same order of magnitude as the

interatomic distances in the material, diffraction occurs with photons scattered by planes of atoms with a repeating structure within the crystal, shown in Fig. 2-6.

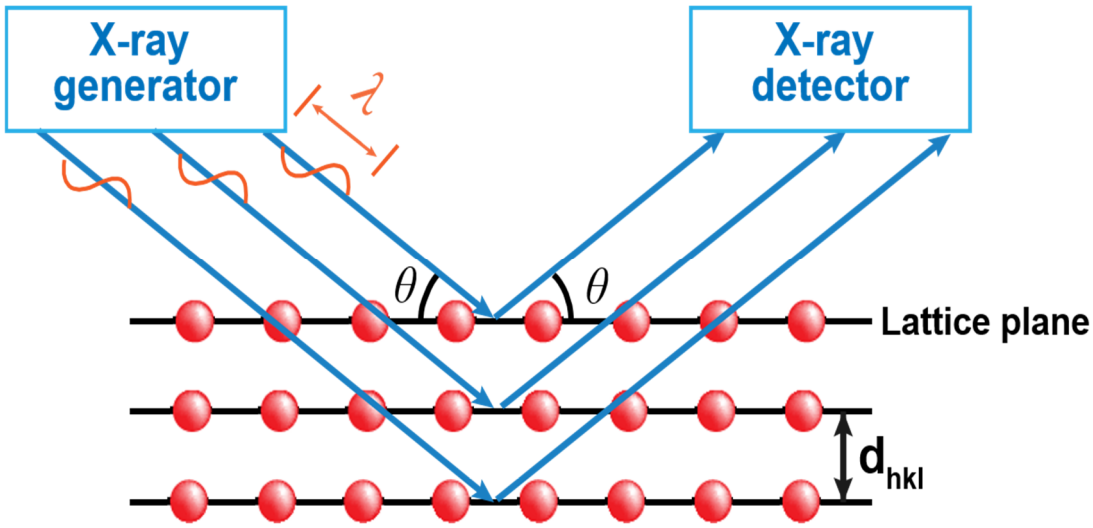


Figure 2-6. A schematic of X-ray diffraction by the molecules. Constructive interference occurs to follow the Bragg's law.

The relationship between the spacing (d) between two planes (hkl) and the diffraction angle (2 θ) is given by the Bragg's law[4], shown in equ. 2.1:

$$2\,d\sin\theta = n\,\lambda \qquad (2.1)$$

where n represents the order of the diffracted beam and λ is the wavelength of the X-ray beam. The order n has to be an integral for the X-ray beams being in phase to have the constructive interference. Otherwise, the X-ray waves are out of phase and the interference is destructive.

In different crystals, all sets of planes diffract with different patterns, resulting in a series of concentric cones, and therefore PXRD is useful to distinguish crystalline substances in a mixture. In this project, PXRD was used to identify the discharge products in Li-O_2 batteries, such as the desirable product, lithium peroxide (Li_2O_2) and possible by-products like lithium

hydroxide (LiOH) and lithium carbonate (Li_2CO_3). Li_2O_2 is a hexagonal structure with its crystal phase shown in Fig. 2-7.

In this work, the dried electrodes were placed on a low-background silicon holder and sealed in a special airtight holder, which was covered with a piece of Kapton® polyimide film to protect the sample from air contamination. The PXRD was carried out in a Rigaku X-ray diffraction with Cu ($K_{\alpha 1}$) radiation (λ = 1.5406 Å)[5].

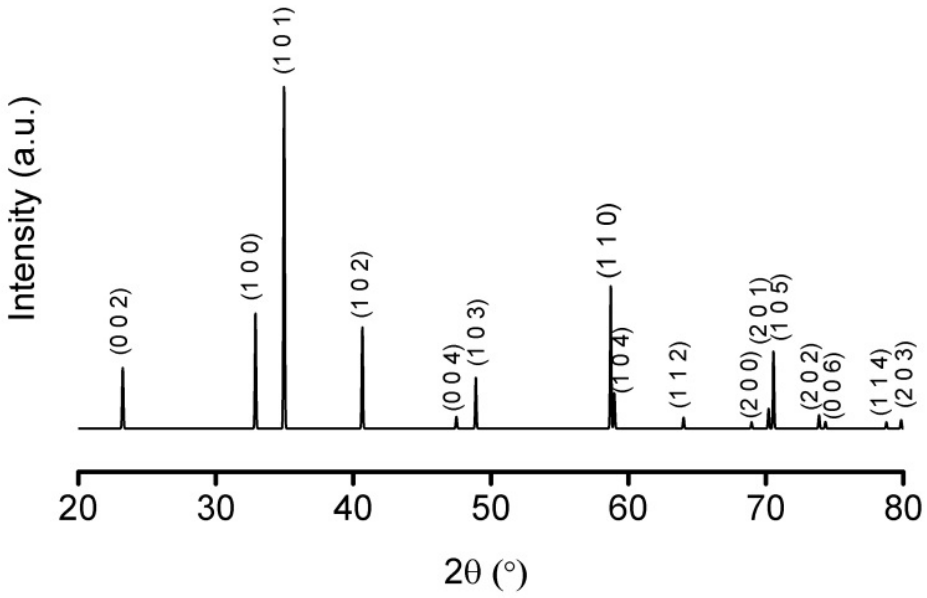


Figure 2-7. PXRD pattern of lithium peroxide in a certain diffraction angle range. (hkl) represents the different planes in a Li_2O_2 lattice.

2.2.4 Fourier transform infrared spectroscopy (FTIR spectroscopy)

FTIR spectroscopy is widely used in organic synthesis, polymer science and pharmaceutical industry. Using FTIR technique, one can easily identify the presence of certain functional groups in a molecule and detect the existence of impurities. The side products like Li_2CO_3 and organic carbonate species have poor crystallinity, and therefore it is difficult to detect

such species by PXRD. FTIR is thus applied in this project to analyse the discharge products to compensate[6].

When a discrete infrared light passes through a molecule, if the vibration or rotation frequency of the molecular is in the range of this discrete infrared light, the molecule will absorb certain radiation and jump to a higher vibrational or rotational energy state. The absorption is recorded and the interferogram is first collected as the infrared spectrum. The Fourier transform function is then used to deconvolute frequency information and translate it into a spectrum.

The infrared portion of an electromagnetic spectrum is divided into: the near-, mid- and far-infrared, which has the frequency of 14000-4000 cm^{-1} (wavelength of 0.7-2.5 μm), 4000-400 cm^{-1} (wavelength of 2.5-25 μm), and 400-10 cm^{-1} (wavelength of 25-1000 μm), respectively. The mid-infrared region is normally used to study the fundamental vibrations and the rotation-vibrational structure analysis. In order to be IR active, firstly the energy state barriers should match the infrared light energy range, and secondly the molecular should have conjugation with the infrared light and the permanent dipole in the molecular should change. If the change in permanent dipole is small, one will get poor IR signals, but such molecular is likely to have strong Raman signals, which is used as a complementary analysis to FTIR spectroscopy.

FTIR was, in this project, carried out on Nicolet 6700 spectrometer (Thermo Fisher Scientific) in a N_2-filled glovebox. The standard FTIR reference spectra of Li_2O_2 and some possible side products in aprotic Li-O_2 cells like Li_2CO_3, CH_3CO_2Li and LiOH are shown in Figure 2-8. The IR adsorption of Li_2O_2 is below 600 cm^{-1}, and therefore CsI is used as the window material. A small piece of the electrode was ground with CsI and compressed

into a transparent pellet. The data was collected in transmission mode at the range of 225-4000 cm^{-1}.

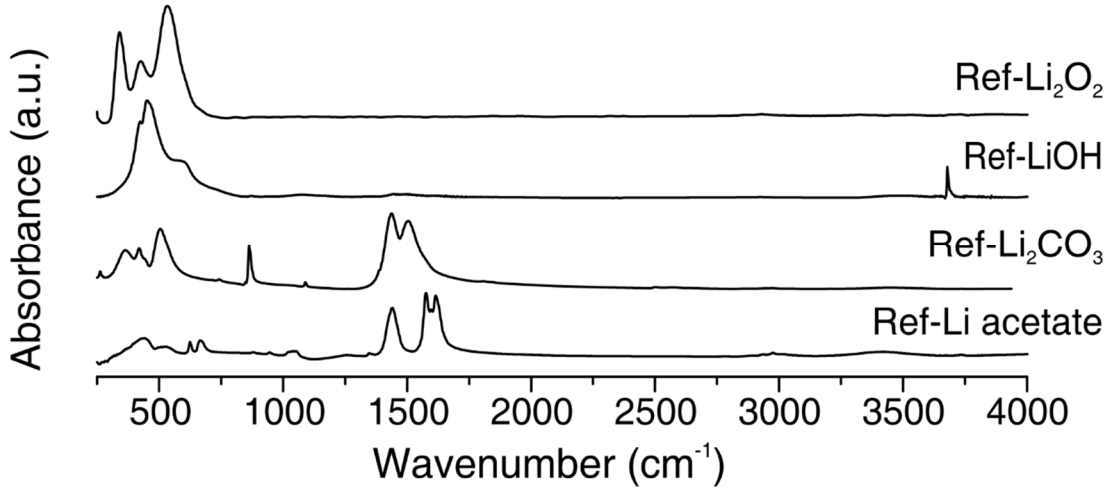


Figure 2-8. FTIR spectra of Li_2O_2, Li_2CO_3 CH_3CO_2Li and LiOH samples.

2.2.5 Raman Spectroscopy

Raman spectroscopy is a vibrational spectroscopy technique always used to observe the vibrational, rotational and other low-frequency modes in a substance to obtain the unique fingerprint of the substance. It is a complementary analysis to FTIR spectroscopy and the combination of these two techniques can provide a comprehensive understanding of the molecular structure.

When a monochromatic light, in this work, a laser in the visible range (red or green light) with a frequency of ν_0 interacts with a substance, a small fraction of the scattered light has a frequency (ν) differing from the original laser is observed and recorded. This is because the photons interact with molecular vibrations and excite the atoms in either the ground state or a lower excited state to the laser energy level depending on the laser used. The excited atoms will instantaneously relax back to a more stable energy level and emit the scattered light with a different frequency. Three scattering process can occur due to different starting

and ending energy state, including stokes, anti-stokes and rayleigh scattering. A schematic of Raman scattering demonstrating the differences of stokes, anti-stocks, rayleigh scattering and infrared absorption is shown in Fig. 2-9, where anti-Stokes scattering has a higher frequency than the initial light while Stokes scattering shows a lower frequency and the frequency of Rayleigh scattering remains the same.

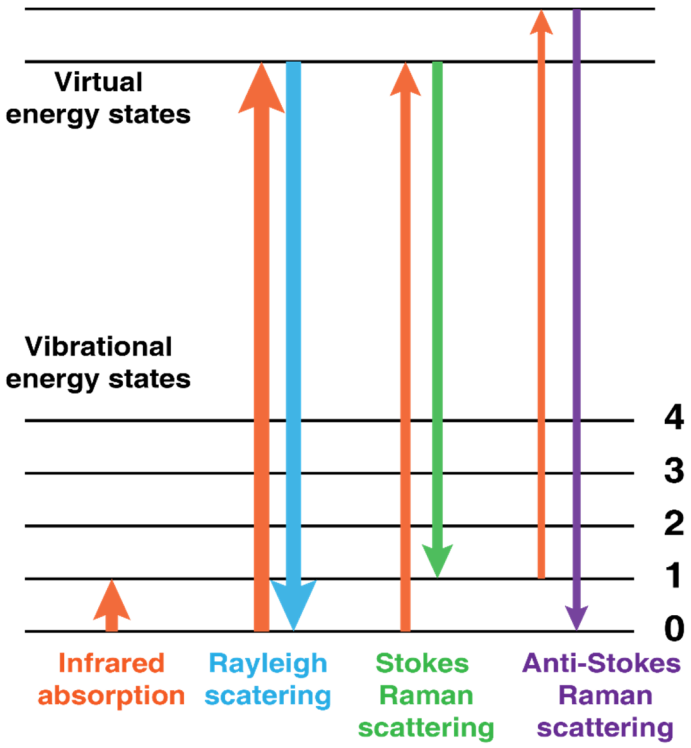


Figure 2-9. An energy-level diagram showing the different Raman scattering processes and infrared absorption.

Surface enhanced Raman spectroscopy (SERS) is an advanced Raman spectroscopy technique with higher sensitivity that enhances the scattering by molecules absorbed on rough metal surfaces or by nanostructures like plasmonic-magnetic silica nanotubes. *In situ* SERS experiments can detect the intermediates on the electrode surface and therefore are applied in mechanism studies in Li-O_2 cells. The working planar electrode, *e.g.* Au and Ag with unique plasmonic properties is roughened to enhance the signal in the electric field, leading to an enhanced Raman intensity.

In this project, Raman spectroscopy is used to identify and distinguish Li_2O_2 and other by-products in Li-O_2 batteries. The experiments were carried out in a Renishaw Raman system with a laser wavelength of 633 nm or 785 nm.

2.2.6 Nuclear Magnetic Resonance Spectroscopy (NMR Spectroscopy)

FTIR and Raman spectroscopy provide clear evidence of solid by-products, and NMR spectroscopy is applied to investigate the by-products in the electrolyte solutions in Li-O_2 batteries. NMR spectroscopy studies the magnetic properties of atomic nuclei based on nuclear magnetic resonance, which is related to the nuclear spin (I) of the nucleus of an atom. In atoms like ^{12}C and ^{16}O where the number of neutrons and protons are both even, the spins are paired against each other with the overall spin as 0. In some nuclei like ^{2}H and ^{6}Li where the number of neutrons and protons are both odd, the nucleus has an integer spin (*e.g.* 1, 2). While in some nuclei like ^{1}H and ^{13}C where the number of neutrons plus protons is odd, the nucleus has a half-integer spin (*e.g.* 1/2, 3/2). Such nuclei with spin 1/2 have an intrinsic magnetic moment and angular momentum, which, according to quantum mechanics, have two possible orientations with equal energy, as shown in Fig. 2-10. When external magnetic field is applied, the spin will split into two different energy levels, shown as - 1/2 (higher energy level) and + 1/2 (lower energy lever), and the nuclei will absorb energy and excite themselves into higher energy level, re-emitting electromagnetic radiation. The energy difference between the two energy levels, corresponding to the resonance frequency recorded, depends on the strength of magnetic field applied and the magnetic moment of the atoms. Electrons are charged and rotate to produce magnetic field opposite to the original magnetic field, which reduces the energy gap and therefore reduce the resonance frequencies. For the same nuclei with different chemical environment, the surrounding nuclei have different interactions and therefore the shielding effect from the

local magnetic field is different, resulting in different resonance frequencies. In practical use, chemical shift (δ/ppm) is used to characterise the resonant frequency change of a nucleus relative to a standard sample in the magnetic field, which is defined as $(\nu_{sample} - \nu_{standard})/\nu_{standard}$ $x10^6$.

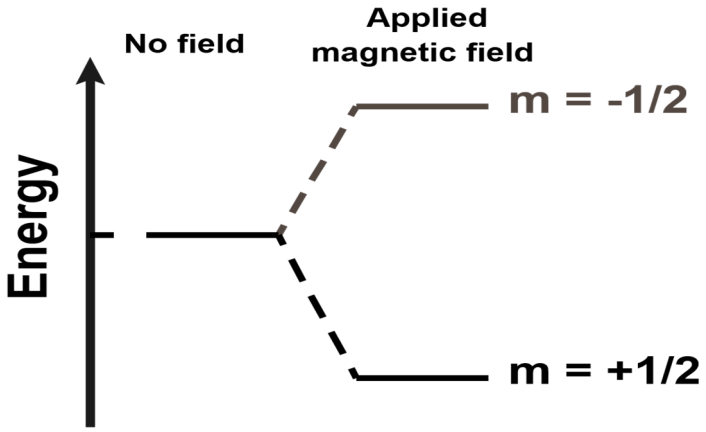


Figure 2-10. Energy levels for a nucleus with spin quantum number 1/2. In the applied magnetic field, the spin will split into two different energy levels.

In this project, solution phase ^1H NMR experiments are applied to measure the by-products in the electrolyte solutions. Tetramethylsilane (TMS) was used as the standard sample, and Chloroform-d ($CDCl_3$) and Deterium oxide (D_2O) were used as the solution. The discharged electrodes and separators, containing 100 µl of electrolyte solution, were rinsed with 0.7 ml $CDCl_3$ and the electrode was soaked in 0.5 g of D_2O, filtered into NMR tubes to be examined on a Bruker spectrometer (400 MHz).

2.2.7 Ultraviolet-Visible Spectroscopy (UV-Vis Spectroscopy)

UV-Vis spectroscopy refers to absorption or reflectance spectroscopy in ultraviolet and visible light region. The principle is similar to FTIR. When a range of ultraviolet and visible light interacts with a molecule, the π-electrons or non-bonding electrons can absorb the energy and are excited to higher anti-bonding molecular orbitals. The spectrometer records

the absorbed energy and the degree of the transmission, which then translates into absorbance (A) versus wavelength (λ) in the spectrum. According to Beer-Lambert law, the absorbance of a solution is proportional to the concentration of the absorbing species in the solution, shown in equ. 2.2:

$$A = \log_{10} (I_0/I) = a * b * c \qquad (2.2)$$

Where A is the absorbance; I_0 is the initial light intensity; I is the detected light intensity after passing through the solution; a is the absorptivity coefficient which is wavelength dependent; b is the path length and c is the concentration of the absorbing species. It should be noted that the linearity of the Beer-Lambert law is deviated at high concentrations because of the electrostatic interactions between molecules in close proximity.

In this work, UV-vis technique was used as a titration method to quantify the amount of Li_2O_2 in the discharge cathode by UV-vis spectrometry (Thermo Evolution 200). First, the purity of commercial Li_2O_2 was determined by titration using $KMnO_4$, and the purity of Li_2O_2 was 93 %. Known amounts (*e.g.* 0.5 mg, 1 mg, 2 mg, *etc.*) of such Li_2O_2 (Aldrich) were added to a known volume of deionized water to form different concentrations of H_2O_2 in solution. 1 ml of this solution was added to 2 ml of 2 % $TiOSO_4$ dissolved in 1 M H_2SO_4 solution and a yellowish complex $[Ti(O_2)]^{2+}$ (λ_{max}= 405 nm) was formed. The absorbance of different solutions was measured and a calibration curve was obtained by plotting the absorbance against the concentration of H_2O_2, which was related to the amount of Li_2O_2. Note that the purity was considered when constructing the calibration curve[5,7].

For analysing the discharge and charge electrodes, the unwashed electrode and separators were added into a known volume of deionized water. Such solution was added to a certain volume of 2 % $TiOSO_4$ dissolved in 1 M H_2SO_4 solution to test the absorbance. In order to fit the Beer-Lambert law, the concentration of $[Ti(O_2)]^{2+}$ was controlled to ensure

absorbance less than 1. After measuring the absorbance, the concentration of peroxide was obtained from the calibration curve and it related to the total amount of Li_2O_2 in the electrode.

The yield is termed by comparing the total Li_2O_2 amount with the total discharge capacity. If there were no side reactions, all the charge passed through the cell during discharge would transform into Li_2O_2 and I would get a 100 % yield. However, in practical cells, due to side reactions involving the intermediates, singlet oxygen and desired discharge product Li_2O_2, the yield is always lower than 100 % and it is an important parameter to evaluate the true performance of an aprotic Li-O_2 cell.

2.2.8 Scanning Electron Microscopy (SEM)

In a Li-O_2 battery system, Li_2O_2 is the desired discharge product. SEM was applied in this project to investigate the morphology of Li_2O_2 in different electrolyte systems and study its structure formation and decomposition during cycling.

SEM is an electron microscopy technique that takes images by scanning the sample with a focused electron beam. Electrons are produced on the top of the column, normally emitted from either thermal emission or field emission gun (FEG). In the FEG system, it applies several-kilovolt potential on the metal emitter surface to induce the field electron emissions, which has over 100 times more brightness, better electron coherence and much longer lifetime comparing to electrons emitted by thermal emission guns. The field-emitted electron beam is focused through magnetic field and then directly strikes and interacts with the sample. The electrons lose energy by random scattering and absorption, while nucleus and electrons of the sample obtain energy from the electron beam. The energy exchange results in the reflection of high-energy electrons by elastic scattering and emission of secondary electrons by inelastic scattering and emission of electromagnetic radiation, which are collected by different detectors to produce images for various demands. In this project,

after washing and drying the cathodes, the samples were transferred into FE-SEM (Zeiss-Merlin) by an air-sensitive holder to avoid exposure to air.

2.2.9 Differential Electrochemical Mass Spectrometry (DEMS)

DEMS combines electrochemical measurements with mass spectrometry, which can test the gas consumption and evolution and detect the gaseous products. It helps to study the intermediate reactions during the electrochemistry performance measurements.

In situ DEMS was used in this project to analyse the gas consumption and evolution during cell discharge and charge. The system contains three parts: an electrochemical cell (*in situ*) or an analysis vial (*ex situ*); a quadrupole mass spectrometer (Prolab, Thermofischer) and carrier gas flow which is pure Ar or Ar/O_2 mixture depending on the needs of different experiments, Fig. 2-11. The setup was first calibrated for gases including Ar, O_2, CO_2, H_2 and N_2 by calibration gases. Different known amounts of calibration gases were applied considering the nonlinearity and cross-sensitivity of gas mixtures.

During the experiments, the carrier gas controlled by a flow meter with a flow rate of 0.2-2 ml min^{-1} went into a DEMS cell and carried the gas phase out of the cell through fused silica capillary tubing into a mass spectrometer. The gas sample was then ionised by electrons in the ion source chamber and separated by different ratio of mass/charge (m/z), quantified by Faraday detectors, which was recorded together with the mass/charge. The DEMS experiments are normally designed merely for non-volatile solvents. Volatile solvents like MeCN and DME are easily carried away by the carrier gas and the cell dies due to the depletion of electrolyte solutions. Besides, the solvents like glycol ethers always have fragments at 28 or 45, the same mass ratio as CO and CO_2, making it difficult to know the right amount of such gases.

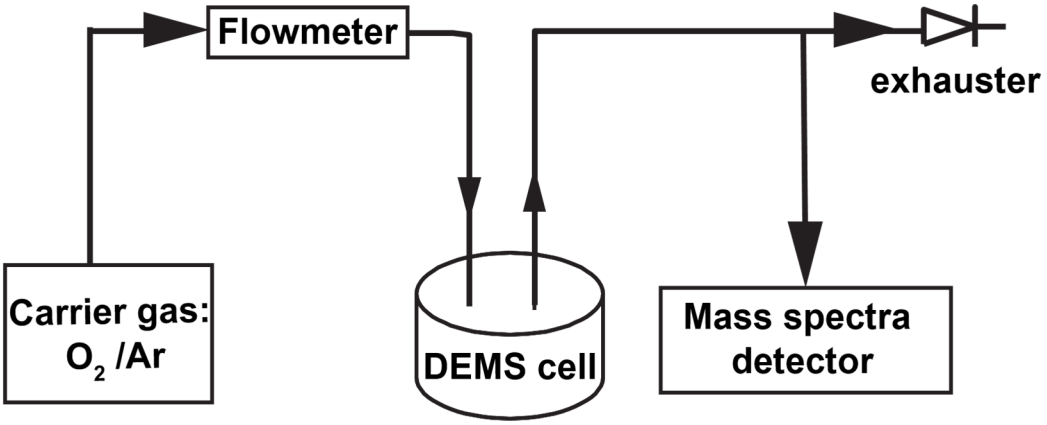


Figure 2-11. A schematic of an *in situ* DEMS system setup. A carrier gas flow with a certain flow rate passed through the DEMS cell and brought the gas phase into the mass spectrometer for analysis.

Ex situ mass spectrometer measurements were also applied in this work to quantify by-products like some carbonates in the electrode. After discharge/charge, the washed and dried electrodes were cut into pieces and transferred into a small glass vial. The vial was connected to the DEMS system with 100 % Ar as the carrier gas. 0.3 ml of 2 M H_3PO_4 was injected into the glass vial to fully decompose the lithium carbonate in the sample. At the very acidic pH-value, CO_3^{2-} is fully converted to CO_2, carried by the Ar gas into the mass spectrometry. After the complete evolution of CO_2, 0.3 ml of 2 M H_3PO_4 containing 0.5 M $FeSO_4$ and 20 µl of 30 % H_2O_2 was added into the vial to decompose the organic carbonates. Fe^{2+} reacts with H_2O_2 to form the very reactive OH• , shown in equ. 2.3:

$$Fe^{2+} + H_2O_2 \rightarrow Fe^{3+} + OH\bullet + OH^- \qquad (2.3)$$

The reactive OH• generated by the process is a powerful and non-selective oxidant, which can oxidise organic compounds rapidly to primarily CO_2 and H_2O. CO_2 was purged by Ar carrier gas to mass spectrometry to quantify the amount of lithium carboxylates.

2.3 References

1 Chai, C. & Armarego, W. L. F. *Purification of laboratory chemicals*. 6th edn, (Butterworth-Heinemann, 2009).

2 Lepoivre, F., Grimaud, A., Larcher, D. & Tarascon, J.-M. Long-time and reliable gas monitoring in Li-O_2 batteries via a Swagelok derived electrochemical cell. *J. Electrochem. Soc.* **163**, A923-A929,(2016).

3 Bard, A. J. & Faulkner, L. R. *Electrochemical methods: fundamentals and applications*. 2nd edn, (John Wiley, 2001).

4 Smart, L. & Moore, E. *Solid State Chemistry: An Introduction*. 3rd edn, (Taylor & Francis, 2005).

5 Gao, X., Chen, Y., Johnson, L. & Bruce, P. G. Promoting solution phase discharge in Li-O_2 batteries containing weakly solvating electrolyte solutions. *Nat. Mater.* **15**, 882–888,(2016).

6 Freunberger, S. A. *et al.* Reactions in the rechargeable lithium-O_2 battery with alkyl carbonate electrolytes. *J. Am. Chem. Soc.* **133**, 8040-8047,(2011).

7 Gao, X., Jovanov, Z. P., Chen, Y., Johnson, L. R. & Bruce, P. G. Phenol-catalyzed discharge in the aprotic lithium-oxygen battery. *Angew. Chem. Int. Ed.* **56**, 6539-6543,(2017).

Chapter 3. Phenol as a phase transfer catalyst in aprotic Li-O_2 batteries

As discussed in Chapter 1, the discharge product Li_2O_2 is insoluble and insulating and once it forms on the cathode via the surface mechanism, typically in a low donor number solvent, it will lead to low capacities, poor rates and early cell death. While if the reduction of O_2 to form Li_2O_2 is displaced from the electrode surface via solution mechanism, typically in a high DN based electrolyte solution, then achieving high discharge capacities with high rates is desirable. However, high DN solvents are more likely to be unstable against superoxide and peroxide species. Therefore, it is always desirable to have solution mechanism of Li_2O_2 formation in a relatively stable low DN solvent[1-6]. In this project, different types of acids as protic additives are studied and phenol as a weak acid is shown to promote discharge via solution mechanism in a low DN ether-based solvent.

3.1 Background of protic additives

Recently, water, as an additive has been investigated and is of high interest in aprotic Li-O_2 batteries. Gasteiger and co-workers reported the significant effect of H_2O in affecting the morphology of the discharge product, the large discharge capacities and the oxidation pathway of Li_2O_2. Their work demonstrated that Li_2O_2 was the main discharge product in the presence of H_2O rather than LiOH, and interestingly, they showed that increased amount of H_2O (with maximum amount of 1 % water in their studies) led to higher Li_2O_2 yield and less side reactions. H_2O was considered to dissolve and solubilise Li_2O_2, resulting in this significant effect[7,8]. Similar results were demonstrated by Nazar and co-workers on Na-O_2 batteries, where they considered H_2O as an example of phase-transfer catalysts that are responsible for the growth and dissolution of micrometre-sized cubic in Na-O_2 batteries[9].

Luntz *et al.* also found that trace amount of water can enhance the discharge capacities, where they believed that H_2O as a high AN solvent promoted the solvation of O_2^-, triggering the solution pathway of Li_2O_2 particles formation. Different from Gasteiger, they claimed that the addition of water led to more parasitic chemistry[4]. Shao-Horn and co-workers claimed that the presence of water decreases the surface Li_2O_2 nucleation rate during the discharge, resulting in the increased capacity and large Li_2O_2 morphologies. Their result indicated that LiOH could form together with Li_2O_2[10]. Recently, Li *et al.* reported that in their cell system with Ru/MnO_2/Super P as the cathode, the ppm-leveled H_2O was shown to reduce the charge overpotential and the total discharge/charge potential gap was 0.32 V. Excellent cycling stability of 200 cycles was demonstrated with LiOH and Li_2O_2 coexisting in the cathode[11].

In conclusion, the addition of H_2O into the low DN solvents can introduce the growth of large toroid Li_2O_2 particles and enhance the discharge capacities. However, it might bring with by-products like LiOH, which would passivate the electrode surface and lead to the cell death. Here, I propose the addition of organic acids with tunable pKa can have the possibility to reach higher solubility of intermediates and discharge product to catalyse the solution mechanisms in low DN solvents. Moreover, the addition of acids can avoid the formation of LiOH.

3.2 Electrochemistry performance with phenol

Phenol has been studied as the proton source in high DN solvents, which is able to combine the free superoxide to form HO_2 and HO_2^- as the intermediates[12,13]. It provides some hint that phenol is able to solubilize the reduced oxygen species and lead to the solution growth of Li_2O_2. Since high DN solvents are less stable against reactive species than the lower DN

solvents, ethers are therefore chosen as the electrolyte solution. To conclude, phenol is chosen as a weak acid additive with higher acidity than H_2O in TEGDME.

CV studies were first carried out to study the electrochemistry performance. Voltammetry for O_2 reduction in a TBATFSI-based electrolyte in TEGDME is known to have the quasi-reversible shape[26], as shown in Fig. 3-1, Fig. 3-2 (a).

The reaction is explained by many groups as:

$$O_2 + e^- \rightarrow O_2^- \qquad (3.1)$$

When 20 mM phenol was added into the TBATFSI-based electrolyte in TEGDME, the reduction peak current increased and the corresponding oxidation peak current decreased. A mixture of two reduction peaks is shown and the oxidation of O_2^- still appears, indicating the existence of free superoxide species and insufficient protons to fully catalyse the oxygen reduction reactions. When the phenol concentration was increased to 30 mM, the O_2/O_2^- wave became irreversible, indicating no free superoxide species. Therefore, 30 mM phenol was chosen for the following studies.

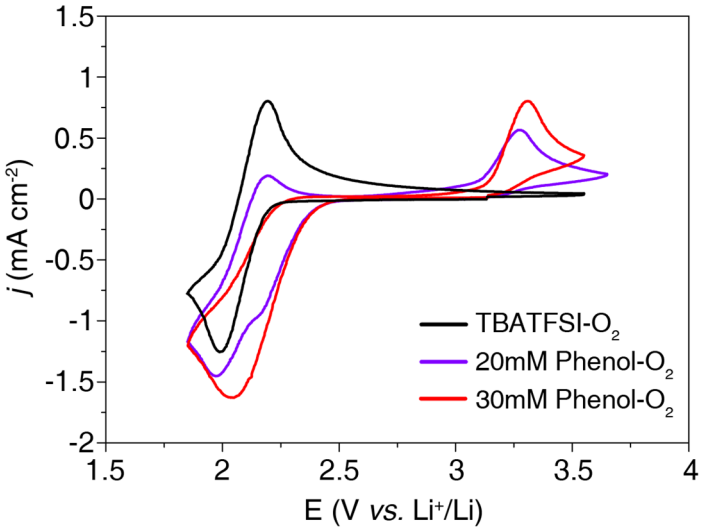


Figure 3-1. CVs for O_2 reduction without phenol (black) and with various amounts of phenol (red, blue) in 0.5 M TBATFSI in TEGDME under O_2. GC electrode. Scan rate 100 mV s^{-1}.

The CVs in Fig. 3-2 (a) are similar to previous studies by Peng *et al.*, where phenol was added into $TBAClO_4$-based electrolyte in DMSO[12]. The loss of O_2/O_2^- wave reversibility and the increase in reduction current were also shown in their work, comparing to that without phenol. Here I observed a positive shift on reduction, indicating the formation of new species rather than O_2^-. The proton prefers the strongest base, and therefore in low DN solvents like TEGDME, the superoxide, rather than the solvent, is more likely to stabilize the proton, which can explain the positive shift on reduction seen in TEGDME and no shift in the previous work in DMSO. It should be noted that no anodic peak at ~ 3.2 V is observed for phenol under Ar, excluding the oxidation of phenate ions as suggested by previous studies[12,13]. It could therefore be the oxidation of H_2O_2 absorbed on the planar electrode surface.

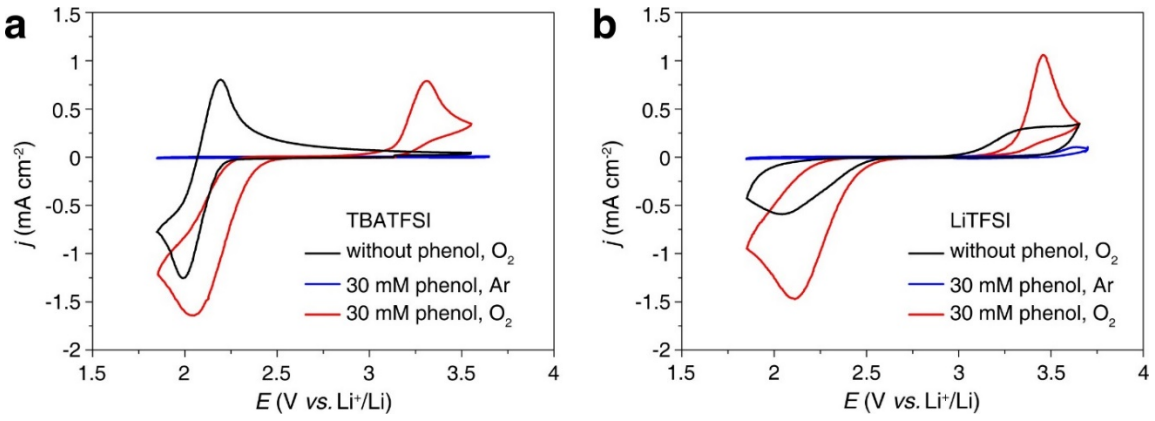


Figure 3-2. CVs for O_2 reduction without phenol (black) and with 30 mM phenol (red) in (a) 0.5 M TBATFSI in TEGDME and (b) 0.5 M LiTFSI in TEGDME under O_2 and under Ar (blue). GC electrode. Scan rate 100 mV s^{-1}.

When the Li^+-free electrolyte was switched to the LiTFSI-based electrolyte in TEGDME, the quasi-reversible peak for O_2/O_2^- became irreversible with the reduction peak current much smaller and no oxidation peaks at potential below 3 V, as shown in black curve in Fig.

3-3 (b)[3]. The reaction mechanisms for this process is well known and given by equations (3.2)-(3.4)[14,15]:

$$O_{2\,(sol)} + Li^{+}{}_{(sol)} + e^{-} \rightarrow LiO_2^* \qquad (3.2)$$

$$LiO_2^* + Li^{+}{}_{(sol)} + e^{-} \rightarrow Li_2O_2^* \qquad (3.3)$$

$$2\,LiO_2^* \rightarrow Li_2O_2^* + O_{2\,(sol)} \qquad (3.4)$$

The equations are written in the form of the surface mechanism, which is expected to be dominant in low DN solvents with the presence of LiTFSI[3,16]. In TBATFSI-based electrolyte, O_2 is reduced to 1 e^- product O_2^-, while in the Li^+-based electrolyte, the reaction forms a 2 e^- product Li_2O_2, where a double peak current should be expected comparing to that in TBA^+-based electrolyte. However, the peak height is now actually lower than that in the equivalent CV in the TBATFSI-based electrolyte in TEGDME, Fig. 3-2 (a), (b), due to the blockage of the planar electrode surface by Li_2O_2 as an insulating surface film[16].

When 30 mM Phenol was added into the LiTFSI-based electrolyte in TEGDME, a big increase in the peak current on reduction is observed, which demonstrates that the insoluble insulating Li_2O_2 formed on reduction is able to dissolve and escape into the electrolyte solution. It confirms that addition of phenol to the electrolyte, LiTFSI in TEGDME, results in a soluble 2 e^- discharge product, like LiOOH and H_2O_2.

3.3 Discharge studies with phenol in Li-O_2 cells

Some previous work also observed an increased peak current on reduction in CV studies with a strong acid additive[8]. The CV measurements only prove a soluble 2 e^- discharge product, which cannot rule out the possibility of H_2O_2 formation and accumulation. In order to prove the concept that the phenol added is acting as a catalyst and is not consumed during

the reduction process, cells containing TEGDME saturated with O_2 (under 1 atm. of O_2) were discharged without and with 30 mM phenol. One piece of GDL (4 mm in diameter), which was heated under 5 % H_2/Ar prior to use, served as the cathode[17,18]; a glass fibre filter (Waterman) as the separator and a partially oxidised $LiFePO_4$ electrode was used as the anode. $LiFePO_4$ was used in this project to isolate the cathode chemistry from the anode side. In reality, protected metallic lithium with a solid-state separator should be considered to avoid crossover of soluble additives and other undesired side reactions[2]. 150 µl of 1 M LiTFSI in TEGDME without or with 30 mM phenol served as the electrolyte. The discharge performances of different cells with several different areal current densities are shown in Fig. 3-3.

The cells died rapidly in the absence of phenol, exhibiting very small capacities and poor rate performances, as is seen in Fig. 3-3 (b), similar to previous studies by other groups in TEGDME[19,20]. 0.18 mAh cm^{-2}_{areal}, equivalent to 0.15 mg of Li_2O_2 was obtained at the current density of 100 uA cm^{-2}_{areal}. The poor discharge performance was caused by the surface growth of insulating discharge product Li_2O_2. However, cells with 30 mM phenol discharged under the same conditions exhibited a dramatic improvement, delivering up to 35 times higher discharge capacities before end of life, *e.g.* 9.1 mAh cm^{-2}_{areal}, equivalent to 7.81 mg of Li_2O_2 was achieved at the current density of 50 uA cm^{-2}_{areal}, comparing to 0.27 mAh cm^{-2}_{areal} without phenol.

Considering the 150 µl of the electrolyte with 30 mM phenol, even if all the protons had been reacted to form H_2O_2, it would correspond to a capacity of 0.48 mAh cm^{-2}_{areal}, much lower than the 9.1 mAh cm^{-2}_{areal} achieved in the real cell with phenol, indicating that phenol was not consumed and indeed it was working as a phase transfer catalyst. The capacity at the current density of 50 uA cm^{-2}_{areal}, 9.1 mAh cm^{-2}_{areal}, represented a utilization of around

20 % of the total GDL electrode pore volume, which might block the pores and severely limit the mass transport.

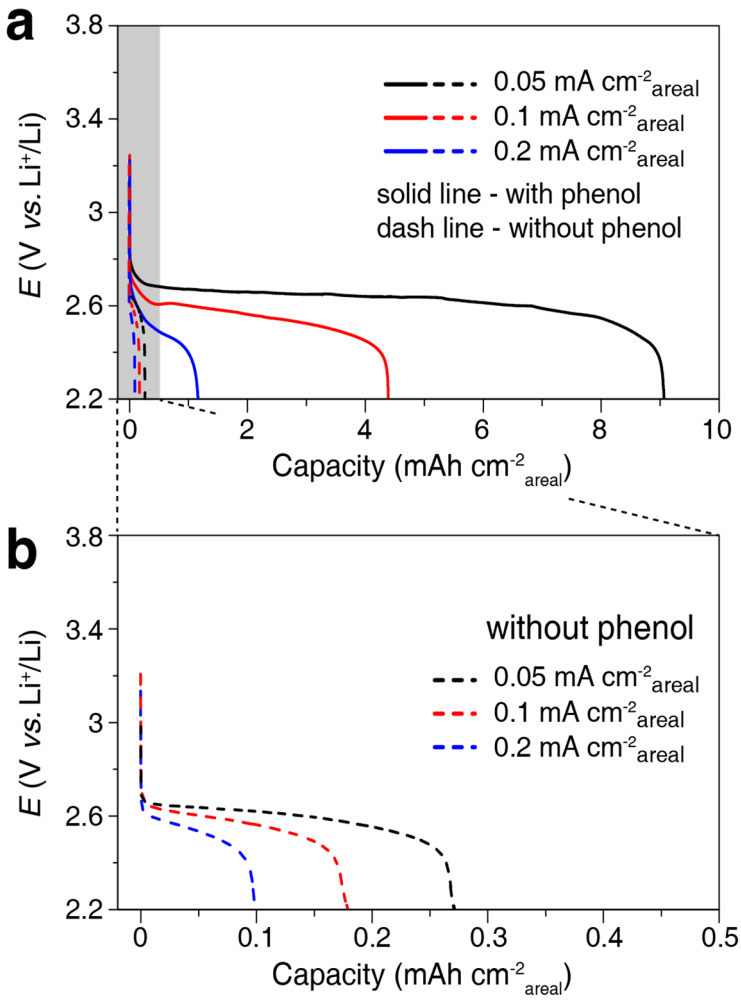


Figure 3-3. Load curves of O_2 reduction at a gas diffusion electrode discharged with and without phenol. (a). cells are discharged under O_2 at various areal current densities from 0.05 mA cm^{-2} to 0.2 mA cm^{-2} in 1 M LiTFSI in TEGDME with 30 mM phenol (solid lines) and without phenol (dash lines) under O_2 at various areal current densities from 0.05 mA cm^{-2} to 0.2 mA cm^{-2}. (b) Enlarged section of the load curves recorded without phenol in (a).

In order to observe the effect of phenol in the absence of mass transport limitations, galvanostatic discharge was carried out on a planar GC electrode. The effect of phenol is even more promising. The capacity with 30 mM phenol is more than 60 times bigger than

that without phenol at the current density of 60 μA cm^{-2}_{areal}, proving a dominant solution mechanism by the addition of phenol, Fig. 3-4. The cell performance in the presence of phenol demonstrates the ability of the phenol catalysed discharge to overcome the limits of electrode surface area. In a practical battery this will enable low carbon fractions in the cathode, which is a requisite for the high performance of a Li-O_2 battery.

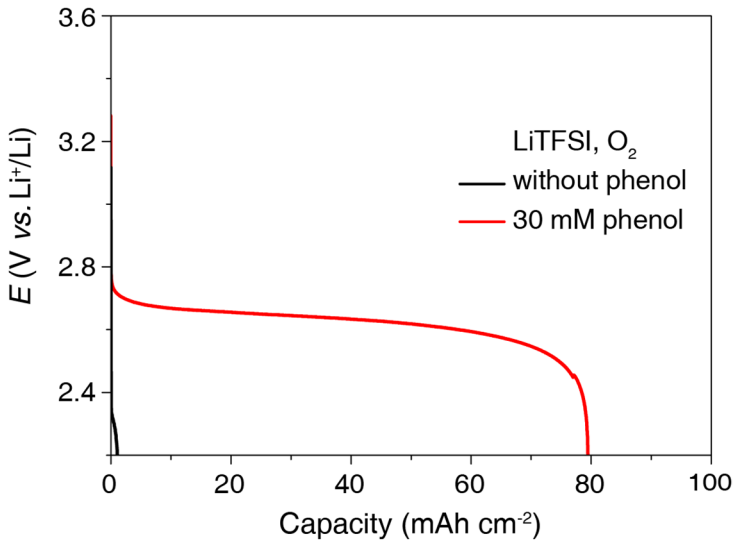


Figure 3-4. Load curves of O_2 reduction at a planar GC electrode discharged in 1 M LiTFSI in TEGEME without phenol (black) and with 30 mM phenol (red) at a current density of 60 μA $cm^{-2}_{(geometric)}$.

3.4 Discharge product characterisations

3.4.1 SEM analysis

After discharging the cells, SEM was carried out on the cathodes with and without phenol. Fig. 3-5 (a) shows the pristine GDL. In the absence of phenol, a film of Li_2O_2 is observed, Fig. 3-5 (b) and no particles of Li_2O_2 are evident, which is consistent with the discharge by a surface mechanism in glycol ethers[4,7,8]. In contrast, the electrode from cells with phenol shows discharge products as large hemispherical particles with 1-2 μm in diameter, Fig. 3-

5 (c), (d), rather than the film formation on the electrode surface shown in Fig. 3-5 (b). The mechanism of such morphology formation is unclear yet and needs further studies. After half way of the discharge, the cell was stopped and the electrode was analysed. No clear film is evident on the cathode surface, Fig. 3-5 (c). At the end of the discharge, the entire carbon structure is covered with similar spherical particles, Fig. 3-5 (d). If the cells had followed the surface discharge mechanism, it should be limited to a 7 nm thick layer mentioned forehead[21]; however, it obviously is not the case here, which confirms the solution mechanism by the addition of phenol.

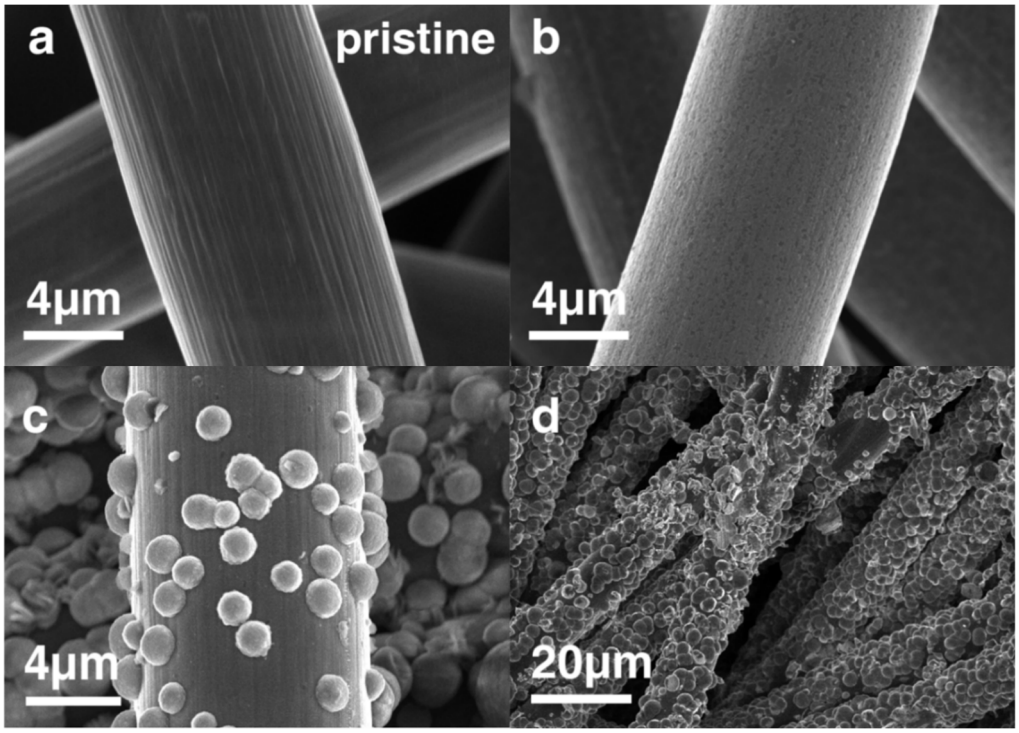


Figure 3-5. SEM images showing the Li_2O_2 morphologies on discharge in 30 mM phenol -1 M LiTFSI in TEGDME under O_2. (a) pristine GDL, (b)without Phenol, (c)half discharge with 30 mM phenol.

3.4.2 PXRD and FTIR analysis

In order to prove the particles observed in SEM in the presence of phenol are indeed Li_2O_2, PXRD and FTIR were carried out to examine the discharge cathode with phenol. The XRD

pattern shows Li_2O_2 peak signals, Fig. 3-6, confirming that Li_2O_2 is the final discharge product. From the PXRD data, it is difficult to confirm or exclude the existence of Li_2CO_3 and LiOH peaks, Fig.3-6. By-products are likely to be small amount and have poor crystallinity in Li-O_2 cells, and therefore hard to be recognized in PXRD. Therefore, FTIR was used to analyse the discharged electrode. The FTIR, shown in Fig. 3-7, also proves that Li_2O_2 is the main discharge product and some lithium acetate and carbonate are the side products. Again, no LiOH signal was detected.

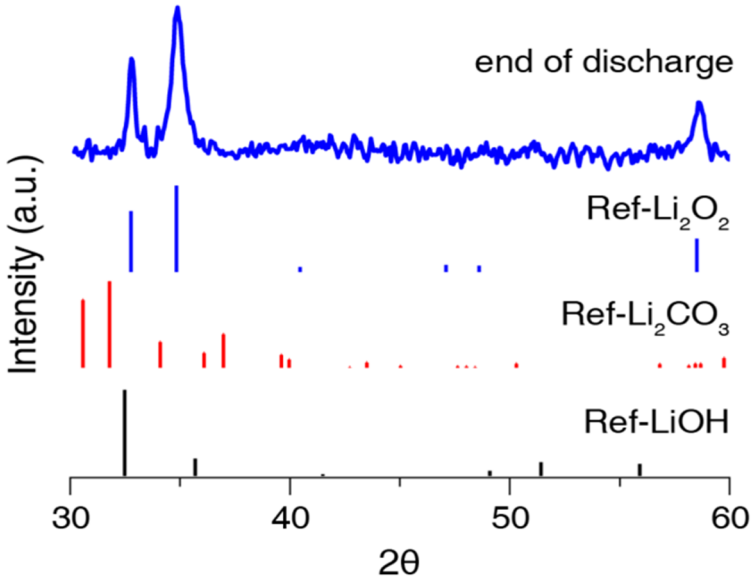


Figure 3-6. PXRD pattern of the GDL discharged in 30 mM phenol -1 M LiTFSI in TEGDME under O_2. Patterns of possible side products are included as the reference.

It is well established that the stability of the electrolyte solutions and component is a major problem in aprotic Li-O_2 cells[22-27]. Glycol ethers are known to suffer from hydrogen abstraction to form lithium formate, acetate and carbonate[25,28]. From Fig. 3-6 and 3-7, I can see that the addition of phenol did not introduce any new side reactions with new side products. Previous work claimed that the addition of protic acids might lead to the formation of LiOH, but both pieces of evidence in this project exclude the existence of LiOH as the possible side product.

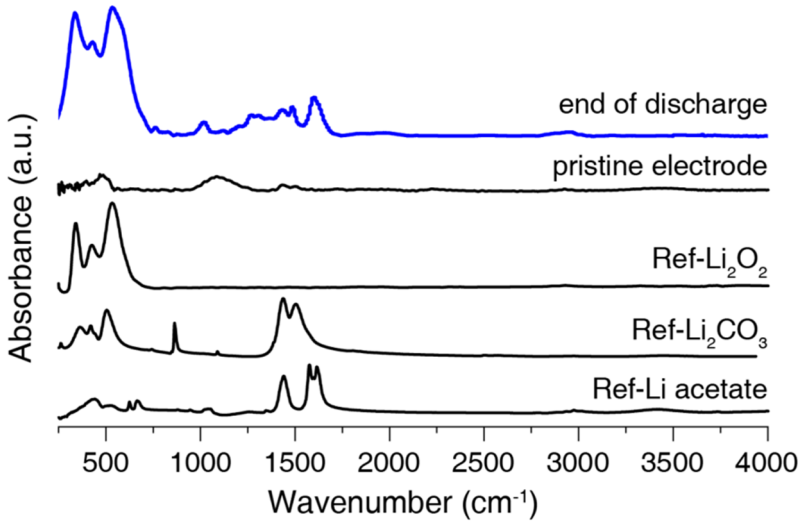


Figure 3-7. Infrared spectrum of the GDL discharged in 30 mM phenol -1 M LiTFSI in TEGDME under O_2. Spectrum of possible side products are included as the references.

3.4.3 DEMS analysis

People always have concerns when adding protic additives that the protons may introduce more side reactions, and indeed ether solvents like DME in aqueous solutions can be oxidised to methanol, formaldehyde and formic acid[29]. Therefore *in situ* DEMS analysis was carried out to investigate the gas consumption during the discharge process with addition of phenol. The carrier gas was 5% Ar : 95% O_2 mixture and the flow rate was 1 ml min^{-1}. CV was applied in the DEMS cell at a scan rate of 0.1 mV s^{-1}, with the voltage *vs.* time recorded in Fig. 3-8 (b). The gas analysis results are shown in Fig. 3-8 (a). A delay on the gas analysis versus the electrochemistry measurement is seen in Fig. 3-8 (a), which is due to the dead volume in the DEMS cell that requires some time to pass the gas to the detector.

Only the O_2 consumption was detected during discharge and no other gas evolution, particularly there is no evidence of CO_2, Fig. 3-8 (a). The ratio of electrons to oxygen consumption was 2.04 e^-/O_2, close to the theoretical value of 2 e^-/O_2, which indicates that

the dominant reaction is the formation of a two electron reduction product of oxygen, typically Li_2O_2, as shown by PXRD and FTIR[23,30]. It again suggests that the addition of phenol, although changes the intermediate species, but does not induce more side reactions. At the same time, the 2.04 e^-/O_2 also indicates that the main side reactions seen in Fig. 3-7 should not come from intermediate species, otherwise, the e^-/O_2 number should largely differs from the theoretical 2 e^-/O_2. It could be Li_2O_2 or singlet oxygen as proposed by previous studied that result in the solvent decomposition after their formation[31-34].

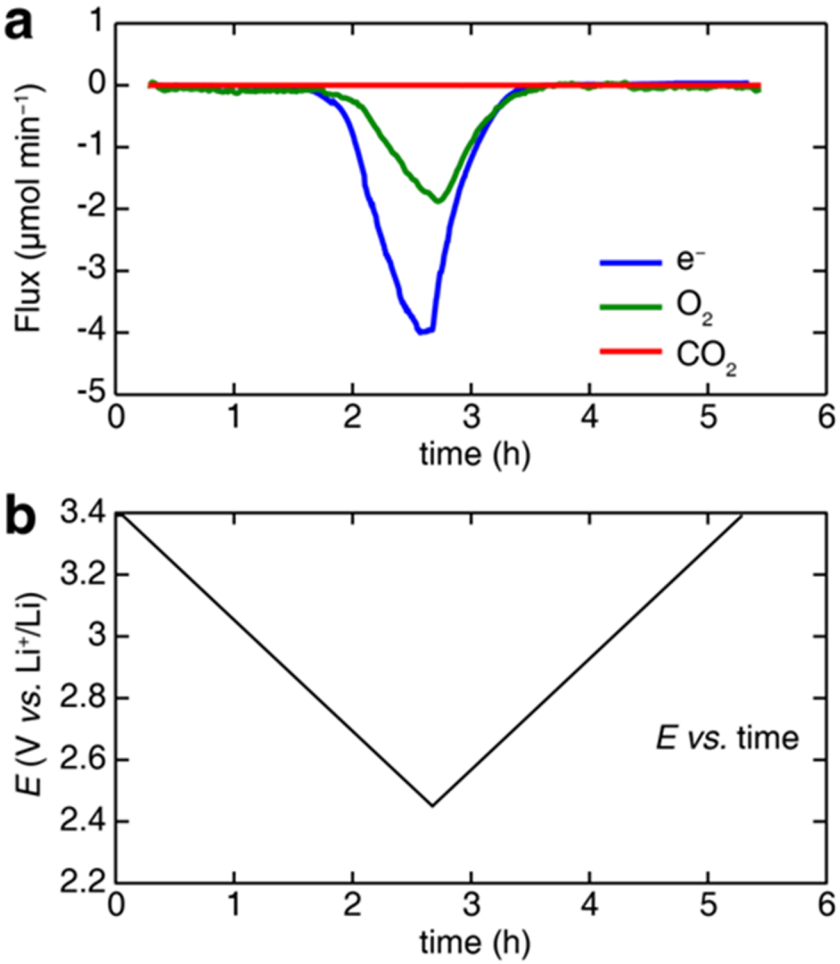


Figure 3-8. ***In situ*** **DEMS of a discharged GDL in phenol-LiTFSI-TEGDME showing 2.04 e^- per O_2 consumed, confirming that Li_2O_2 is the dominant discharge product.** (a) Discharge current (blue), O_2 consumption (green) and CO_2 evolution (red) in 30 mM phenol- 1 M LiTFSI in TEGDME; (b) voltage profile of the DEMS cell.

3.4.4 Yield measurements

The FTIR measurements have shown the existence of side products in the cell and the DEMS results indicate that the discharge product Li_2O_2 might contribute to the solvent decomposition. In order to quantify the amount of Li_2O_2 after discharge, the yield measurement was carried out by a chemical analysis of Li_2O_2 against $TiOSO_4$ solution. In the presence of 30 mM phenol, the discharged electrode had the yield percentage of 62 %. It should be noted that the low yield of 62 % does not result from the addition of phenol into the system and actually when GDL served as the electrode, the yield was only 58 % without phenol, which is similar to previous studies by other groups[8]. The similar yields with and without phenol quantitatively tells that the level of side reactions does not increase with the addition of phenol during discharge. Instead, the low yield comes from the property of the GDL electrode and the TEGDME-based electrolyte. By switching the GDL electrodes to other types of carbon, I can get a different yield value. When ketjen black carbon was used as the cathode, a yield of 86 % without phenol was achieved and the yield in the presence of 30 mM phenol, 82 %, is similar to that without phenol[23]. Again, it proves that phenol does not induce more side reactions. Combining the DEMS analysis with yield measurements, the main side reactions should probably be related to the TEGDME solvent and Li_2O_2.

3.4.5 Summary of characterisations

From the discharge curve combining with SEM, I can conclude that weak acid phenol as a phase transfer catalyst is able to enhance the discharge performance, favouring a solution mechanism during discharge, forming large particles in the pores of electrode rather than a thin film on the carbon surface. The CV and DEMS measurements showed the main reaction as a two-electron reduction and the intermediate is very unlikely to be largely involved in

side reactions, while PXRD and FTIR data proved the discharge product as Li_2O_2, with some lithium carbonate and acetate as the side products. The yield measurement quantified the Li_2O_2 formed and it indicated that the side products may rise from the instability of Li_2O_2 with the electrolyte solution.

It should be noted that the addition of phenol does not induce more side reactions in the short term during discharge, and ethers are known to be unstable and can be easy attacked by the intermediate and Li_2O_2 in the lithium-air battery. Identification of truly stable solvents is required and possibly one of the most important challenges in the field, but that is beyond the discussion in this project.

3.5 Discharge studies with perchloric acid in Li-O_2 cells

The success of phenol catalysing the solution mechanism triggered my interest in studying homogeneous additives with higher acidity than phenol. Stronger acids should have higher solubility of Li_2O_2 and can combine intermediates more strongly, which will lead to even higher discharge capacities. Therefore, another stronger type of acid, perchloric acid ($HClO_4$), was explored, which at the same time could help me better understand the relationship between acid types and the discharge pathways.

$HClO_4$ was added to LiTFSI-based electrolyte in TEGDME for discharge studies. The cells were assembled under the same conditions that GDL served as the cathode, except that the electrolyte was changed to 150 μl of 1 M LiTFSI in TEGDME with 30 mM $HClO_4$. The discharge performance is shown in Fig. 3-9.

The load curve shows a different pattern comparing to that with or without phenol. A new plateau at a more positive potentials (~ 3.3 V) is observed, much higher than the E^0 for O_2/Li_2O_2 (2.96 V), which indicates that new reactions are happening rather than the Li_2O_2

formation. Following this new plateau comes to the expected plateau for Li_2O_2 formation, similar to previous studies[8]. Importantly, no apparent increase in discharge capacities is observed comparing to that in the electrolyte with phenol, Fig. 3-3 (a). According to Schwenke *et al.*, the new plateau before the formation of Li_2O_2, rises from the formation of H_2O_2 by the following equations (3.5, 3.6 and 3.7):

$$O_{2(sol)} + HA_{(sol)} + e^- \rightarrow HOO_{(sol)} + A^- \quad (3.5)$$

$$HOO_{(sol)} + e^- + HA_{(sol)} \rightarrow H_2O_{2\,(sol)} + A^- \quad (3.6)$$

$$2\,HOO_{(sol)} \rightarrow H_2O_{2\,(sol)} + O_{2(sol)} \quad (3.7)$$

After the protons are consumed to form H_2O_2 at the first plateau, normal oxygen reduction reaction in aprotic Li-O_2 chemistry takes over to show the second plateau[8].

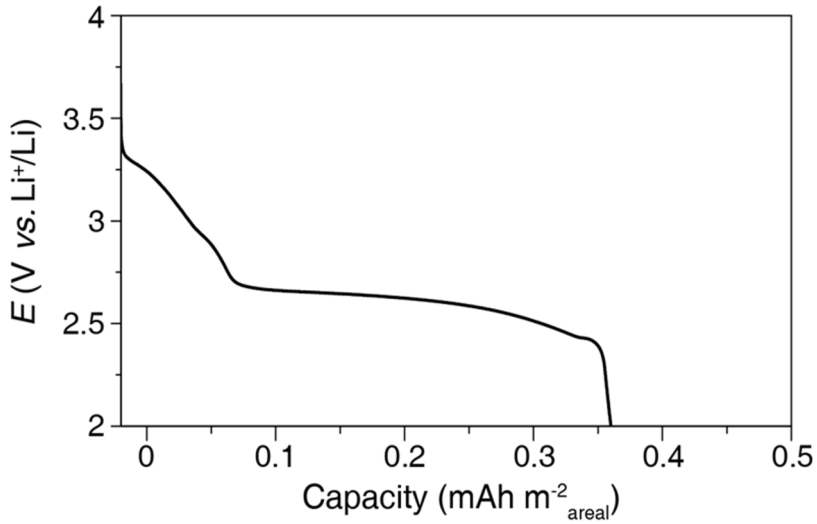


Figure 3-9. Load curves of O_2 reduction at a gas diffusion electrode discharged in 1 M LiTFSI in TEGDME with 30 mM $HClO_4$.

As Gastiger *et al.* reported, when $HClO_4$ was added into the electrolyte, the electrolyte decomposition was playing the dominant role. The Li_2O_2 formed may decompose in contact with degraded solvent fragments in electrolytes with strong acid, leading to more side

reactions and unwanted lower discharge yield[8]. All these data show little or no benefit in capacity by any catalytic behaviour of strong acids like perchloric acid and it indicates that the chemistry of the protic additives should play critical roles to serve as phase transfer catalysts.

3.6 Mechanism of catalytic effect of acid additives

After studying the effect of different types of acids (perchloric acid and phenol) in the discharge performance in Li-O_2 batteries, some weak acids are able to catalyst solution mechanisms, while the addition of strong acids have no apparent benefits. The mechanisms of strong and weak acid as electrolyte additives are therefore discussed to give some idea of the relationship between acids and the discharge performance.

3.6.1 The effect of proton activity

In the case of strong acids like $HClO_4$, H^+ activity is much higher than Li^+ activity, and therefore when O_2 is reduced, it is more likely to combine with the proton to form H_2O_2 rather than the desired Li_2O_2, and therefore a new plateau is observed in Fig. 3-9. After all protons are consumed, O_2 continues to be reduced and then it has to combine with Li^+ to form Li_2O_2 in the cell, which means that the addition of strong acids like perchloric acid has no benefits in capacity or apparent catalysis.

While in the case of weak acids, the proton activity is much reduced, comparing to that in strong acids. Li^+ activity is therefore greater than the H^+ activity, and thus when oxygen is reduced, it combines Li^+ and forms Li_2O_2 as the final product. Equilibrium then should exist between solid and dissolved peroxide by equation 3.8.

$$Li_2O_{2(s)} + AH_{(sol)} \rightleftharpoons HOOLi_{(sol)} + Li^+_{(sol)} + A^-_{(sol)} \qquad (3.8)$$

A similar reaction should exist for the superoxide species, but given its short life time as the intermediate, here I only focus on peroxide species.

To evaluate the equation 3.8, quantitative analysis of concentrations of dissolved Li_2O_2 in TEGDME with varying amounts of phenol was measured. Excess dry Li_2O_2 powder was added into certain volume of TEGDME solutions containing 0, 10, 25, 50 and 100 mM phenol and the solutions were stirred to fully dissolve the maximum amount of Li_2O_2. The emulsion was then centrifuged to obtain the clear solution. It was then slowly heated to evaporate the solvent under vacuum at a temperature of 70 ^oC. Finally, 1 M nitric acid solution was added to prepare samples for elemental analysis by inductive coupled plasma mass spectroscopy measurements (ICP-MS). The Li^+ was analysed versus different concentrations of phenol. The ICP-MS results are shown in Fig. 3-10.

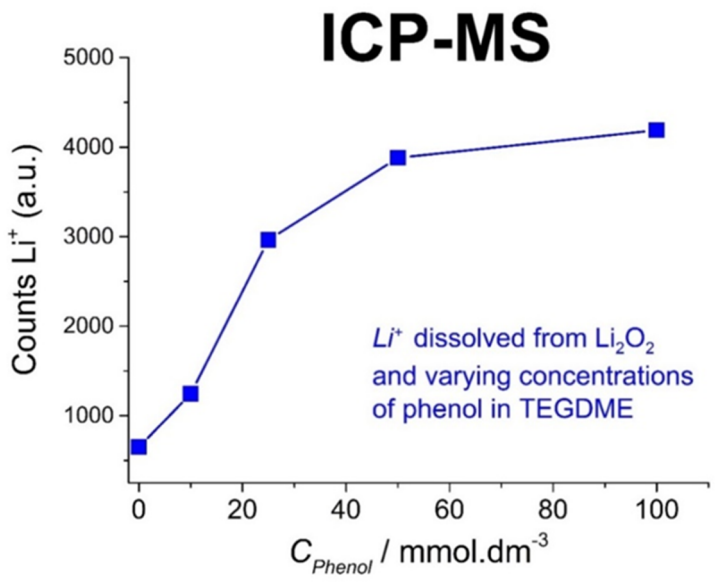


Figure 3-10. Quantitative analysis of the total amount of Li^+ in TEGDME-based solutions containing varying concentrations of phenol. The Li^+ amount was measured by ICP-MS.

Tiny Li^+ concentration is observed in pure TEGDME, in accord with the poor Li_2O_2 solubility in TEGDME. While after addition of phenol, an increase in Li^+ concentration is

seen and more phenol leads to higher concentrations of Li^+, which relates to soluble peroxide species. The ICP-MS results confirm the above equation 3.8.

Considering the equation 3.8: $Li_2O_{2(s)} + AH_{(sol)} \rightleftharpoons HOOLi_{(sol)} + Li^+_{(sol)} + A^-_{(sol)}$, I can shift the equilibrium to the left favouring Li_2O_2 formation by invoking the Li^+ activity. The formation of LiOOH, even in small amounts, allows solid Li_2O_2 to dissolve into solution and recrystallize as larger particles by an Ostwald ripening process, shown in Fig. 3-5 (c), which is tantamount to a solution mechanism and possesses all the associated benefits[3].

3.6.2 The effect of conjugate bases

Combining the discussions above, a cartoon of schematic comparing different pathways with strong and weak acids is shown in Fig. 3-11.

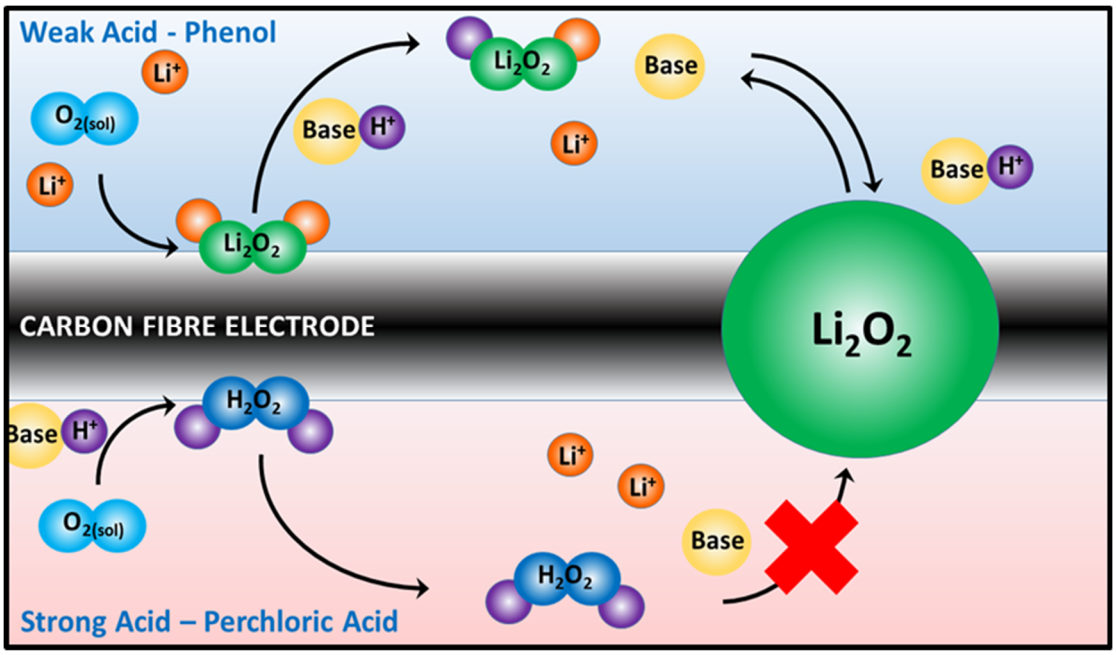


Figure 3-11. Cartoon of schematic comparing the action of a strong and weak acid during discharge process in a lithium oxygen cell.

In the presence of a strong acid with weak conjugate base, the major product is H_2O_2 and the exchange between H^+ and Li^+ is inhibited by the poor base. With a weak acid (strong

conjugate base), the major product is Li_2O_2 and the exchange of H^+ between Li_2O_2 and the conjugate base is facile, enabling phase transfer catalysis and a solution mechanism. Such differences in weak and strong acids also demonstrate the importance of conjugate bases to meet the requirements as a proper phase transfer catalyst. The conjugate bases, A^-, should be strong enough to accept the proton from LiOOH so that the equilibrium in equation 3.8 lies to the left forming Li_2O_2. If this is not the case, then protonation will effectively be irreversible. It is observed when using perchloric acid and H_2O_2 forms as the product. While a relatively strong conjugate base such as the phenolate ion, the proton can reversibly transfer between $LiOO^-$ and phenolate, becoming catalytic and greatly enhancing the performance of the battery.

In practice, the strongest base in the system, which could be the salt or solvent when using a strong acid, will control proton activity and therefore, determine where the equilibrium lies. It should be noted that the concentration of Li^+ and H^+ and the nature of the electrolyte (salt and solvent) will all play a role in the equilibrium position. It is important to tune this equilibrium in order to maximize the capacity.

3.7 Conclusions

In this project, I successfully demonstrated that the addition of phenol to TEGDME-based electrolyte solution is able to introduce a solution mechanism in low DN solvents. The performance of a 35-fold increase in capacities and growth of large deposited particles far in excess of that possible in the absence of phenol is satisfying. In all cases, the characterisation confirmed Li_2O_2 as the main product, and the data indicated that phenol, acting as a phase transfer catalyst, did not increase the amount of side reactions in short term period.

As for the mechanisms for acid additives, the data show that protic phase transfer catalysts for Li-O_2 batteries must be selected such that a balance exists between Li^+ and H^+ activity. The balance between protonation of the discharge product to induce solubility and removal of the proton of the conjugate base and recrystallization of Li_2O_2 particles is then struck. The critical component for this process is the strength of the conjugate bases, which must be strong enough to remove the proton from LiOOH to regenerate the catalyst. It is important to tune the equilibrium between solid Li_2O_2 and dissolved peroxide species to maximize the capacity.

However, all effects of introducing protic additives are by no means understood and it remains a question whether such additives could be used over a longer time period. It is an interesting system and protic acids should be considered along with other emerging additives able to enhance discharge in the aprotic Li-O_2 battery. It should be mentioned that regardless of the presence of phenol, solvents like ethers are not truly stable and till now no stable solvent have been identified in aprotic Li-O_2 batteries.

3.8 References

1 Gao, X., Jovanov, Z. P., Chen, Y., Johnson, L. R. & Bruce, P. G. Phenol-catalyzed discharge in the aprotic lithium-oxygen battery. *Angew. Chem. Int. Ed.* **56**, 6539-6543 (2017).

2 Aurbach, D., McCloskey, B. D., Nazar, L. F. & Bruce, P. G. Advances in understanding mechanisms underpinning lithium–air batteries. *Nat. Energy* **1**, 16128 (2016).

3 Johnson, L. *et al.* The role of LiO_2 solubility in O_2 reduction in aprotic solvents and its consequences for Li–O_2 batteries. *Nat. Chem.* **6**, 1091-1099 (2014).

4 Aetukuri, N. B. *et al.* Solvating additives drive solution-mediated electrochemistry and enhance toroid growth in non-aqueous Li-O_2 batteries. *Nat. Chem.* **7**, 50-56 (2015).

5 Kwabi, D. G. *et al.* Experimental and computational analysis of the solvent-dependent O_2/Li^+-O_2^- redox couple: standard potentials, coupling strength, and implications for lithium-oxygen batteries. *Angew. Chem. Int. Ed.* **55**, 3129-3134 (2016).

6 Koper, M. T. M. Thermodynamic theory of multi-electron transfer reactions: implications for electrocatalysis. *J. Electroanal. Chem.* **660**, 254-260 (2011).

7 Meini, S., Piana, M., Tsiouvaras, N., Garsuch, A. & Gasteiger, H. A. The effect of water on the discharge capacity of a non-catalyzed carbon cathode for Li-O_2 batteries. *Electrochem. Solid-State Lett.* **15**, A45-A48 (2012).

8 Schwenke, K. U., Metzger, M., Restle, T., Piana, M. & Gasteiger, H. A. The influence of water and protons on Li_2O_2 crystal growth in aprotic Li-O_2 cells. *J. Electrochem. Soc.* **162**, A573-A584 (2015).

9 Xia, C., Black, R., Fernandes, R., Adams, B. & Nazar, L. F. The critical role of phase-transfer catalysis in aprotic sodium oxygen batteries. *Nat. Chem.* **7**, 496-501 (2015).

10 Kwabi, D. G. *et al.* The effect of water on discharge product growth and chemistry in Li-O_2 batteries. *Phys. Chem. Chem. Phys.* (2016).

11 Li, F. *et al.* The water catalysis at oxygen cathodes of lithium-oxygen cells. *Nat. Commun.* **6**, 7843 (2015).

12 Peng, Z., Chen, Y., Bruce, P. G. & Xu, Y. Direct detection of the superoxide anion as a stable intermediate in the electroreduction of oxygen in a non-aqueous

electrolyte containing phenol as a proton source. *Angew. Chem. Int. Ed.* **54**, 8165-8168 (2015).

13 Andrieux, C. P., Hapiot, P. & Saveant, J. Mechanism of superoxide ion disproportionation in aprotic solvents. *J. Am. Chem. Soc.* **109**, 3768-3115 (1987).

14 Adams, B. D. *et al.* Current density dependence of peroxide formation in the Li-O_2 battery and its effect on charge. *Energy Environ. Sci.* **6**, 1772-1778 (2013).

15 Laoire, C., Mukerjee, S., Plichta, E. J., Hendrickson, M. A. & Abraham, K. M. Rechargeable Lithium/TEGDME-$LiPF_6/O_2$ battery. *J. Electrochem. Soc.* **158**, A302-A308 (2011).

16 Burke, C. M., Pande, V., Khetan, A., Viswanathan, V. & McCloskey, B. D. Enhancing electrochemical intermediate solvation through electrolyte anion selection to increase nonaqueous Li-O_2 battery capacity. *Proc. Natl. Acad. Sci. U. S. A.* **112**, 9293-9298 (2015).

17 Gao, X., Chen, Y., Johnson, L. & Bruce, P. G. Promoting solution phase discharge in Li-O_2 batteries containing weakly solvating electrolyte solutions. *Nat. Mater.* **15**, 882–888 (2016).

18 Ottakam Thotiyl, M. M., Freunberger, S. A., Peng, Z. & Bruce, P. G. The carbon electrode in nonaqueous Li-O_2 cells. *J. Am. Chem. Soc.* **135**, 494-500 (2013).

19 Girishkumar, G., McCloskey, B., Luntz, A. C., Swanson, S. & Wilcke, W. Lithium−air battery: promise and challenges. *J. Phys. Chem. Lett.* **1**, 2193-2203 (2010).

20 Lu, Y.-C. *et al.* The discharge rate capability of rechargeable Li-O_2 batteries. *Energy Environ. Sci.* **4**, 2999-3007 (2011).

21 Viswanathan, V. *et al.* Electrical conductivity in Li_2O_2 and its role in determining capacity limitations in non-aqueous Li-O_2 batteries. *J. Chem. Phys.* **135**, 214704 (2011).

22 Sharon, D. *et al.* Reactivity of amide based solutions in lithium–oxygen cells. *J. Phys. Chem. C* **118**, 15207-15213 (2014).

23 McCloskey, B. D. *et al.* Combining accurate O_2 and Li_2O_2 assays to separate discharge and charge stability limitations in nonaqueous Li–O_2 batteries. *J. Phys. Chem. Lett.* **4**, 2989-2993 (2013).

24 Khetan, A., Pitsch, H. & Viswanathan, V. Solvent degradation in nonaqueous Li-O_2 batteries: oxidative stability versus H-abstraction. *J. Phys. Chem. Lett.* **5**, 2419-2424 (2014).

25 Freunberger, S. A. *et al.* The lithium-oxygen battery with ether-based electrolytes. *Angew. Chem. Int. Ed.* **50**, 8609-8613 (2011).

26 Bardé, F. *et al.* Sulfone-based electrolytes for nonaqueous Li–O_2 batteries. *J. Phys. Chem. C* **118**, 18892-18898 (2014).

27 Chen, Y., Freunberger, S. A., Peng, Z., Barde, F. & Bruce, P. G. Li-O_2 battery with a dimethylformamide electrolyte. *J. Am. Chem. Soc.* **134**, 7952-7957 (2012).

28 Adams, B. D. *et al.* Towards a stable organic electrolyte for the Lithium oxygen battery. *Adv. Energy Mater.* **5**, 1400867 (2015).

29 Nagai, Y., Matubayasi, N. & Nakahara, M. Mechanisms and kinetics of noncatalytic ether reaction in supercritical water. 2. proton-transferred fragmentation of dimethyl ether to Formaldehyde in competition with hydrolysis. *J. Phys. Chem. A* **109**, 3558-3564 (2005).

30 Peng, Z., Freunberger, S. A., Chen, Y. & Bruce, P. G. A reversible and higher-rate Li-O_2 battery. *Science* **337**, 563-566 (2012).

31 Mahne, N. *et al.* Singlet oxygen generation as a major cause for parasitic reactions during cycling of aprotic lithium–oxygen batteries. *Nat. Energy* **2**, 17036 (2017).

32 García, J. M., Horn, H. W. & Rice, J. E. Dominant decomposition pathways for ethereal solvents in Li–O_2 batteries. *J. Phys. Chem. Lett.* **6**, 1795-1799 (2015).

33 Sharon, D. *et al.* On the challenge of electrolyte solutions for Li–air batteries: monitoring oxygen reduction and related reactions in polyether solutions by spectroscopy and EQCM. *J. Phys. Chem. Lett.* **4**, 127-131 (2012).

34 Wandt, J., Jakes, P., Granwehr, J., Gasteiger, H. A. & Eichel, R.-A. Singlet oxygen formation during the charging process of an aprotic lithium–oxygen battery. *Angew. Chem. Int. Ed.* **55**, 1-5 (2016).

Chapter 4. Redox mediator promoting solution phase discharge in aprotic Li-O_2 batteries containing weakly solvating electrolyte solutions

As discussed in the introduction and Chapter 3, due to the insoluble and insulating property of Li_2O_2 as the discharge product, there is always a need to promote discharge via solution mechanism and to do so in relatively stable solvents[1-5]. Another problem encountered with aprotic Li-O_2 cells is the fact that the discharge potential, even at modest rates, lies c.a. 0.3 V below the thermodynamic discharge potential for the O_2/Li_2O_2 reaction (2.96 V)[6]. The potential determining step in an aprotic Li-O_2 battery is the formation of LiO_2 intermediate that has a higher free energy than Li_2O_2, inevitably leading to the large discharge overpotential[3]. Phenol has been discussed in Chapter 3 as a possible candidate to induce a solution mechanism by solubilizing the discharge products[1]. However, the addition of acid additives does not change the formation of superoxide and therefore can hardly solve the overpotential problem. The existence of the equilibrium also limits the high rate performance.

In this work, I will focus on promoting solution phase discharge in ether-based electrolyte solutions with attempts to minimise the discharge overpotential. Since the formation of LiO_2 is the potential determining step, as long as LiO_2 still forms as the intermediate, the discharge overpotential remains thermodynamically.

Here, I propose that homogeneous catalysts and discharge mediators can be used to promote the solution phase discharge in low DN solvents and at the same time, it can lower the activation energy of the intermediate, provide new discharge routes avoiding LiO_2, and therefore increase the discharge potentials.

4.1 Selection criteria for the discharge mediator

Some requirements are considered when selecting the suitable discharge mediators that can promote solution phase discharge in low DN solvents with low activation energy intermediate. Firstly, the potential of the mediator should be lower than 2.96 V, the thermodynamic potential for O_2/Li_2O_2, otherwise, Li_2O_2 will not be formed during the mediator reduction process. Furthermore, in order to maximise the energy that a cell delivers, a stabilised superoxide or a new low-energy intermediate is required to facilitate the ORR. In addition, an effective mediator should operate as a redox shuttle to keep the oxygen reduction reaction away from the electrode surface and therefore a larger discharge capacity with higher rates is achievable. In conclusion, it is necessary to carry out the reduction of O_2 to Li_2O_2 in solution at a higher potential than the surface route, avoiding the formation of LiO_2 and therefore reducing the discharge overpotential[3].

Quinones are well known to catalyse the oxygen reduction reactions, and therefore they are studied as the candidate discharge mediators[7,8]. Several quinones with potentials in the relevant ranges were investigated, including 3,5-di-tert-butyl-o-benzoquinone, 2,5-di-tert-butyl-1,4-benzoquinone and thymoquinone. Their CVs obtained in 1 M LiTFSI in TEGDME at a gold electrode under Ar and O_2 are shown in Fig. 4-1. The potentials of these three quinones are all below 2.96 V under Ar, shown as blue lines in Fig. 4-1. When the gas atmosphere was switched to O_2, the reduction peak currents of both 3,5-Di-tert-butyl-o-benzoquinone and thymoquinone are similar to that under Ar, which do not exhibit the enhancement of oxygen reduction, Fig. 4-1 (a), (c). However, CVs with 2,5-di-tert-butyl-1,4-benzoquinone (DBBQ) under O_2 show a large increase in the peak current, demonstrating promising electrochemistry. The reasons why different quinones have different responses to O_2 remained unknown yet: the quinones might need to have specific

structures. It is not the focus of this project, but the catalytic effect of DBBQ is obvious and therefore, I choose DBBQ as the discharge mediator for the following studies in this project.

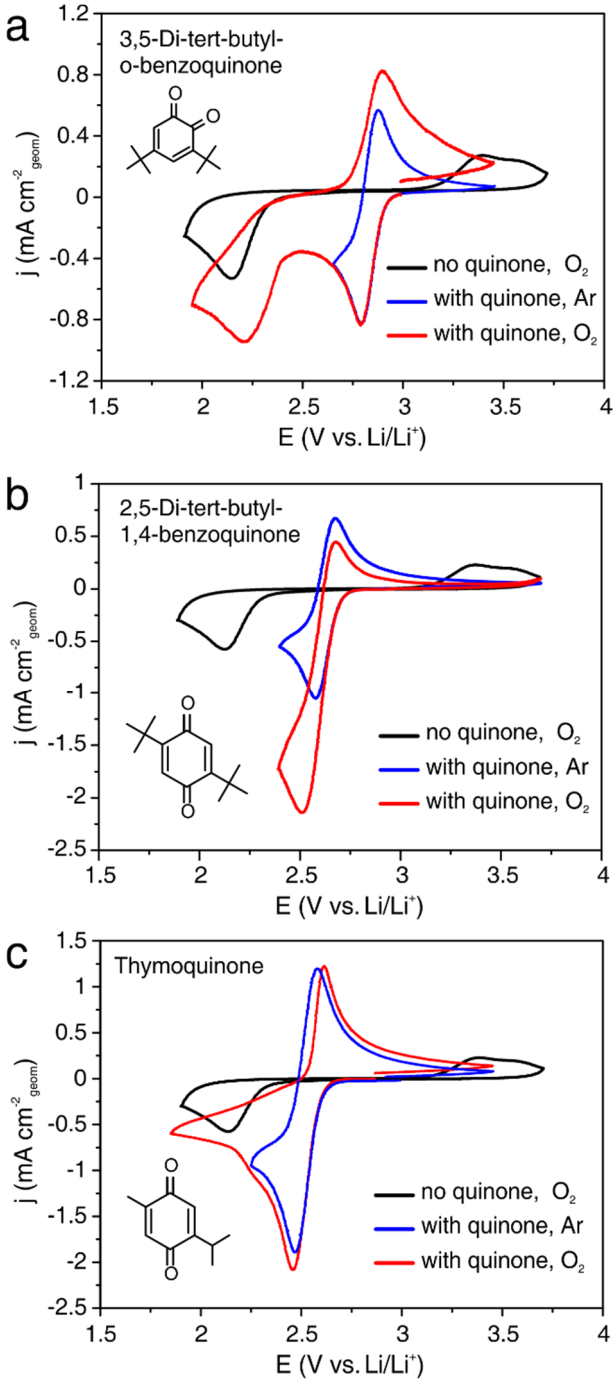


Figure 4-1. Cyclic voltammograms for electrolytes without quinone (black) and with various quinones in 1 M LiTFSI in TEGDME at a Au electrode under Ar (blue) and O_2 (red) **(a)** 3,5-di-tert-butyl-o-benzoquinone, **(b)** 2,5-di-tert-butyl-1,4-benzoquinone and **(c)** thymoquinone. Scan rate: 100 mV s^{-1}.

4.2 Electrochemistry studies with DBBQ

The CV curves for DBBQ obtained in 1 M LiTFSI in TEGDME and DME at a gold electrode under Ar exhibit quasi-reversible behavior, Fig. 4-2. In the presence of O_2, the reduction peaks are greatly enhanced in both solvent systems, indicating the regeneration of DBBQ. It is similar to that of a catalyzed reduction, where DBBQ is reduced first and then takes part in the following chemical reaction with O_2 to form Li_2O_2, regenerating more DBBQ, and at the same time giving rise to the increased reduction current. The reduction potential with the presence of DBBQ is much higher than the direct reduction of O_2, marked as black curves in Fig. 4-2, thus effectively suppressing the direct formation of Li_2O_2 on the electrode surface.

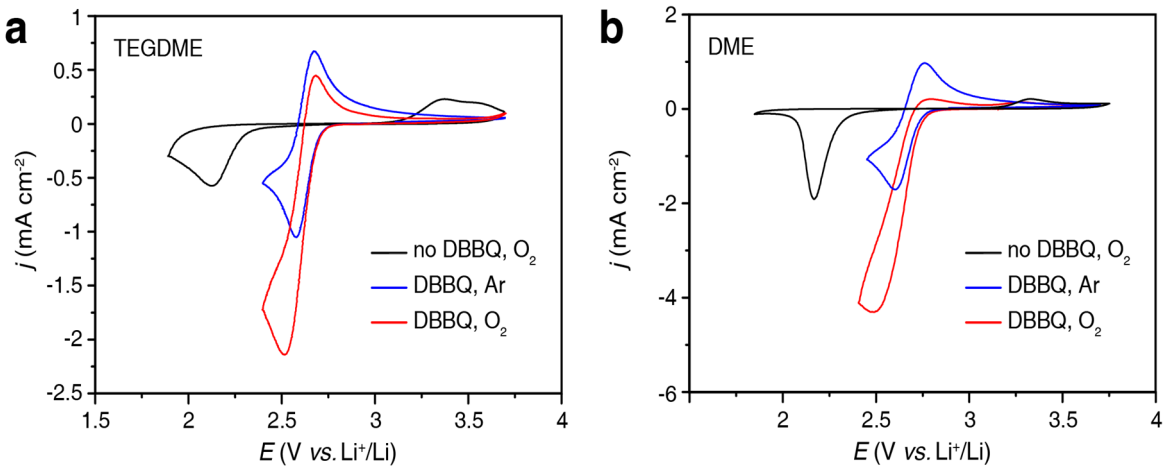


Figure 4-2. CVs demonstrating the significant effect DBBQ has on O_2 reduction in ethers. CVs for DBBQ in 1 M LiTFSI in **(a)** TEGDME and **(b)** DME. CVs under Ar (blue) and O_2 (red) and for direct O_2 reduction without DBBQ (black). DBBQ concentration was 10 mM and CVs were carried out at planar Au electrodes, at a scan rate of 100 mV s^{-1}.

No apparent current is observed below 3 V on oxidation without DBBQ. While in the presence of DBBQ, the oxidation of DBBQ is seen under O_2, but the current is much smaller than that under Ar, which is possibly due to some $DBBQ^-$ involved in chemical reactions

during the reduction. The oxidation of Li_2O_2 seen in the LiTFSI-based electrolyte is missing in the presence of DBBQ, which indicates that the reduction product, presumably Li_2O_2, might be dissolved in the electrolyte solution, away from the planar electrode surface.

4.3 Enhancing the cell performance of Li-O_2 cells with DBBQ

4.3.1 Discharge performance with DBBQ

The CV curves show the catalytic effect of DBBQ, and further studies of the effect of DBBQ on discharge in the cells are carried out. Cells containing TEGDME and DME saturated with O_2 (under 1 atm. of O_2) were each discharged at several different current densities with and without DBBQ, shown in Fig. 4-3. Three pieces of GDLs (3 mm * 3 mm) were stacked to form the cathode, similar to cathodes used widely for aprotic O_2 cells[1,9,10]. The electrolyte solution was 1 M LiTFSI dissolved in TEGDME or DME, without or with 10 mM DBBQ. Here, I only focus on the cathode and $LiFePO_4$ was chosen as the anode to avoid unwanted reactions involving lithium metal[1,11]. If lithium metal were directly used as the anode, it would react and reduce DBBQ to its reduction state, and therefore protected lithium would be required[12].

In the absence of DBBQ, the cells died rapidly, Fig. 4-3 (c) and (d), even at modest current densities, exhibiting very small capacities and poor rate capabilities, in accord with previous observations[1,12-14]. The same cells with the presence of DBBQ show dramatic improvements, delivering up to around 80-100 times higher discharge capacities before end of life and ensuring that areal current densities of 0.5 mA to 2 mA cm^{-2}_{areal} are possible, Fig. 4-3 (a), (b). In TEGDME with DBBQ, a capacity of 10.6 mAh cm^{-2}_{areal} (equivalent to 9.1 mg of Li_2O_2) was obtained at a current density of 0.2 mA cm^{-2}_{areal}, while in DME with DBBQ, 7.3 mAh cm^{-2}_{areal} (equivalent to 6.3 mg of Li_2O_2) was obtained at 0.5 mA cm^{-2}_{areal} and 4 mAh

cm^{-2}_{areal} (equivalent to 3.4 mg of Li_2O_2) at 1 mA cm^{-2}_{areal}. Moreover, the discharge potentials in the presence of DBBQ are higher by 0.1-0.15 V than without DBBQ, *i.e.* halving the discharge overpotential.

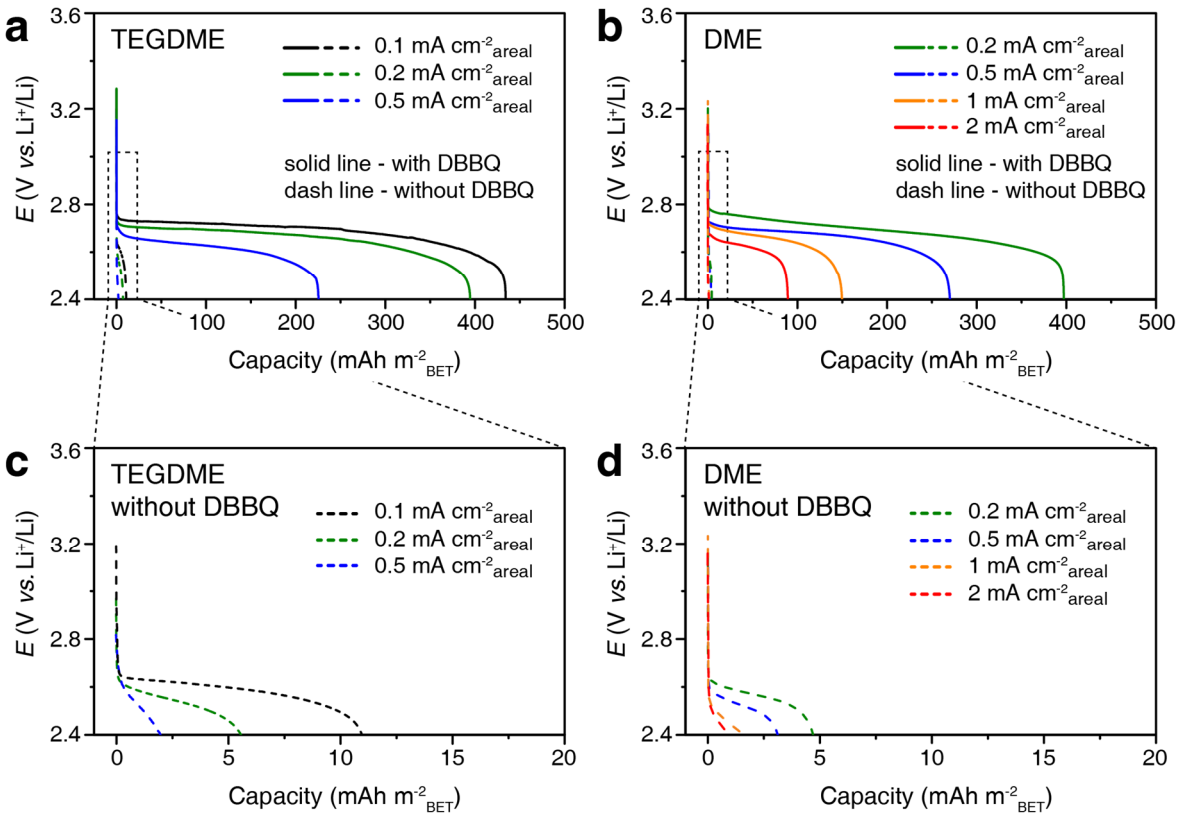


Figure 4-3. Significant effect of DBBQ on discharge in Li-O_2 cells. Load curves of O_2 reduction at gas diffusion electrodes discharged in 1 M LiTFSI in **(a)** TEGDME and **(b)** DME with 10 mM DBBQ (solid lines) and without DBBQ (dash lines) at various areal current densities from 0.1 mA cm^{-2} to 2 mA cm^{-2}. **(c)**, **(d)** enlarged section of load curves recorded without DBBQ in **(a)**, **(b)**, dash lines. The roughness factor of the cathode is 270.

It has been reported that the thickness of the Li_2O_2 film growth is limited to ~ 7 nm[6], which equates to a maximum capacity of ~ 15 mAh m^{-2}_{BET}. As is shown in Fig. 4-3 (c), (d), the cells without DBBQ exhibit end of life below this limit, indicating that Li_2O_2 is predominantly formed by the surface mechanism in both ether-based electrolytes. However, cells with DBBQ exceed this limit substantially, reaching ~ 400 mAh m^{-2}_{BET}, providing

some indirect evidence that Li_2O_2 is probably displaced away from the electrode surface. A close look at the load curves with DBBQ in Fig. 4-3 (c), (d) finds that the discharge curves remain quite flat during most of the discharge process. Until at some point, it reaches the potential where Li_2O_2 surface film formation commences at the late discharge stage and the voltage drops rapidly to the end of discharge. The rapid downturn is consistent with previous studies, in the absence of a mediator that assigns the end of discharge to Li_2O_2 film formation[15,16].

4.3.2 Charge performance with DBBQ

After discharge, the cycling performance of the cells with DBBQ in TEGDME and DME was evaluated, and the attempts to charge the cells with DBBQ proved to be fruitless, as shown in Fig. 4-4. No apparent capacity is seen on charge below 4 V, and only small amount of capacity, ~ 12 mAh m^{-2}_{BET} was charged back, which stands for only 2-3 % of the total discharge capacity.

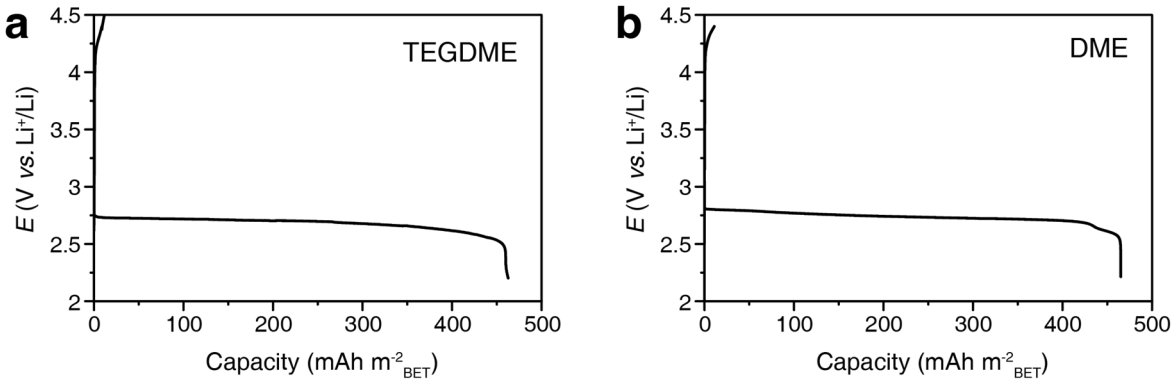


Figure 4-4. Discharge-charge profiles of cells with DBBQ in TEGDME and DME. Load Curves of GDLs discharged and charged in 10 mM DBBQ – 1 M LiTFSI in (a) TEGDME and (b) DME under O_2 at an areal current density of 0.1 mA cm^{-2}.

The failure to charge the cell actually indicates that Li_2O_2 is formed away from the electrode surface. Considering the large Li_2O_2 particles grown from the solution, they are not well

connected to the electrode surface and therefore it is difficult to be electrochemically oxidised directly[11]. The capacity charged back might be the oxidization of some Li_2O_2 film grown on the electrode surface at the end of discharge. Therefore, especially in the presence of a discharge mediator, it is necessary to employ a proper charge mediator to oxidise Li_2O_2 particles chemically[11,12,17-20], which will be discussed in Chapter 5.

4.4 Discharge product characterisations

4.4.1 SEM analysis

The CV measurements, the discharge curves and the failure to charge the cell in the presence of DBBQ all indicate the solution phase formation of Li_2O_2 in ether-based electrolytes. To confirm this directly, the discharged cells with and without DBBQ were extracted and examined by SEM, shown in Fig. 4-5. In both TEGDME and DME, in the absence of DBBQ, the electrode surface was covered with a thin film and there was no clear evidence of large particles, Fig. 4-5 (b), (f). In contrast, discharge in identical cells under the same conditions, except for the presence of 10 mM DBBQ in the electrolyte, showed substantial growth of large particles with ~ 200 nm particle size in the electrode pores. These particles have the toroidal morphologies expected for Li_2O_2, Fig. 4-5 (c)-(e), (g)-(i). However, the mechanism of the toroid formation is poorly understood. After half of the discharge, the electrode surface shows little evidence of film growth, Fig. 4-5 (c), (g). At the end of discharge, the electrode was filled with large Li_2O_2 particles and it was difficult to study the electrode surface. It has been proposed that Li_2O_2 toroids are more prevalent when significant quantities of H_2O are present in the electrolyte[9,21-23]. Therefore, rigorous care was taken to rule out the presence of large amounts of H_2O in the cell. The solvents were dried under molecular sieves, and the electrodes and all the cell components were dried under vacuum prior to use. After discharge, the H_2O amount in the cell was measured as well. The H_2O

content at the beginning and end of discharge did not exceed 30 ppm, considerably smaller than the quantities required for toroid particles formation, which is at least 200-500 ppm[9,21] and significant capacity increases. The SEM data demonstrate that DBBQ has successfully displaced O_2 reduction away from the electrode surface.

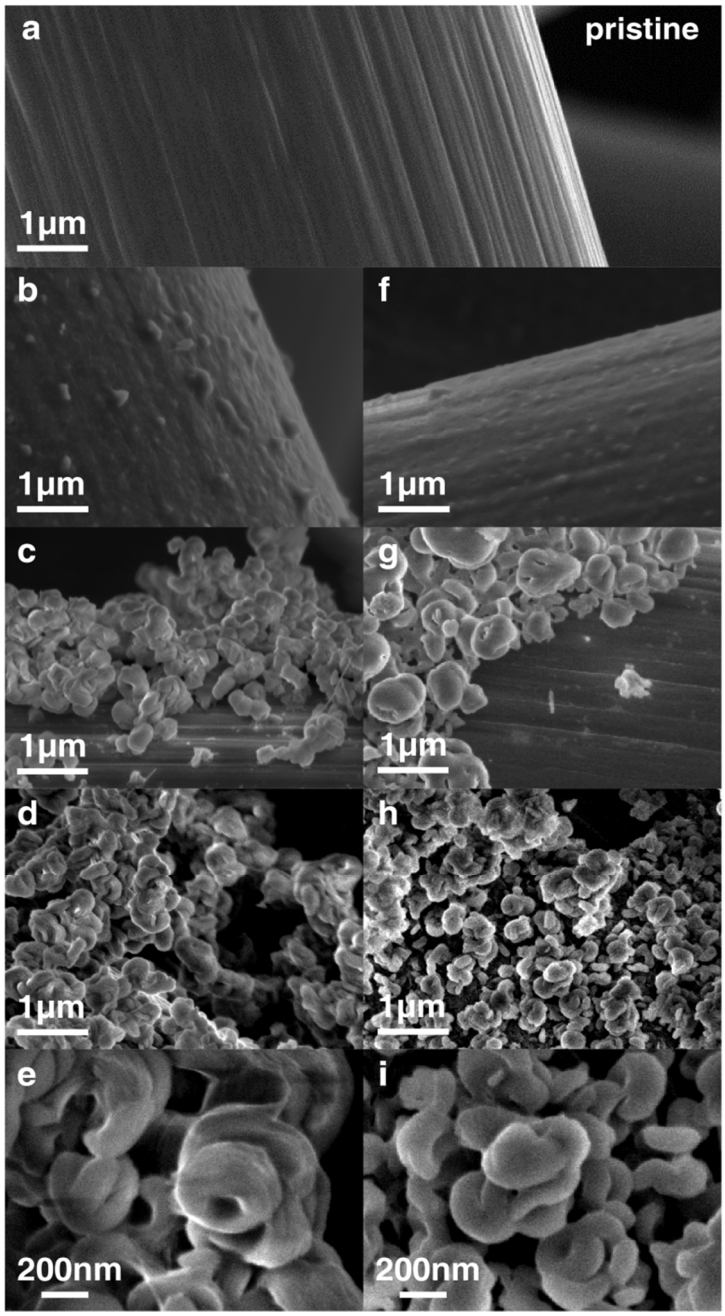


Figure 4-5. SEM images showing the Li_2O_2 morphologies on discharge in 1 M LiTFSI in ethers with and without DBBQ. (a) the pristine GDL; **(b-e)** discharge in TEGDME and **(f-i)** in DME. **(b, f)** full discharge without DBBQ; **(c, g)** half discharge and **(d, e, h, i)** full discharge with DBBQ.

4.4.2 PXRD, FTIR and Raman characterisations

SEM images in Fig. 4-5 prove the existence of large toroid particles after discharge. To confirm that the particles are indeed Li_2O_2, PXRD, FTIR and Raman characterisations were carried out on the discharge electrode. The results are shown in Fig. 4-6.

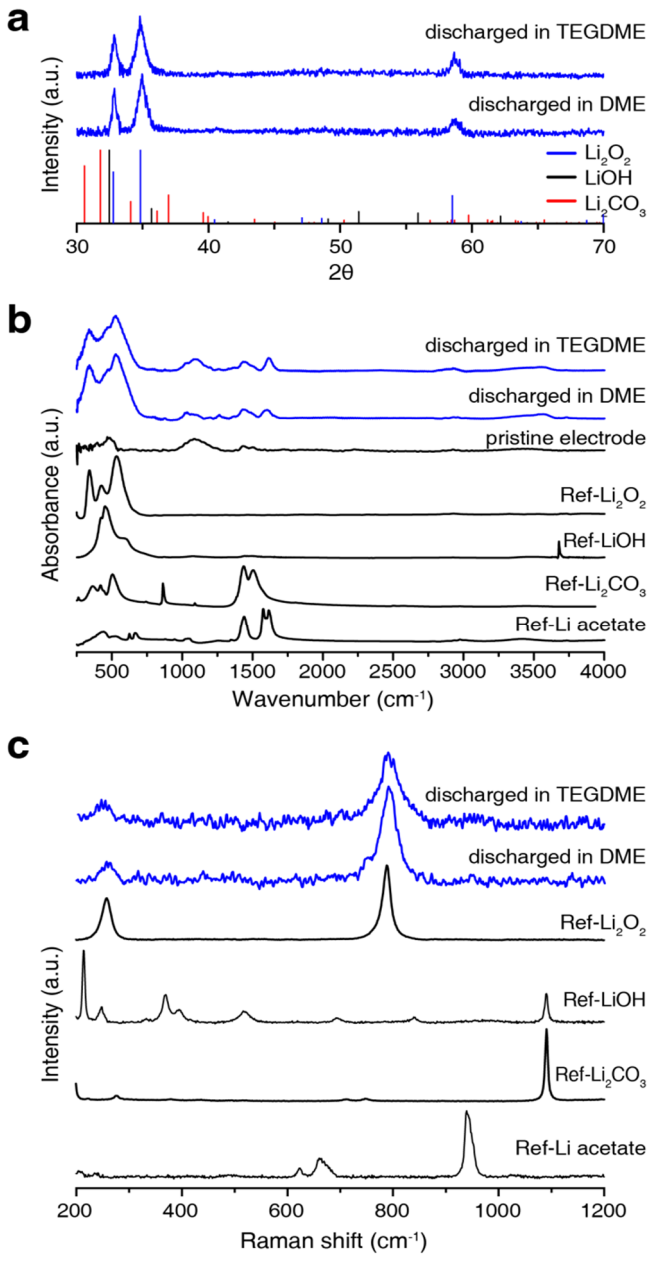


Figure 4-6. Characterisation of the discharge product confirming Li_2O_2 is dominant. (a) PXRD pattern, **(b)** IR and **(c)** Raman spectra of GDLs discharged in 10 mM DBBQ- 1 M LiTFSI in TEGDME and DME under O_2.

The PXRD patterns collected on GDLs discharged both in TEGDME and DME exhibit peaks associated with Li_2O_2, Fig. 4-6 (a). In particular, there is no clear evidence of LiOH and Li_2CO_3, confirming that Li_2O_2 is the dominant solid product on discharge. The results are further confirmed by FTIR and Raman spectra in Fig. 4-6 (b), (c), which also show Li_2O_2 as the primary products in both TEGDME and DME. No other peaks are observed in Raman spectra, Fig. 4-6 (c). However, in FTIR spectra in Fig. 4-6 (b), some other peaks besides Li_2O_2 are shown. There is little evidence of LiOH in the discharged electrode. Small peaks besides Li_2O_2 patterns in Fig. 4-6 (b), around 1000-2000 cm^{-1} are associated with lithium acetate, formate and carbonate that are common by-products due to the decomposition of glycol ether solvents[24,25]. These results show that the addition of DBBQ did not introduce new side products in the electrode and prove that the discharge represents the formation of Li_2O_2 rather than the DBBQ redox shuttling.

4.4.3 NMR analysis

To further study the side reactions and investigate the presence of soluble by-products, NMR was carried out on the electrolyte solutions after discharge. D-Chloroform was chosen as the base solvent. The results are shown in Fig. 4-7. Main peaks observed in Fig. 4-7, around 3~4 ppm, correspond to the electrolyte solvents like TEGDME and DME. The peaks with chemical shift of ~ 1.2 ppm and ~ 6.5 ppm are associated with the dissolved DBBQ in the electrolyte. In addition to these main peaks, a tiny peak is observed around 2 ppm chemical shift in both glycol ethers. It can be assigned to lithium acetate, in accord with the FTIR results. Although glycol ethers are one of the more stable solvents in Li-O_2 batteries[24], it is known that they are not completely stable and are readily to be attacked by superoxide and peroxide species to form lithium formate, acetate and carbonate, seen in Fig. 4-6, 4-7[24,25].

The NMR results indicate that DBBQ does not degrade during discharge nor introduce new side reactions.

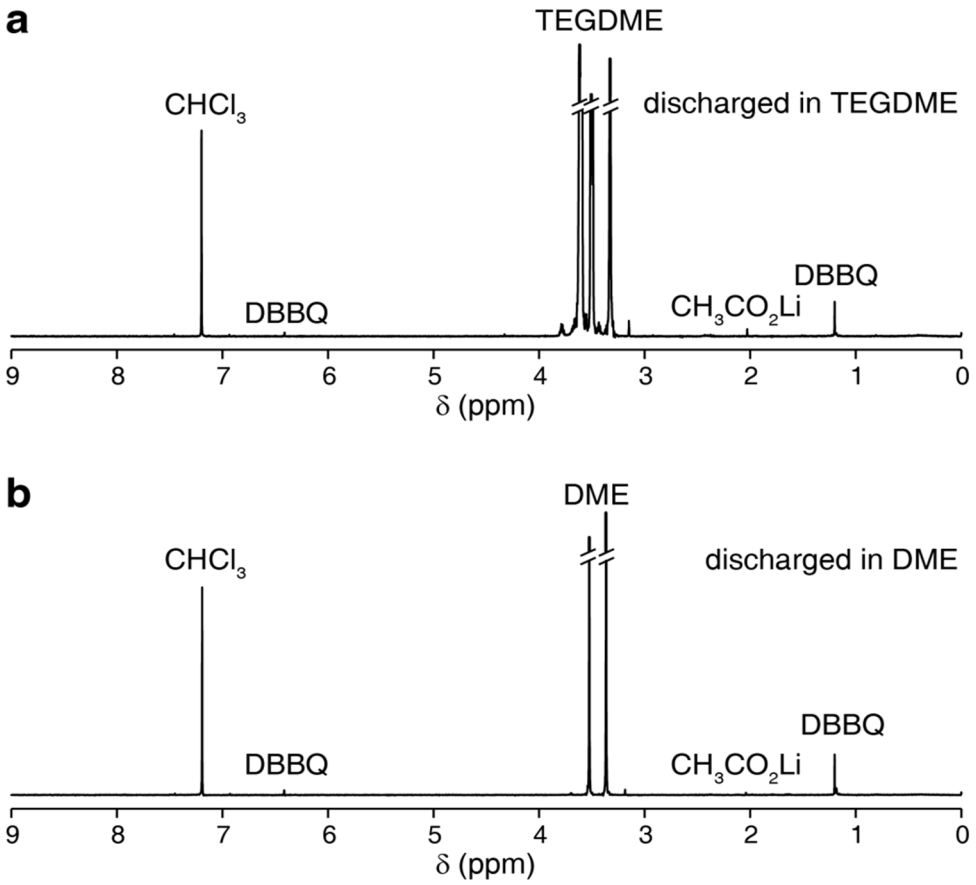


Figure 4-7. ^{1}H NMR spectra of electrolyte solutions after discharge demonstrating little side-reaction product. $CDCl_3$ extract from electrodes and separators in cells discharged in (**a**) TEGDME and (**b**) DME with 10 mM DBBQ - 1 M LiTFSI.

4.4.4 *In situ* DEMS analysis

FTIR and NMR results show the presence of side reactions. To further study the source of the side reactions, *in situ* DEMS was carried out to investigate the gas consumption during the discharge process with DBBQ. GDL served as the cathode and a partially oxidised $LiFePO_4$ composite electrode served as the anode. Considering the volatility of DME, here I only analysed the cell in TEGDME and the electrolyte solution was 10 mM DBBQ in 1 M

LiTFSI in TEGDME. A continuous 95% O_2 : 5% Ar gas flow was purged through the cell with the carrier gas at a flow rate of 0.3 ml min^{-1}. The results are presented in Fig. 4-8.

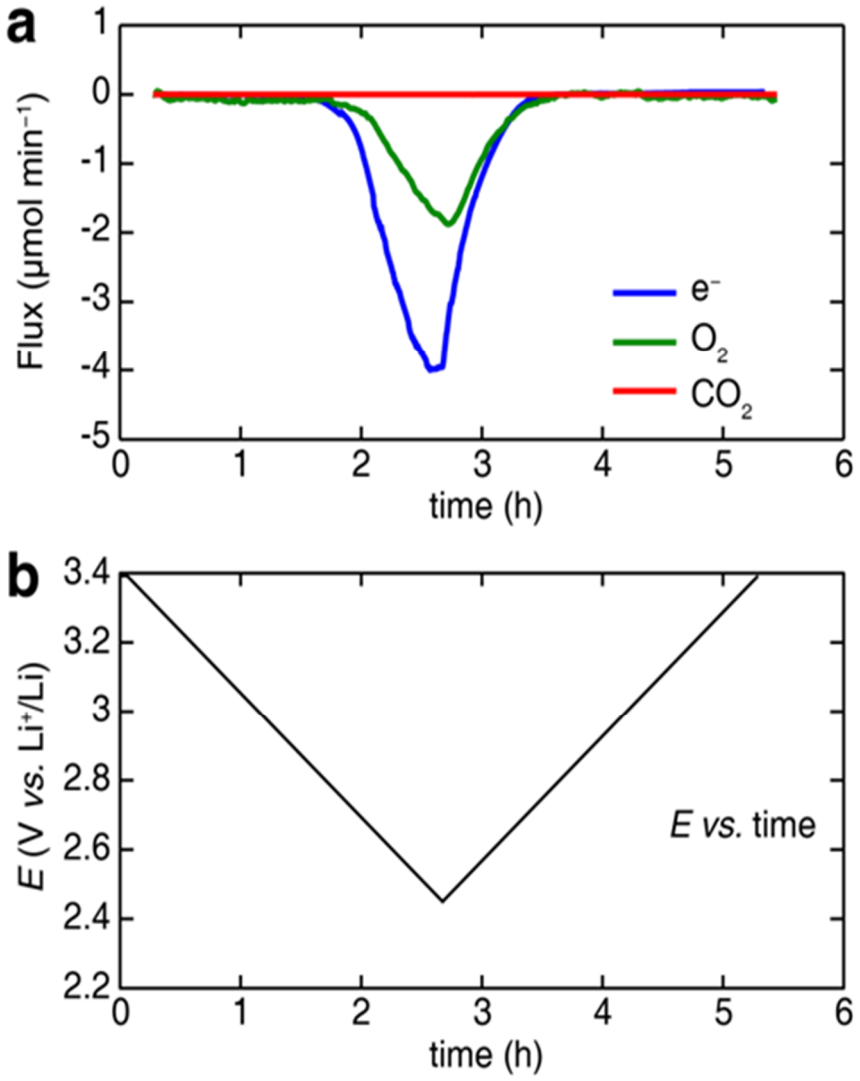


Figure 4-8. ***In situ*** **DEMS in DBBQ-TEGDME showing 2.03 e^- per O_2 consumption, consistent with formation of Li_2O_2. (a)** discharge current (blue), O_2 consumption (green) and CO_2 evolution (red) in 10 mM DBBQ - 1 M LiTFSI in TEGDME; **(b)** voltage profile of the DEMS cell. Cyclic voltammetry was applied. e^-/O_2 ratio was obtained from the integral of charge passed and total O_2 consumption.

No gases are detected other than O_2 consumption and in particular there is no evidence of CO_2 evolution, consistent with the side reactions being small in glycol ethers. The total O_2

consumed and total charge passed were measured and gave a charge to mass ratio of 2.03 e^-/O_2. It proves that the discharge is not the redox shuttling of DBBQ and the dominant reaction on discharge is a 2 e^- oxygen reduction, expected to be the formation of Li_2O_2[1,24,26]. The oxygen-charge ratio close to the theoretical 2 e^-/O_2 for Li_2O_2 formation also indicates that the intermediate is not heavily involved in side reactions, in accord with charge/mass ratio seen in previous studies in ethers[24]. Side reactions probably result from the instability of solvents with Li_2O_2 or singlet oxygen.

4.4.5 Yield measurements

FTIR, XRD, Raman and NMR shows that the addition of DBBQ does not induce new side reactions. DEMS indicates that Li_2O_2 might contribute to the solvent decomposition. In order to exclude the possibility of redox shuttling of DBBQ together with Li_2O_2 formation, yield measurements were carried out to quantify the amount of Li_2O_2 formed in the presence of DBBQ by chemical analysis with $TiOSO_4$ solution[1]. The yield percentage of Li_2O_2 with DBBQ was 95 % and 86 % in DME and TEGDME, respectively. This is even slightly higher than 91 % and 81 % reported for DME and TEGDME[24] and the yield with GDL as the electrode in TEGDME was even lower, ~ 60 %[1,9].

If the redox shuttling was happening together with the formation of Li_2O_2, the yield would be much lower. In fact, the higher yields in the presence of DBBQ suggest that the addition of DBBQ alleviates the side reactions between reactive Li_2O_2 with the electrolyte solutions. Considering the same amount of Li_2O_2, a Li_2O_2 film has a much higher surface area than large Li_2O_2 particles. The relatively high surface area of the Li_2O_2 film that grew on the electrode surface in the absence of DBBQ is likely to contribute to more electrolyte decomposition than the case for the large particles growing in solution with DBBQ. Furthermore, it has been suggested that the reactive intermediate LiO_2 is responsible for

some decomposition of ether-based electrolyte solutions[25-29]. With the presence of DBBQ, a more stable and low-energy intermediate would result in the higher yields as well.

4.5 Mechanism of O_2 reduction with DBBQ

4.5.1 Comparisons of several discharge electrocatalysts

Several soluble electrocatalysts like quinones[7], viologens[30-32] and phthalocyanines[33,34] have been investigated to improve the discharge performance. It is important to make a comparison among these electrocatalysts to understand the mechanisms of ORR with DBBQ. In some quinone cases, only electrochemical measurements alone were carried out to evaluate the performance[7]. Yet past work on Li-O_2 batteries have shown the necessity and importance of providing more than electrochemical evidence in this field[35]. It is difficult to evaluate the performance of quinones by the electrochemistry measurements alone.

Viologens work by transferring electrons from the electrode surface to O_2 in solution and reduce it by an outersphere electron transfer to LiO_2 and further to Li_2O_2[30-32]. It has a lower potential than for the direct reduction of O_2, which will still occur at this potential, therefore such redox shuttles cannot effectively avoid Li_2O_2 film formation on the electrode surface. In the case of DBBQ, if DBBQ worked as a simple redox shuttle, then the reaction

$$LiDBBQ + O_2 \rightarrow DBBQ + LiO_2 \qquad (4.1)$$

would be spontaneous, having a negative free energy charge. However, it is not this case by comparing the onset potentials of O_2 and DBBQ reduction in Fig. 4-1. Calculations based on E^0 for DBBQ/$DBBQ^-$ and the free energy of formation for LiO_2 indicates a ΔG^0 of approximately + 28 kJ mol^{-1} for reaction 4.1, which suggests that such a reaction is not happening and DBBQ is not acting as a redox shuttle as viologens.

Phthalocyanines works by binding O_2 first and the complex is reduced in solution to form Li_2O_2[33,34]. In this case, it shows an increase in discharge voltage (lower overpotential) as small as *e.g.* 50 mV, which is very unlikely to be sufficient to shutoff the direct reduction of O_2 to Li_2O_2, essential to stop detrimental Li_2O_2 film formation[34]. DBBQ is different from phthalocyanines as well. After binding with O_2, the reduction potential of the phthalocyanine has an innegligible potential shift comparing to that under Ar, however, such a potential shift is not observed in the case of DBBQ in Fig. 4-2.

It is further confirmed in Li^+-free electrolyte solution. The reduction potential of DBBQ in TBATFSI-based electrolyte in TEGDME and DME did not change when the gas atmosphere was switched from Ar to O_2, Fig. 4-9. The voltammograms for DBBQ under O_2 including the peak current and the redox potential position, remained the same as that under Ar in TBATFSI-based electrolyte. It is different from that seen in LiTFSI-based electrolyte shown in Fig. 4-2 where an increase in the reduction peak is observed under O_2, indicating the following chemical reaction and the regeneration of DBBQ requires the presence of Li^+. Li^+ activity will tune the DBBQ potential.

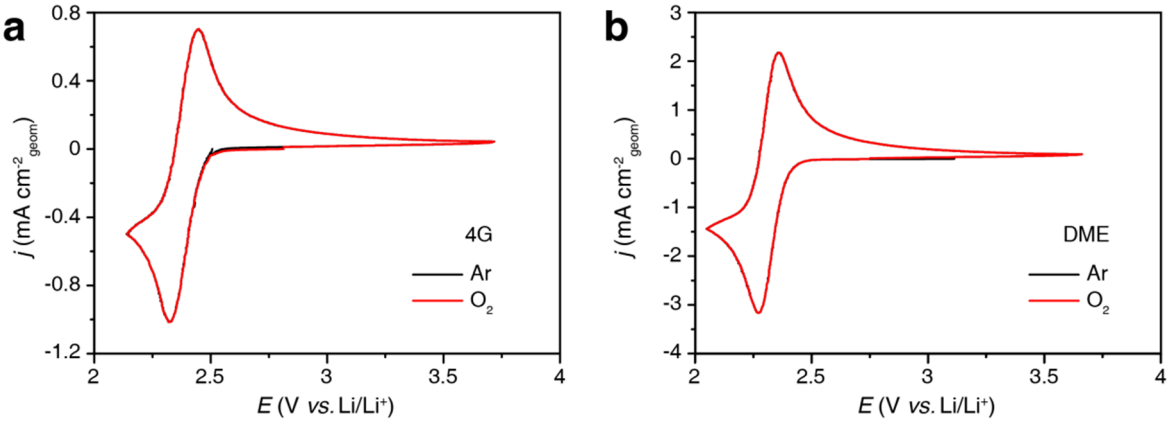


Figure 4-9. CVs of DBBQ in 1 M TBATFSI in (a) 4G and (b) DME under Ar and O_2 at a planar gold electrode at a scan rate of 100 mV s^{-1}.

Consequently, I can conclude that the reduction process with DBBQ is different from some other electrocatalysts mentioned above. Cells with DBBQ operate by a different mechanism that changes the pathway of O_2 reduction to Li_2O_2.

4.5.2 Mechanism

The reduction of quinones, such as DBBQ, in Li^+-based electrolyte solutions under Ar is known to form Li-quinone complexes[36-38], in this case, LiDBBQ, Fig. 4-1. In the presence of O_2, the reduction potential for DBBQ/LiDBBQ does not change, as shown in Fig. 4-2, indicating that the same reduction occurs and that there is no binding of O_2 to DBBQ before the initial electron transfer. The first step is DBBQ being reduced to LiDBBQ and is written in equation 4.2. However, the reduction current for DBBQ is enhanced significantly under O_2. Such a CV is similar to that of an EC_{cat} reaction, that the electrochemical reduction followed by a chemical step, in which the reduced form of the redox couple takes part in a chemical reaction that regenerates the oxidised form of the couple to feed the reduction. Here DBBQ is regenerated from LiDBBQ by the latter reducing O_2 in a chemical reaction, which goes on to form Li_2O_2.

In the absence of any discharge mediator, reduction of O_2 to Li_2O_2 proceeds via the reactive LiO_2 intermediate[3,9,22,39-41], and it is the need of reaching the potential for formation of LiO_2 that pins the O_2 reduction at a potential much lower than 2.96 V, the standard potential for O_2 reduction to Li_2O_2. As long as LiO_2 still forms as the intermediate, the discharge overpotential remains thermodynamically. A low-energy intermediate is required to facilitate the reduction to deliver a higher discharge plateau[42]. Here in the presence of DBBQ in Fig. 4-2, O_2 reduction effectively takes place at the potential for DBBQ reduction, which is significantly higher than that for direct ORR process via the LiO_2 intermediate in solution. This indicates that the oxygen reduction process involves the formation of a different

intermediate complex between LiDBBQ and O_2, as written in equation 4.3. By complexing Li^+, $DBBQ^-$ with O_2, the free energy of the intermediate (now a complex of the form $LiDBBQO_2$ rather than LiO_2) is lowered (Fig. 4-10) and the potential correspondingly shifted positive, as seen in the higher discharge voltage in galvanostatic discharge of Li-O_2 cells in Fig. 4-3. The sequences of the proposed reaction steps at the cathode on discharging a Li-O_2 cell containing DBBQ are summarised in following equations 4.2 to 4.4:

$$DBBQ_{(sol)} + Li^+_{(sol)} + e^- \rightarrow LiDBBQ_{(sol)} \qquad (4.2)$$

$$LiDBBQ_{(sol)} + O_{2(sol)} \rightleftharpoons LiDBBQO_{2(sol)} \qquad (4.3)$$

$$2\ LiDBBQO_{2(sol)} \rightarrow Li_2O_{2(s)} + O_{2(sol)} + 2\ DBBQ_{(sol)} \qquad (4.4a)$$

$$LiDBBQ_{(sol)} + LiDBBQO_{2(sol)} \rightarrow Li_2O_{2(s)} + 2\ DBBQ_{(sol)} \qquad (4.4b)$$

These reactions are summarised by the schematic shown in Fig. 4-10.

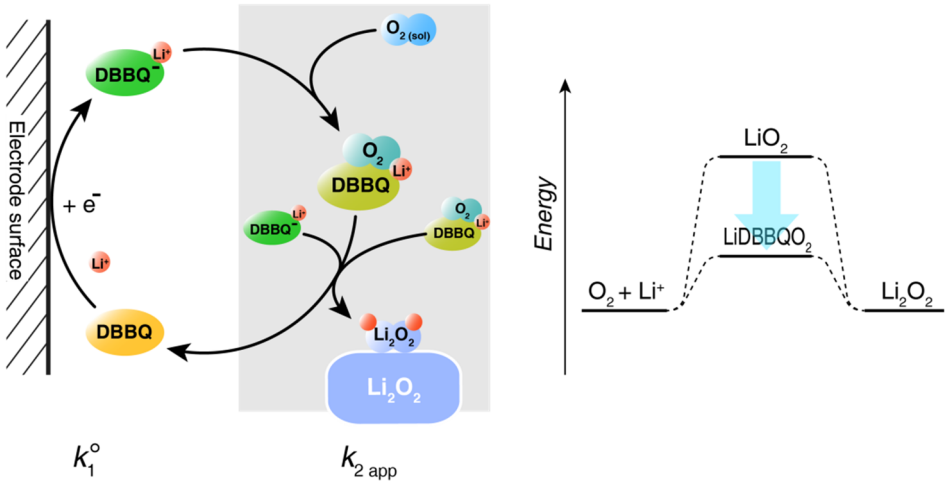


Figure 4-10. Schematics (left) of reactions on discharge and (right) the effect of DBBQ on the potential determining step. DBBQ is reduced at the electrode surface forming LiDBBQ, and then LiDBBQ reacts with O_2, producing Li_2O_2 and itself being regenerated to DBBQ. Schematic of free energy plot is at E^o for O_2/Li_2O_2.

DBBQ is reduced to LiDBBQ (equ 4.2), which then binds O_2 to form $LiDBBQO_2$ (equ 4.3). Equations (4.4a) and (4.4b) are two examples of possible steps by which the intermediate

$LiDBBQO_2$ could disproportionate or react with another LiDBBQ to form Li_2O_2 that grows from solution, and this liberates DBBQ molecules that can continue the cycle. The consequences of this scheme are relatively simple electron transfer and dominant formation of solution phase product that translate into high rates and capacities during cell discharge.

4.5.3 Kinetics of the catalytic reactions

To measure the rate of O_2 reduction to Li_2O_2 mediated by DBBQ, the kinetic rate constants of the initial heterogeneous electron transfer to DBBQ forming LiDBBQ, k_1^0, were obtained from the analysis of the relative peak-to-peak separation at different scan rates from CVs shown in Fig. 4-11. k_1^0 in TEGDME and in DME are 0.0011 cm s^{-1} and 0.0031 cm s^{-1}, respectively.

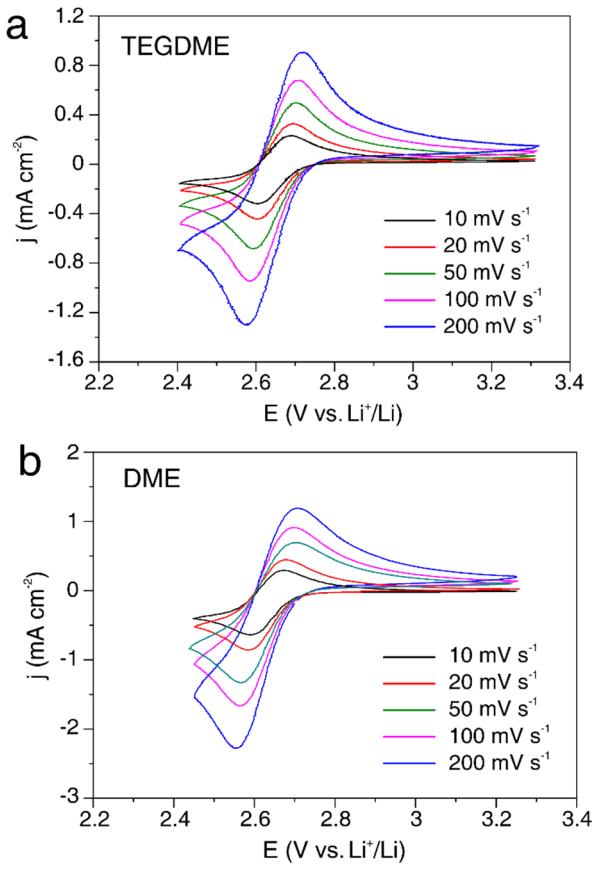


Figure 4-11. CVs in 10 mM DBBQ – 1 M LiTFSI in (a) TEGDME and (b) DME at GC electrode under Ar, at various scan rate from 10 mVs^{-1} to 200 mV^{-1}.

The overall kinetic rates of LiDBBQ reacting with O_2 to form Li_2O_2 were measured by UV-vis spectroscopy. The rate constant could not be obtained in DME due to the fast reaction, beyond the measurement limit. It was also impossible to separate the two chemical pathways; instead, an apparent overall kinetic rate constant for the combined chemical reactions in TEGDME, $k_{2\ app}$ was obtained. First, 2 mM DBBQ in TEGDME was allowed to react with Li metal pieces to form LiDBBQ. The yellowish solution was decanted into a vial and the exact concentration of LiDBBQ was determined by measuring steady state current using a gold ultramicro electrode. The concentration of LiDBBQ formed after an hour in TEGDME was 0.2 mM. 1 ml of such LiDBBQ solution was added into a quartz cuvette in a glovebox and transferred to measure its UV-vis spectra. LiDBBQ has a strong absorption band at 408 nm, shown as blue line in Fig. 4-12 (a). When O_2 was added into the LiDBBQ solution, the yellow colour faded and no apparent peak at 408 nm was observed after some time, shown as the red line in Fig. 4-12 (a). The absorbance at 408 nm, A, was recorded as a function of time. A sharp decrease of absorbance was observed when various amounts of O_2 saturated TEGDME was injected into the cuvette, Fig. 4-12 (b).

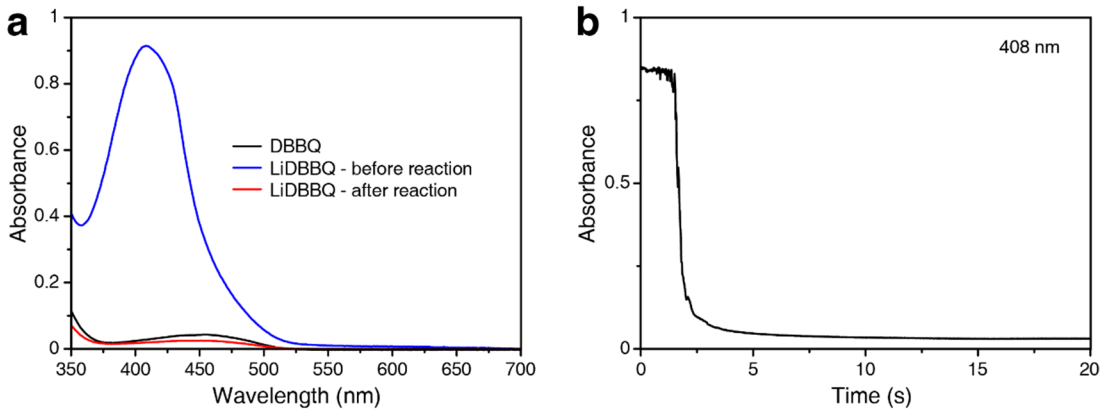


Figure 4-12. Schematics (left) of reactions on discharge and (right) the effect of DBBQ on the potential determining step. DBBQ is reduced at the electrode surface forming LiDBBQ, and then LiDBBQ reacts with O_2, producing Li_2O_2 and itself being regenerated to DBBQ. Schematic of free energy plot is at E^o for O_2/Li_2O_2.

The overall kinetic rates of LiDBBQ reacting with O_2 to form Li_2O_2 vary with the O_2 concentration, which shows that the overall chemical reaction is not a simple first-order reaction. In fact, the resulting plots of 1/A against time, shown in Fig. 4-13, is consistent with a pseudo-second-order reaction. The rate constants for the chemical reactions in TEGDME are shown in Table 4-1.

However, since the electrochemical reduction of DBBQ and the reaction of LiDBBQ with O_2 to form Li_2O_2 are not in the same order, comparing the reaction rate of these two is not trivial. Besides, it is impossible to separate the two chemical pathways and therefore it is difficult to know which step is rate determining.

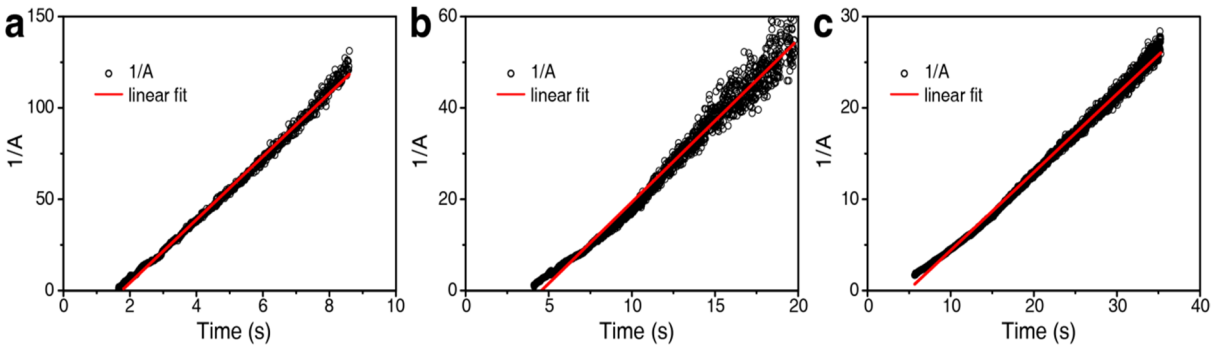


Figure 4-13. Analysis of kinetic rate of LiDBBQ reacting with O_2 in TEGDME. UV-Vis adsorption recorded at 408 nm of LiDBBQ in TEGDME after addition of (a) 1 ml, (b) 0.2 ml, (c) 0.1 ml of O_2 saturated TEGDME. Circles-experimental points, solid line-linear least squares fit.

Table 4-1 Rate constants for LiDBBQ reacting with various O_2 concentrations in TEGDME.

$[O_2]$ (mM)	**$k_{2\ app}$ (L mol^{-1} s^{-1})**
2	7100
0.67	1500
0.36	360

4.6 Conclusions

In this chapter, the addition of DBBQ to weakly solvating electrolyte solutions is shown to promote O_2 reduction to Li_2O_2 in solution via a new route that avoids the reactive LiO_2 intermediate. DBBQ is reduced to LiDBBQ, which acts as the reducing agent for O_2. O_2 binds to LiDBBQ, forming a $LiDBBQO_2$ complex, which is a new low-energy intermediate. The latter step is vital to catalysing the reaction, which is otherwise limited by surface LiO_2 formation. By the addition to the catalysis, this new cell chemistry introduces a number of benefits. The electrochemistry at the electrode surface is now DBBQ reduction rather than direct formation of Li_2O_2, and therefore, Li_2O_2 formation is shifted into solution without the need of high donor/acceptor number solvents or salts. DBBQ blocks off the direct formation of Li_2O_2 thin film on the cathode, thus postponing cell death and at the same time, increasing capacity 80-100 fold and facilitating discharge rates of > 1 mA cm^{-2}_{areal} for cathodes with capacities of > 4 mAh cm^{-2}_{areal}. The discharge potential is increased to gain more energy the cell delivers.

The discharge mediators might bring some issues to the cell. The characterisations show that DBBQ does not bring any new side reactions to the cell. However, the long-time stability of the mediator is not examined. Besides, the large Li_2O_2 particles growing from solution are poorly connected to the electrode surface and the direct oxidation proves to be difficult. Charge mediators are required to oxidise such large particles discharged via a solution mechanism.

From FTIR and NMR results, it is known that the ethers used in this project still suffer from decomposition. Parasitic reactions involving the electrolyte remained a significant source of decomposition. The good news is that there is no need to search for highly polar solvents which are easier to decompose. The search for truly stable electrolyte solutions for Li-O_2

batteries can focus on very low polarity and hence weakly solvating solvents. If such stable solvents can be identified, then DBBQ provides a route to solution growth of Li_2O_2 and hence potentially high rates, high capacities and sustained cycling can be achieved, avoiding early cell death.

4.7 References

1 Gao, X., Jovanov, Z. P., Chen, Y., Johnson, L. R. & Bruce, P. G. Phenol-catalyzed discharge in the aprotic lithium-oxygen battery. *Angew. Chem. Int. Ed.* **56**, 6539-6543 (2017).

2 Aurbach, D., McCloskey, B. D., Nazar, L. F. & Bruce, P. G. Advances in understanding mechanisms underpinning lithium–air batteries. *Nat. Energy* **1**, 16128 (2016).

3 Johnson, L. *et al.* The role of LiO_2 solubility in O_2 reduction in aprotic solvents and its consequences for Li–O_2 batteries. *Nat. Chem.* **6**, 1091-1099 (2014).

4 Burke, C. M., Pande, V., Khetan, A., Viswanathan, V. & McCloskey, B. D. Enhancing electrochemical intermediate solvation through electrolyte anion selection to increase nonaqueous Li-O_2 battery capacity. *Proc. Natl. Acad. Sci. U. S. A.* **112**, 9293-9298 (2015).

5 Gao, X., Chen, Y., Johnson, L. & Bruce, P. G. Promoting solution phase discharge in Li-O_2 batteries containing weakly solvating electrolyte solutions. *Nat. Mater.* **15**, 882–888 (2016).

6 Luntz, A. C. *et al.* Tunneling and polaron charge transport through Li_2O_2 in Li–O_2 batteries. *J. Phys. Chem. Lett.* **4**, 3494-3499 (2013).

7 Matsuda, S., Hashimoto, K. & Nakanishi, S. Efficient Li_2O_2 formation via aprotic oxygen reduction reaction mediated by quinone derivatives. *J. Phys. Chem. C* **118**, 18397-18400 (2014).

8 Guin, P. S., Das, S. & Mandal, P. C. Electrochemical reduction of quinones in different media: a review. *Int. J. Electrochem.* **2011**, 1-22 (2011).

9 Schwenke, K. U., Metzger, M., Restle, T., Piana, M. & Gasteiger, H. A. The influence of water and protons on Li_2O_2 crystal growth in aprotic Li-O_2 cells. *J. Electrochem. Soc.* **162**, A573-A584 (2015).

10 Hartmann, P. *et al.* A rechargeable room-temperature sodium superoxide (NaO_2) battery. *Nat. Mater.* **12**, 228-232 (2013).

11 Chen, Y., Freunberger, S. A., Peng, Z., Fontaine, O. & Bruce, P. G. Charging a Li–O_2 battery using a redox mediator. *Nat. Chem.* **5**, 489–494 (2013).

12 Aurbach, D., McCloskey, B. D., Nazar, L. F. & Bruce, P. G. Advances in understanding mechanisms underpinning lithium–air batteries. *Nat. Energy* **1**, 16128 (2016).

13 Girishkumar, G., McCloskey, B., Luntz, A. C., Swanson, S. & Wilcke, W. Lithium−air battery: promise and challenges. *J. Phys. Chem. Lett.* **1**, 2193-2203 (2010).

14 Lu, Y.-C. *et al.* The discharge rate capability of rechargeable Li-O_2 batteries. *Energy Environ. Sci.* **4**, 2999-3007 (2011).

15 Grübl, D., Bergner, B., Schröder, D., Janek, J. & Bessler, W. G. Multistep reaction mechanisms in nonaqueous lithium–oxygen batteries with redox mediator: a model-based study. *J. Phys. Chem. C* **120**, 24623-24636 (2016).

16 Hojberg, J. *et al.* An electrochemical impedance spectroscopy investigation of the overpotentials in Li-O_2 batteries. *ACS Appl. Mater. Interfaces* **7**, 4039-4047 (2015).

17 Bergner, B. J., Schurmann, A., Peppler, K., Garsuch, A. & Janek, J. TEMPO: a mobile catalyst for rechargeable Li-O_2 batteries. *J. Am. Chem. Soc.* **136**, 15054-15064 (2014).

18 Lim, H. D. *et al.* Superior rechargeability and efficiency of lithium-oxygen batteries: hierarchical air electrode architecture combined with a soluble catalyst. *Angew. Chem. Int. Ed.* **53**, 3926-3931 (2014).

19 Kundu, D., Black, R., Adams, B. & Nazar, L. F. A highly active low voltage redox mediator for enhanced rechargeability of Lithium–oxygen batteries. *ACS Cent. Sci.* **1**, 510-515 (2015).

20 Yao, K. P. C. *et al.* Utilization of cobalt bis(terpyridine) metal complex as soluble redox mediator in Li–O_2 batteries. *J. Phys. Chem. C* **120**, 16290-16297 (2016).

21 Meini, S., Piana, M., Tsiouvaras, N., Garsuch, A. & Gasteiger, H. A. The effect of water on the discharge capacity of a non-catalyzed carbon cathode for Li-O_2 batteries. *Electrochem. Solid-State Lett.* **15**, A45-A48 (2012).

22 Aetukuri, N. B. *et al.* Solvating additives drive solution-mediated electrochemistry and enhance toroid growth in non-aqueous Li-O_2 batteries. *Nat. Chem.* **7**, 50-56 (2015).

23 Zhu, Y. G. *et al.* Proton enhanced dynamic battery chemistry for aprotic lithium-oxygen batteries. *Nat. Commun.* **8**, 14308 (2017).

24 McCloskey, B. D. *et al.* Combining accurate O_2 and Li_2O_2 assays to separate discharge and charge stability limitations in nonaqueous Li–O_2 batteries. *J. Phys. Chem. Lett.* **4**, 2989-2993 (2013).

25 Freunberger, S. A. *et al.* The lithium-oxygen battery with ether-based electrolytes. *Angew. Chem. Int. Ed.* **50**, 8609-8613 (2011).

26 Chen, Y., Freunberger, S. A., Peng, Z., Barde, F. & Bruce, P. G. Li-O_2 battery with a dimethylformamide electrolyte. *J. Am. Chem. Soc.* **134**, 7952-7957 (2012).

27 Sharon, D. *et al.* Oxidation of dimethyl sulfoxide solutions by electrochemical reduction of oxygen. *J. Phys. Chem. Lett.* **4**, 3115-3119 (2013).

28 Adams, B. D. *et al.* Towards a stable organic electrolyte for the Lithium oxygen battery. *Adv. Energy Mater.* **5**, 1400867 (2015).

29 Zhang, Z. *et al.* Increased stability toward oxygen reduction products for lithium-air batteries with oligoether-functionalized silane electrolytes. *J. Phys. Chem. C* **115**, 25535-25542 (2011).

30 Lacey, M. J., Frith, J. T. & Owen, J. R. A redox shuttle to facilitate oxygen reduction in the lithium air battery. *Electrochem. Commun.* **26**, 74-76 (2013).

31 Yang, L., Frith, J. T., Garcia-Araez, N. & Owen, J. R. A new method to prevent degradation of lithium-oxygen batteries: reduction of superoxide by viologen. *Chem. Commun.* **51**, 1705-1708 (2015).

32 Lodge, A. W., Lacey, M. J., Fitt, M., Garcia-Araez, N. & Owen, J. R. Critical appraisal on the role of catalysts for the oxygen reduction reaction in lithium-oxygen batteries. *Electrochim. Acta* (2014).

33 Trahan, M. J. *et al.* Cobalt phthalocyanine catalyzed lithium-air batteries. *J. Electrochem. Soc.* **160**, A1577-A1586 (2013).

34 Sun, D. *et al.* A solution-phase bifunctional catalyst for lithium-oxygen batteries. *J. Am. Chem. Soc.* **136**, 8941-8946 (2014).

35 Imanishi, N., Luntz, A. C. & Bruce, P. G. *The lithium air battery: fundamentals*. (Springer, 2014).

36 Lee, M. *et al.* Redox cofactor from biological energy transduction as molecularly tunable energy-storage compound. *Angew. Chem. Int. Ed.* **52**, 8322-8328 (2013).

37 Hanyu, Y. & Honma, I. Rechargeable quasi-solid state lithium battery with organic crystalline cathode. *Sci. Rep.* **2**, 453 (2012).

38 Peover, M. E. & Davis, J. D. The influence of ion-association on the polarography of quinones in dimethylformamide. *J. Electroanal. Chem.* **6**, 46-53 (1963).

39 Hummelshoj, J. S., Luntz, A. C. & Norskov, J. K. Theoretical evidence for low kinetic overpotentials in Li-O_2 electrochemistry. *J. Chem. Phys.* **138**, 034703 (2013).

40 Laoire, C. O., Mukerjee, S., Abraham, K. M., Plichta, E. J. & Hendrickson, M. A. Influence of nonaqueous solvents on the electrochemistry of oxygen in the rechargeable lithium−air battery. *J. Phys. Chem. C* **114**, 9178-9186 (2010).

41 Adams, B. D. *et al.* Current density dependence of peroxide formation in the Li-O_2 battery and its effect on charge. *Energy Environ. Sci.* **6**, 1772-1778 (2013).

42 Koper, M. T. M. Thermodynamic theory of multi-electron transfer reactions: implications for electrocatalysis. *J. Electroanal. Chem.* **660**, 254-260 (2011).

Chapter 5. A rechargeable aprotic Li-O_2 battery with dual mediators stabilizing the carbon electrode

In Chapter 4, the addition of DBBQ has successfully displaced the formation of Li_2O_2 away from the electrode surface via solution mechanism. Li_2O_2 is the product formed and discomposed, which results in the advantages of its high specific capacity to store charge, 3500 Wh kg^{-1}. However, the disadvantages arise at the same time due to its insulating and insoluble nature[1-12]. By forming Li_2O_2 particles from solution in low DN solvents, it avoids the thin passivating film formation and enables the high discharge capacities and high rates in relatively stable solvents[2,5,10,13,14].

However, the large Li_2O_2 particles formed from solution are poorly connected to the electrode surface and therefore electronically isolated during charging. The attempts to charge the cells with the presence of DBBQ proves to be fruitless and oxidation/charge mediators are required[15]. A charge redox mediator is a molecule that can be oxidised at the electrode surface on charging and transfer holes to the electronically isolated Li_2O_2 particles in solution. Thus, Li_2O_2 can be oxidised and O_2 is accordingly regenerated, with the mediator molecular being reduced and regenerated back to the electrode surface for the cycle to be repeated[16-26].

Here I propose that Li_2O_2 can be formed and oxidised in solution by combining the dual mediators in the electrolyte. Such a dual-mediator cell would decouple completely the process of energy storage (formation and decomposition of Li_2O_2 in solution) from the electrochemistry reactions at the electrode surface. By avoiding the insulating and insoluble properties of Li_2O_2, the cell should achieve relatively high capacities and high rates with low polarisation on charge and discharge.

5.1 Selection criteria for the charge mediator

As discussed in Chapter 1, many charge mediators have been reported with various properties, which must be considered when choosing a charge mediator for a high performance cell. To act as a suitable charge mediator, it must have a redox potential above the thermodynamic potential for the O_2/Li_2O_2 reaction (2.96 V vs. Li^+/Li). The redox process has to be highly reversible to sustain the regeneration of the mediator and the heterogeneous rate constant is preferably high enough to support the charging rates. The molecule needs to be relatively stable against reduced oxygen species and singlet oxygen to minimise the decomposition, resulting in extended cycling performance.

In this work, TEMPO is chosen as the charge mediator, as it is known to exhibit desirable redox potential (higher than 2.96 V), reversible redox process itself, high electrochemical stability, relatively fast redox kinetics for oxidation of Li_2O_2 and enables sufficient oxygen solubility[16,27,28].

5.2 Electrochemistry performance with dual mediators

Fig. 5-1 presents the voltammograms for DBBQ and TEMPO under Ar and O_2 in 0.3 M $LiClO_4$ in DME at a scan rate of 100 mV s^{-1}. $LiClO_4$ is chosen in this work as the source of Li^+, rather than LiTFSI, because $LiClO_4$ is easier to purify and has higher stability against reactive oxygen species, and thus is a better choice for long time cycling[29]. A concentration of 0.3 M $LiClO_4$ is set for this work due to its moderate solubility in DME.

Under Ar, clean voltammograms for both DBBQ and TEMPO are observed in Fig. 5-1 (blue line), indicating that the two mediators do not interact with each other. The E^0 of DBBQ and TEMPO are 2.55 V and 3.72 V respectively in DME, which is similar to previous studies[15,16]. When the gas was switched to O_2, both the reduction and oxidation peak current were greatly

enhanced (red line in Fig. 5-1), indicating the regeneration of DBBQ on reduction and TEMPO on oxidation, similar to the catalysed reactions on reduction and oxidation. The voltammogram data gives me some evidence of both mediators catalysing the electrochemistry in the cell.

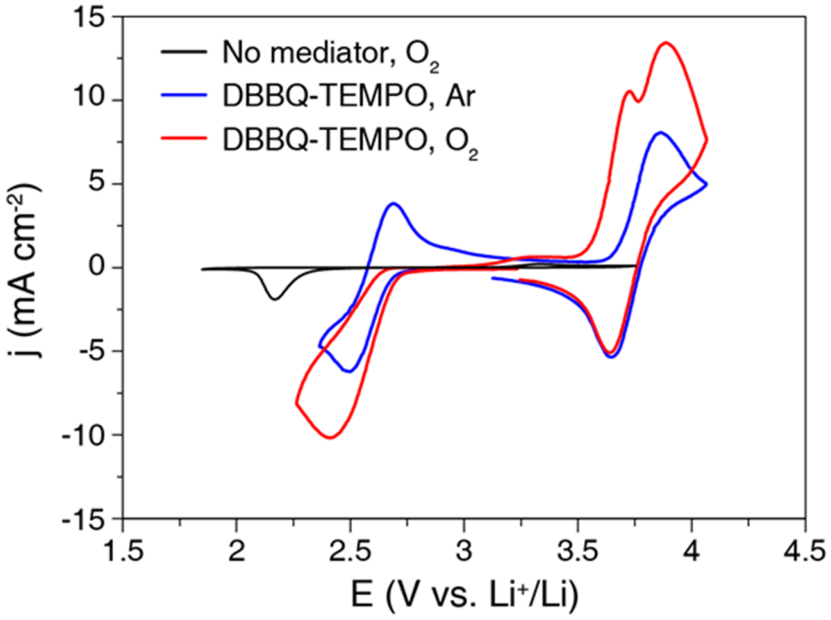


Figure 5-1. CVs for DBBQ and TEMPO in 0.3 M $LiClO_4$ in DME under Ar (blue) and O_2 (red) and for direct O_2 reduction without mediators under O_2 (black). 25 mM DBBQ and 25 mM TEMPO were used. Au electrode. Scan rate 100 mV s^{-1}.

5.3 Enhancing the cell performance with dual mediators

5.3.1 Cell design

In order to study the effect of both mediators during cycling in the cell, a dual-mediator Li-O_2 cell was constructed, where 3 pieces of GDL (4 mm in diameter) served as the cathode, and LFP served as the anode to avoid side reactions involving the lithium metal[14,15,30]. The cell potentials were corrected and given with respect to Li^+/Li. The electrolyte was 300 mM $LiClO_4$ in DME with 25 mM DBBQ and 25 mM TEMPO. The schematic of the cell is

shown in Fig. 5-2. It should be noted that the so-called GDL electrode is not a true gas diffusion electrode used in fuel cell studies where O_2 is delivered along gas channels to the electrolyte/electrode interface. Here it is simply a porous carbon cathode flooded with the electrolyte solution and only the side opposite to the electrolyte saturated separator is exposed to the O_2 atmosphere.

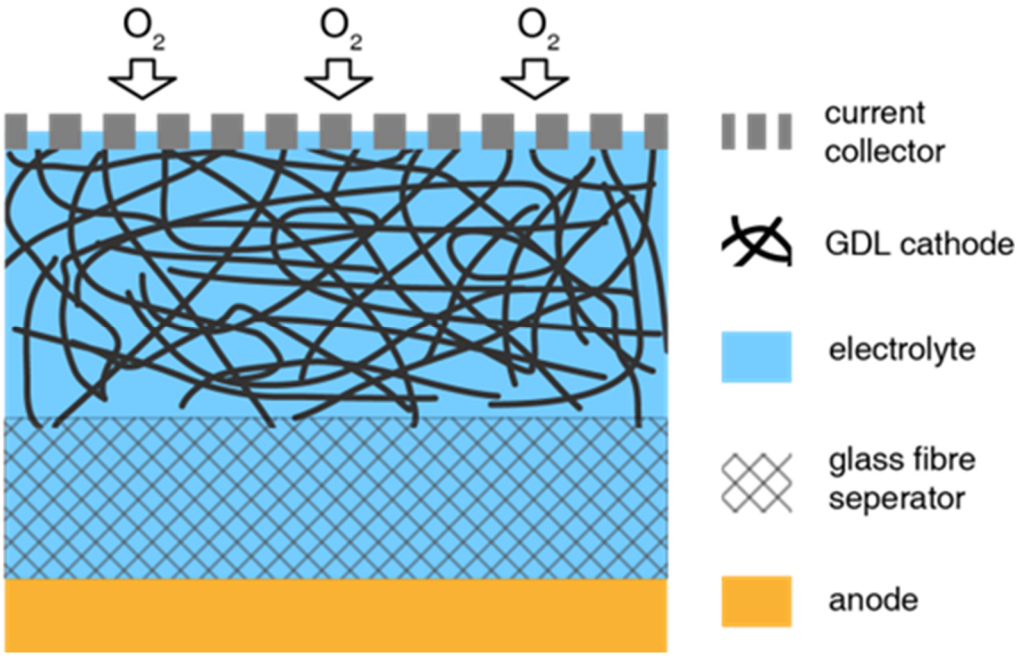


Figure 5-2. Schematic of a cell with a GDL based porous carbon electrode, which is flooded with electrolyte and lacks gas diffusion channels for O_2.

5.3.2 Optimising cycling conditions

The cell with DBBQ and TEMPO was first discharged to the maximum capacities with the voltage cut off at 2 V and charged back at a current density of 1 mA cm^{-2}_{areal}, shown in Fig. 5-3 (a). After discharge, the electrodes were washed, dried and analysed, with the SEM images shown in Fig. 5-3. A close observation on the discharge load curve shows that the voltage did not change significantly until it reached a capacity of ~ 2 mAh cm^{-2}_{areal}. When the cathode was analysed *ex situ* by SEM at 2 mAh cm^{-2}_{areal}, the image shows large toroid

particles, expected for Li_2O_2 and no obvious surface film is found, Fig. 5-3 (b). This is similar to the cell discharged with DBBQ sorely as the discharge mediator in the cell. As the discharge continued beyond 2 mAh cm^{-2}_{areal}, a gentle decrease on the voltage becomes more and more obvious, until the cell suddenly died after 3 mAh cm^{-2}_{areal}. As is mentioned, the GDL cathode was exposed to O_2 only on the side opposite to the electrolyte/separator, therefore, when DBBQ was reduced to LiDBBQ, it preferentially combined with O_2 to form Li_2O_2 at the electrode/gas interface where O_2 was readily available. Li_2O_2 is therefore distributed unevenly in the electrode. As is shown in Fig. 5-3 (c), the pores became clogged at the electrode/gas interface, while at the electrode/electrolyte interface, much less Li_2O_2 is found with the pores unclogged, shown in Fig. 5-3 (d).

At the capacity above 2 mAh cm^{-2}_{areal}, the pores at the electrode/gas interface were heavily clogged, impeding mass transport, leading to the large polarization that further reduced the discharge voltage more significantly as observed. As the voltage continued to decrease, it reached a potential where Li_2O_2 film formation commenced and the voltage then dropped rapidly to the end of discharge, shown in Fig. 5-3 (a). This rapid downturn is consistent with previous studies, in the absence of a mediator, that assign the end of discharge to Li_2O_2 film formation[31,32]. At the beginning of charge, a large overpotential is observed in Fig. 5-3 (a). This was probably due to the fact that the cathode surface was covered by an insulating film of Li_2O_2 with some side products like lithium formate and acetate at the end of discharge. Besides, the pores at the electrode/gas interface were heavily clogged, impeding the mass transportation, contributing to the large overpotential as well.

In conclusion, the low voltage cut-off could result in higher discharge capacities, however, such measurement brought with it more side reactions due to the large overpotential, pore clogging at the gas/electrode interface, surface passivation, higher charge potential, *etc.* In order to avoid the disadvantages rising from large discharge overpotentials, the capacity was

deliberately limited to 2 mAh cm^{-2}_{areal} for further studies, where SEM image Fig. 5-3 (b) shows clean surface on the electrode.

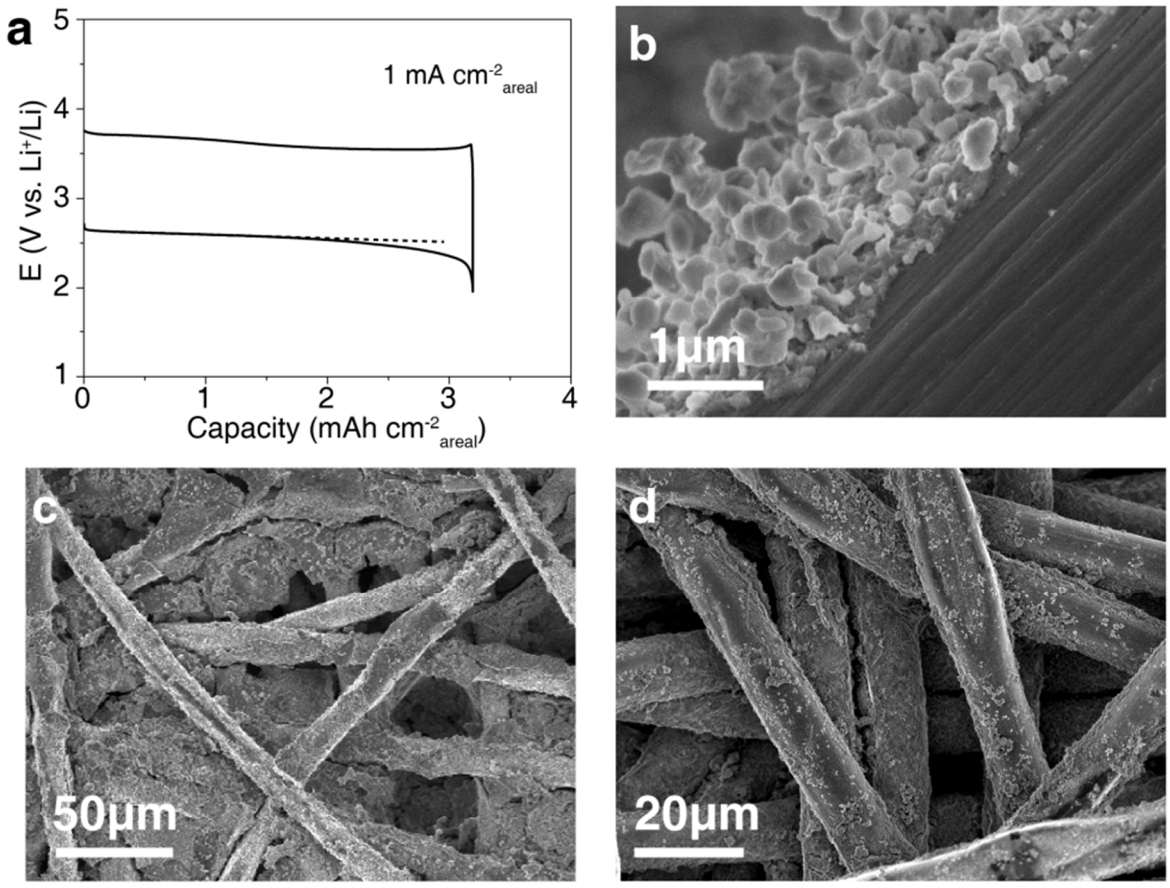


Figure 5-3. a) Discharge and charge curves of GDL based porous carbon electrodes, cycled in 25 mM DBBQ- 25mM TEMPO in 0.3 M $LiClO_4$ in DME under 1 atm O_2 at an areal current density of 1 mA cm^{-2}. At ~ 2 mAh cm^{-2}_{areal}, the discharge curve bends downwards (dash line). SEM images beyond 2 mAh cm^{-2}_{areal} discharge showing (b) little evidence of a passivating Li_2O_2 film on the carbon surface; (c) the clogged pores at the electrode/gas interface of the porous carbon GDL and (d) the unclogged pores at the electrode/electrolyte interface of the GDL.

5.3.3 Cell performance analysis

For the cells with the capacity limited to 2 mAh cm^{-2}_{areal}, plots of the voltage versus capacity on discharge and charge on the 1st, 10th and 50th cycle are shown in Fig. 5-4 (a). Identical cells without dual mediators were cycled and the cycling plots are shown in Fig. 5-4 (a), (b).

However, the capacities in such cells were very small, much less than 2 mAh cm^{-2}_{areal}, and full cycles with voltage cut-off were applied.

Without the dual mediators, the cells died quickly. The discharge plateau at the 1st cycle was ~ 2.5 V and a capacity of only 0.1 mAh cm^{-2}_{areal} was achieved. Charging requires a high potential of ~ 4.5 V. Within 5 cycles, the capacity was reduced to only 0.02 mAh cm^{-2}_{areal}, Fig. 5-4 (b). These results were consistent with previous studies in glycol ethers[14,15,33].

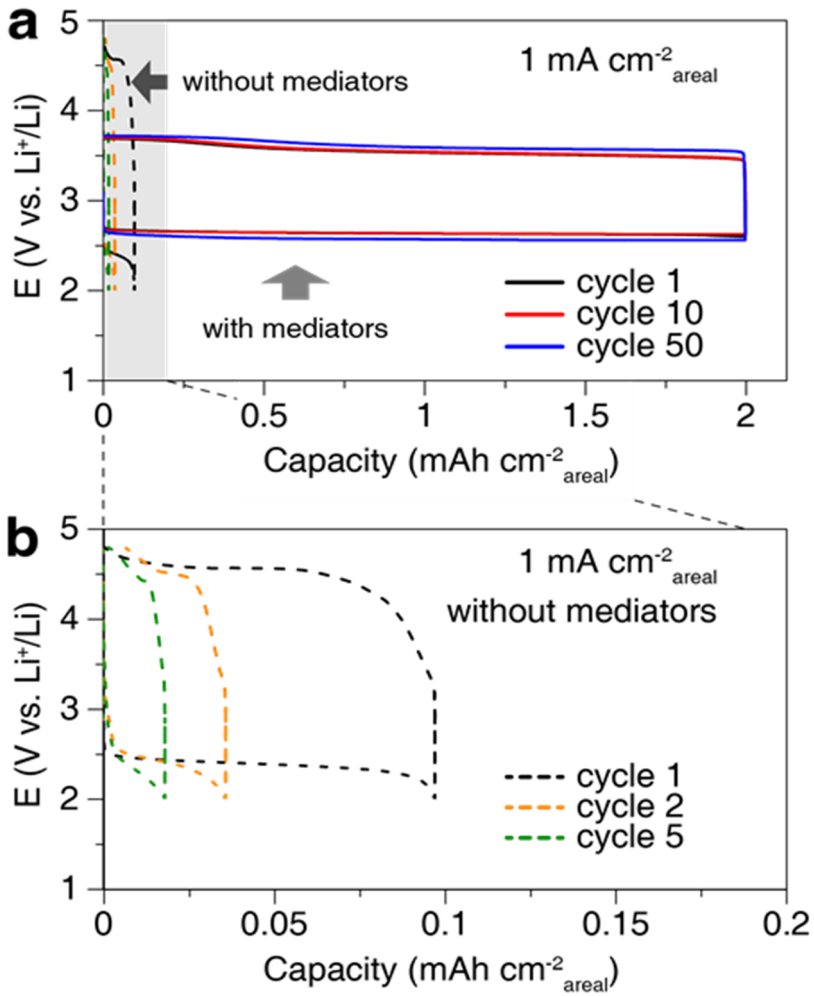


Figure 5-4. Discharge-charge curves of GDL based porous carbon electrode with and without mediators. (a) Cycled in 0.3 M $LiClO_4$ in DME with 25 mM DBBQ-25 mM TEMPO (solid lines) and without DBBQ-TEMPO (dash lines) under 1 atm O_2 at an areal current density of 1 mA cm^{-1}_{areal}. (b) Enlarged section of the discharge-charge curves recorded without DBBQ-TEMPO in (a).

On the contrary, with 25 mM DBBQ and TEMPO as the discharge and charge mediator, a capacity of 2 mAh cm^{-2}_{areal} was sustained over 50 cycles at a current density of 1 mA cm^{-2}_{areal}. A higher discharge voltage, at ~ 2.7 V, comparing to that without DBBQ and only tiny decrease on voltage during the whole discharge process was observed. The charging voltage was much lower than that without TEMPO. A close observation on the load curves in Fig. 5-4 (a) finds that most of the charging curve is flat, at ~ 3.55 V, and a slight increase at the end of charge to ~ 3.7 V in each cycle is seen. The potential rising becomes more apparent after 50 cycles.

In the dual-mediator cell, the discharge voltage is set by the DBBQ mediated reduction and the charge voltage is set by the TEMPO mediated oxidation reaction. The discharge voltage is higher than E^0 of DBBQ (~ 2.55 V) and the charging voltage is lower than E^0 of TEMPO (~ 3.72 V). This is due to the catalytic effect between mediators and Li_2O_2 regenerating the mediators back to the electrode surface, which is in accord with previous studies[10,15]. Note that the observed potentials of redox mediators are affected by the electrolyte solution composition and by the ratio of the reduced and oxidised forms present as well.

5.4 Characterisations

5.4.1 Product analysis

After discharging and charging at the current density of 1 mA cm^{-2}_{areal} with the capacity limited to 2 mAh cm^{-2}_{areal}, the electrodes were collected, washed and dried for further analysis. SEM images of the electrodes at 1st cycle, 10th cycle and 50th cycle are shown in Fig. 5-5. Large toroid particles, expected for Li_2O_2 are seen in the 1st discharge in Fig. 5-5 (b) and their absence with a clean electrode surface shown in Fig. 5-5 (c) indicates that Li_2O_2 are oxidised on the 1st charge. Same toroid shape particles are observed in the 10th and 50th

discharge, showing that Li_2O_2 is the main discharge product[15]. The origin for this toroid shape in this system needs further studies. The SEM images after charging show Li_2O_2 is fully oxidised during cycling. However, an accumulation of fine particles is seen in the extended cycles, Fig. 5-5 (e), (g), possibly due to the accumulation of side products.

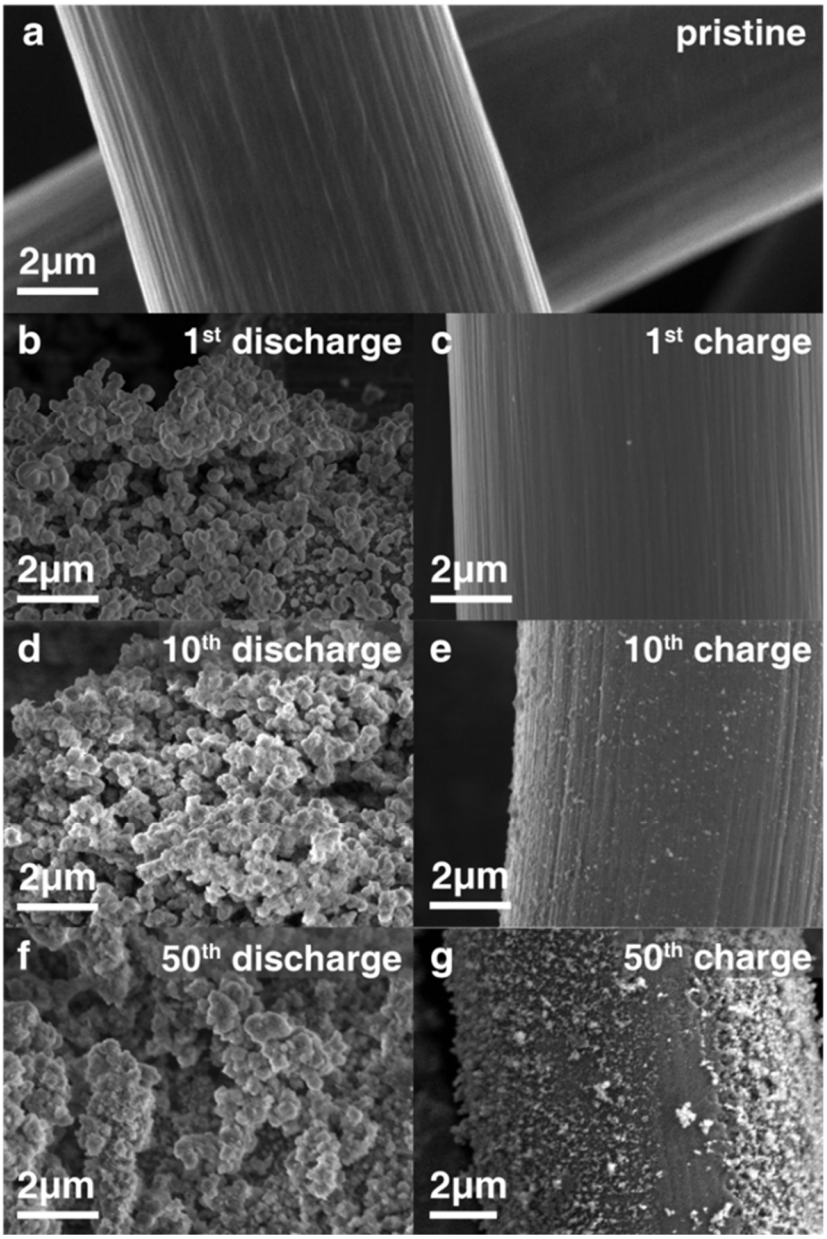


Figure 5-5. SEM images of the porous GDL based porous carbon electrodes after cycling in a dual-mediator Li-O_2 cell. (a) Pristine cathode. After cycling in 25 mM DBBQ-25 mM TEMPO-0.3 M $LiClO_4$ in DME under 1 atm O_2: cathodes at end of (b) 1st discharge, (c) 1st charge, (d) 10th discharge, (e) 10th charge, (f) 50th discharge and (g) 50th charge.

To confirm the toroid shape particles as Li_2O_2 and identify the fine particles seen on extended cycling, FTIR was carried out. It confirmed the formation and removal of Li_2O_2, with the data presented in Fig. 5-6. FTIR is very sensitive to the by-products of any side reactions[33,34] and some lithium acetate (CH_3CO_2Li) and carbonate (Li_2CO_3) was observed at the end of the 1st discharge, consistent with previous reports for Li-O_2 cells with ether based electrolyte solutions[9,33,35]. According to the FTIR spectra for the 1st, 10th and 50th charge processes in Fig. 5-6, CH_3CO_2Li was not observed in the spectra, but Li_2CO_3 was accumulated during cycling. The accumulation presented in FTIR was in accord with the particles seen in SEM images, Fig. 5-5 (c), (e), (g).

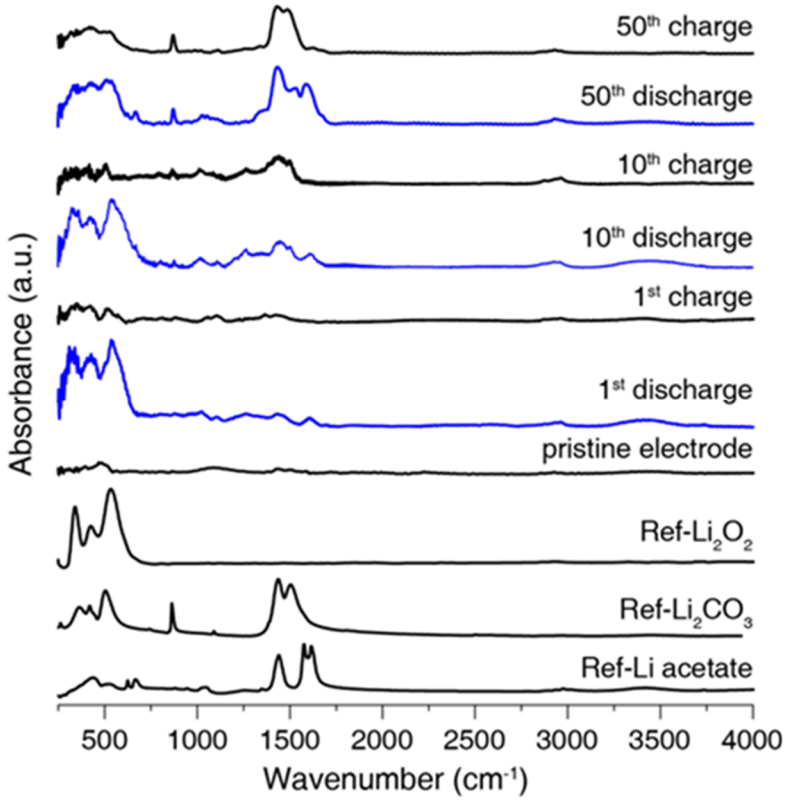


Figure 5-6. FTIR spectra of GDL based porous carbon electrodes discharged and charged in 25 mM DBBQ-25 mM TEMPO-0.3 M $LiClO_4$ in DME under 1 atm O_2.

It suggests that CH_3CO_2Li can be oxidised at such potentials either via direct electrochemical oxidation or chemical oxidation by TEMPO, while Li_2CO_3 cannot be

effectively oxidised within the cell charge window. Thus, Li_2CO_3 remained and accumulated during cycling and it becomes quite obvious in the SEM images and FTIR spectra at the 10^{th} and 50^{th} cycle.

DEMS experiments were carried to investigate whether CH_3CO_2Li can be oxidised by $TEMPO^+$. CH_3CO_2Li was placed over Celgard membrane, separated with GDL electrode and the electrolyte was 25 mM DBBQ-25 mM TEMPO-0.3 M $LiClO_4$ in DME. When the cell was charged by chronoamperometry at 3.6 V, CO_2 evolution was detected, exhibited in Fig.5-7, confirming CH_3CO_2Li being oxidised. With the Celgard membrane separating CH_3CO_2Li and the cathode, the direct electrochemical oxidation of CH_3CO_2Li was impossible. The only possible CO_2 evolution route is that GDL electrode oxidises TEMPO to $TEMPO^+$, which diffuses through Celgard membrane and then oxidises CH_3CO_2Li to evolve CO_2. The DEMS experiment confirms that CH_3CO_2Li can be oxidised by $TEMPO^+$, in accord with the FTIR results.

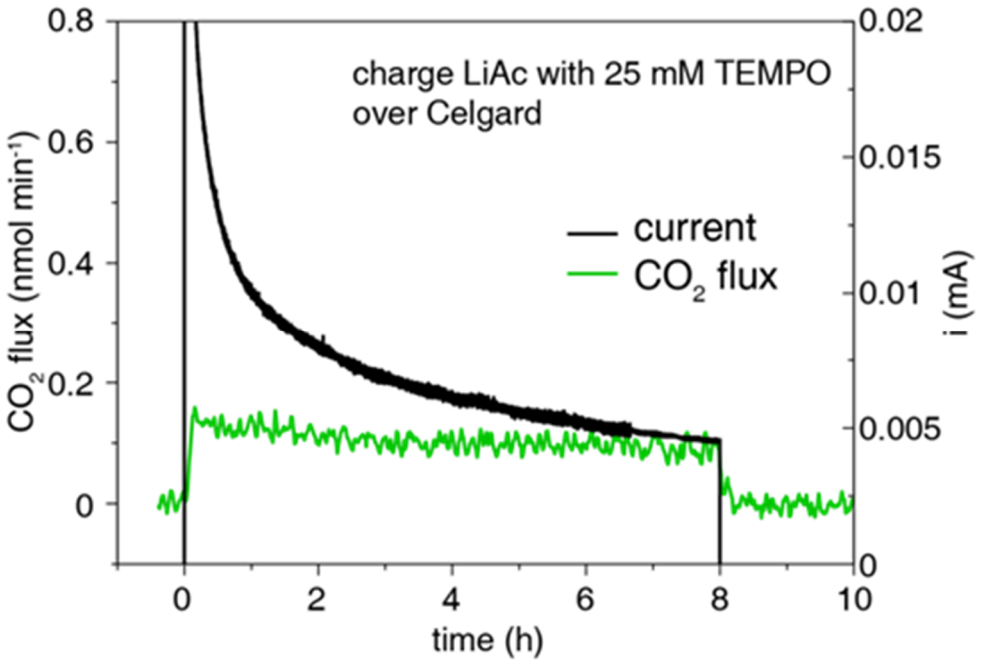


Figure 5-7. DEMS in TEMPO-DME showing the acetate oxidation and CO_2 evolution. CH_3CO_2Li was charged with 25 mM TEMPO over Celgard under Ar.

The same experiment was carried out on Li_2CO_3, and no CO_2 was detected, which indicates that Li_2CO_3 cannot be oxidised at this potential, in agreement with previous studies and the accumulation seen in FTIR and SEM.

The slight increase in the voltage seen on the 50th cycle across the whole charge process can be attributed to the accumulating Li_2CO_3 resulted from side reactions during previous cycling. It is the build-up of Li_2CO_3 on cycling and its accumulation on the electrode surfaces that result in the cell death after cycle 50.

5.4.2 Pressure cell and DEMS analysis

To understand the decomposition, *in situ* DEMS was first carried out to investigate the gas consumption and evolution during cycling in the dual-mediator cell. Considering the volatility of DME, a cold trap was introduced to minimise the amount of DME flowing into the spectrometer by the carrier gas. Both CO and CO_2 were not recorded as DME had fragments in 28 and 44, and once it was flowed into the mass spectrometer, it became impossible to truly quantify the evolution of CO and CO_2 in the cell. Besides, long time measurements were difficult since DME could be flown away by the carrier gas, leading to the depletion of electrolyte solution in the cell. Therefore, only the consumption and evolution of O_2 in the first cycle was recorded and shown in Fig. 5-8. The total O_2 consumed and total charge passed in the 1st discharge were calculated and gave a charge to mass ratio of 2.03 e^-/O_2, which suggested the dominant reaction was a 2 e^- reaction, expected to form Li_2O_2. On charge, around 86 % of the O_2 consumed on discharge was evolved, giving an e^-/O_2 ratio of 2.32. The yield of Li_2O_2 was 88 % (±2 %) on the 1st discharge, which was calculated by titrating the amount of Li_2O_2 formed using UV-vis spectrometry with addition of $TiOSO_4$ solution[15,36,37]. Given the 2.03 e^-/O_2 ratio, this suggested that the CH_3CO_2Li and Li_2CO_3 by-products, identified by FTIR, were formed by the reaction between the

electrolyte solution with Li_2O_2 rather than any intermediate. Although the e^-/O_2 on the 1st charge was calculated as 2.32, which was much higher than the desired 2 e^-/O_2 evolution. However, if we consider the chemical yield of 88 %, the O_2 evolution based on the total Li_2O_2 amount was 98 %, i.e. most Li_2O_2 remaining on discharge was removed on the following charge. It was further confirmed by titration at the end of charge that no Li_2O_2 was detected, in agreement with its absence from FTIR spectra and SEM images of the charged electrode.

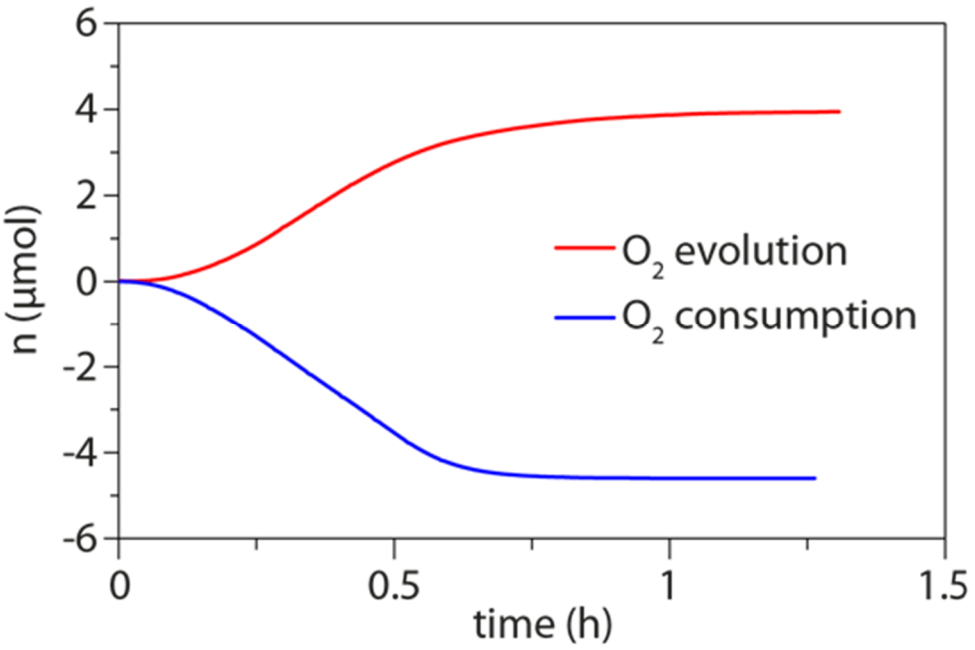


Figure 5-8. Amount of O_2 consumption on discharge (blue) and evolution on charge (red) in DEMS experiment with 25 mM DBBQ- 25mM TEMPO in 0.3 M $LiClO_4$ in DME during the 1st cycle.

It is noted that our 1st discharge yield of 88 % is similar to that of the state-of-art non-mediated Li-O_2 cells and the phenol-catalysed cell with ketjen black based cathode[38]. However, such cells without mediators are plagued with unacceptably high polarisation on charging, typically over 4 V and cannot achieve the capacities and rates possible with dual mediators. The phenol-catalysed cell cannot achieve high rates as well due to the

equilibrium and it also requires charge mediators. Solution phase discharge and charge with mediators is still a better approach to achieve higher capacities with reasonably rates.

To studying the extended cycling, a pressure cell was designed to monitor the gas pressure change in the headspace in the cell to investigate the gas consumption and evolution[39], shown in Fig. 5-9. The pressure drop on the 1st discharge, due to O_2 consumption, corresponds to 2.03 e^-/O_2, showing the same ratio and consistent with the DEMS analysis in Fig. 5-8. On charge, the curve tracked that on discharge over most of its length, Fig. 5-9, indicating that the reduction reaction was reversed on charge.

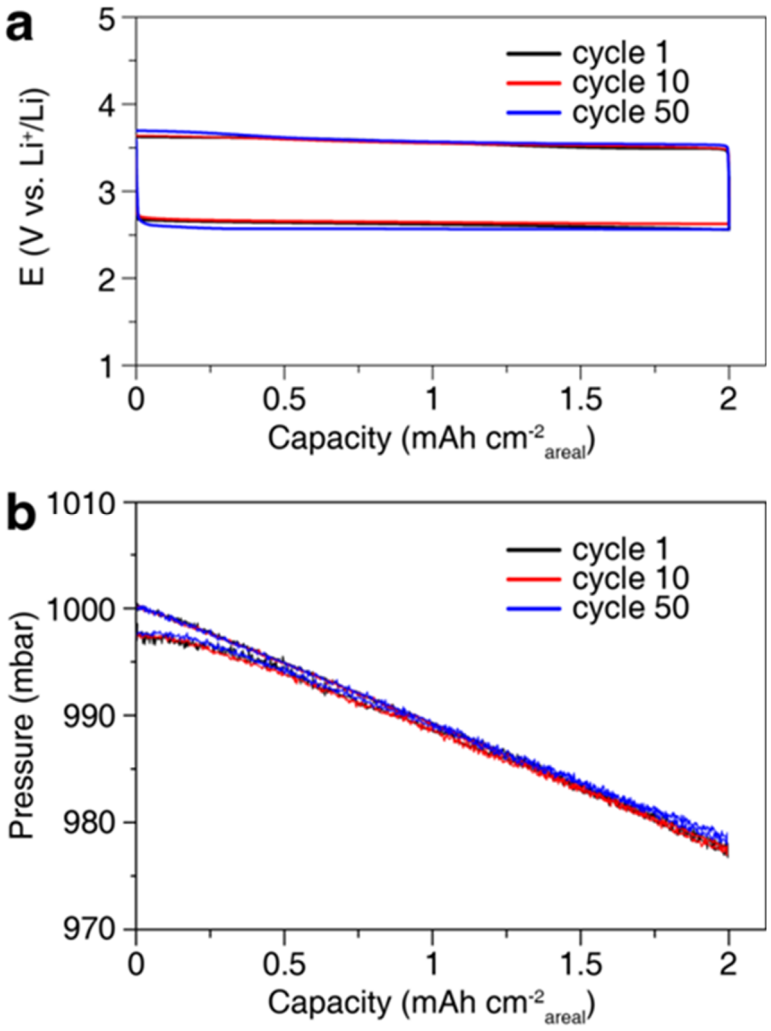


Figure 5-9. (a) Cycling profiles and (b) corresponding pressure response in head space above the Li-O_2 cell with GDLs cycling in 25 mM DBBQ-25 mM TEMPO-0.3 M $LiClO_4$ in DME at 20 °C.

At the later stage of charge, all Li_2O_2 was consumed, with nothing to be oxidised by $TEMPO^+$ and hence the pressure ceased to increase. Due to the increasing ratio of $[TEMPO^+]/[TEMPO]$ at the end of charge, the voltage started to increase on each cycle[28,31]. This is consistent with the chemical yield of 88 % in the 1st discharge and showed the last ~10 % of charge capacity was due to TEMPO oxidation alone. The pressure change remained similar in each cycle, with a slight drop seen in the 50th cycle. Yield measurements after 10th and 50th discharge of 84 % and 75 % suggested that the side reactions increased with cycling, which was in accord with the slight decrease in the pressure drop in the 50th cycle, Fig. 5-9. The lost 10 % yield and the loss of O_2 evolution were possibly due to the instability of the electrolyte solutions or electrodes with Li_2O_2, which is another problem to tackle in this field[9-11,40]. The decrease of yields is likely due to the increasing decomposition products reacting with the Li_2O_2 during the extended cycling process. It should be noted that in this project, the glycol ether DME is used and therefore the reactions between Li_2O_2 and the electrolyte solution is unavoidable.

5.5 Rate capability of the dual-mediator cell

All characterisations have proved that Li_2O_2 is formed as the main discharge product and decomposed on charge. The successful cycling at the current density of 1 mA cm^{-2}_{areal} triggered my interest in pushing the current density higher and therefore I studied the rate capability of the dual-mediator cells. Cells were operated at three different current densities from 0.5 mA cm^{-2}_{areal} up to 2 mA cm^{-2}_{areal}, with the capacity limited to 2 mAh cm^{-2}_{areal}, shown in Fig. 5-10 (a). The discharge and charge load curves are quite similar at 0.5 and 1 mA cm^{-2}_{areal}, with slight higher discharge plateau and lower charge plateau at the current density of 0.5 mA cm^{-2}_{areal}. When I pushed the current density over 1 mA cm^{-2}_{areal}, the discharge voltage was much lower and the voltage decay occurred severely at capacities

lower than 2 mAh cm^{-2}_{areal}. Accordingly, a much higher charge voltage was observed as well and it rise steadily to a potential of ~ 4 V, indicating much less Li_2O_2 product. This probably resulted from the rate performance being limited by O_2 or mediators mass transport, resulting in even more of the Li_2O_2 deposition occurring at the electrode/gas interface and earlier pore clogging and thus earlier Li_2O_2 surface formation, leading to more side reactions and earlier cell death.

When considering the diffusion coefficients (D_0) of O_2 and mediators by measuring the peak current in the CV, which is proportional to $D_0^{1/2}$, for a given concentration, D_0 can be calculated[41], and it turned out that the diffusion coefficient of O_2, DBBQ and TEMPO are 4 x 10^{-5} cm^2 s^{-1}, 5.5 x 10^{-6} cm^2 s^{-1} and 8.6 x 10^{-6} cm^2 s^{-1}, respectively. The diffusion coefficient of O_2 is 5-10 times larger than DBBQ and TEMPO, and therefore one is easy to think that the mediator mass transport should be the rate limiting factor rather than O_2. However, the O_2 solubility in DME is 8-10 mM, which means that the dual mediators have approximately three times higher concentrations and as they are regenerated fast, the rate limitations cannot be assumed based on simple comparison of diffusion coefficients.

In order to determine the rate limiting factor, the effect of the dual mediators was examined by reducing the concentrations of DBBQ and TEMPO to 12.5 mM and 6.25 mM while keeping O_2 concentration constant in all cells. Compared with the discharge and charge curves in the cell with 25 mM DBBQ and TEMPO, there was no significant effect on the performance when hthe concentration was reduced to 12.5 mM, Fig. 5-10 (b), which supported the assumption that the rate capability was limited by O_2 diffusion rather than the dual mediators. However, when the concentration was further reduced to 6.25 mM, major differences are seen: polarisation on discharge increased; the discharge potential dropped faster and the discharge capacity decreased dramatically, Fig. 5-10 (b). This very low

mediator concentrations could contribute to polarisation. The rate determining factor varies in different systems.

Due to the O_2 mass transport limitations, the cycling capacity was deliberately limited to 2 mAh cm^{-2}_{areal} and it represented a utilisation of only c.a. 4 % of the total electrode pore volume, considering the tap density of Li_2O_2 as 1.15 g cm^{-3}. The low utilisation of the electrode pore volume suggests a large increase in the discharge capacity is achievable if we can improve the O_2 mass transport. Unfortunately, there is no true gas diffusion electrode for aprotic Li-O_2 battery so far. The gas diffusion electrodes from fuel cells or aqueous metal-air batteries does not work as they rely on the hydrophilic nature of the electrolyte channels *vs.* the hydrophobic gas channels.

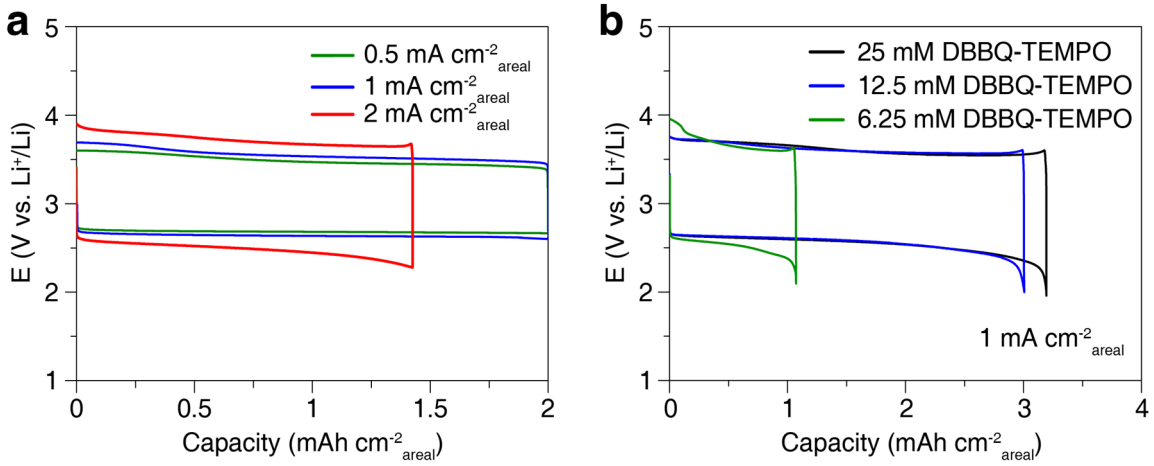


Figure 5-10. Discharge-charge curves of GDL based porous carbon electrodes (a) cycled in 25 mM DBBQ-25 mM TEMPO in 0.3 M $LiClO_4$ in DME under 1 atm O_2 at various areal current densities from 0.5 mA cm^{-2}_{areal} to 2 mA cm^{-2}_{areal}; and (b) cycled with different concentrations of DBBQ and TEMPO in 0.3 M $LiClO_4$ in DME under 1 atm O_2 with the areal current density fixed at 1 mA cm^{-2}.

If a true gas diffusion electrode could be designed to alleviate the mass transport limitation problem, where they can deliver O_2 evenly throughout the electrode, it is then possible to

access a much higher proportion of the electrode volume and achieve a significantly higher capacity to store charge at higher rates. Assuming 80 % of the porosity is filled with Li_2O_2, leaving 20 % of the porosity for the electrolyte passing through[42], an encouragingly large capacity of 40 mAh cm^{-2}_{areal} could be achieved. This exceeds the range of 5 to 30 mAh cm^{-2}_{areal} estimated to be necessary for a practical Li-O_2 cell to achieve the capacity up to 500-600 Wh kg^{-1}, meeting the market needs[12,43]. Designing a true gas diffusion electrode to alleviate O_2 mass transport limitations with proper mediators becomes one of the barriers to achieve higher capacities and higher rates.

5.6 Stability

The FTIR, SEM and pressure cell analysis have proved the existence of side reactions. It is important to find the source of side reactions. Since the dual mediators have shifted the Li_2O_2 formation and decomposition to the electrolyte solution, side reactions probably should have shifted to the solution as well, making the electrode more stable. To confirm this, the stability analysis on the electrode and electrolyte were carried out.

5.6.1 Carbon electrode stability

Carbon has been shown to be unsuitable for Li-O_2 cells, decomposing to form Li_2CO_3, with deleterious consequences for the performance, such as large charging voltages, low rates and severe capacity fading, as illustrated in Fig. 5-4 (b) [3,11,30]. Alternatives like Au, Ru, TiC, TiO_x and Mo_2C have been proposed[44-49], which show better performance but at the same time such electrode materials add large cost and weight to the cell, making the system less attractive and competitive. There are also extensive efforts to modify carbon surfaces or apply coatings[50-53]. In this work, I also studied the carbon electrode decomposition in the dual-mediator cell to see the effect of dual mediators on cathode stability.

Li-O_2 cells were constructed using ^{13}C-carbon to form the porous cathode, and then subjected to cycling with and without dual mediators under the same conditions. ^{13}C-carbon was used to separate the decomposition arising from the carbon electrode ($Li_2{}^{13}CO_3$) and the decomposition originating from the electrolyte solutions ($Li_2{}^{12}CO_3$)[3,30]. ^{13}C-Carbon was treated under an Ar: H_2 (95: 5, v: v) atmosphere at 900 ^oC prior to use[14,15]. Its Brunauer-Emmett-Teller surface area is 150 $m^2\ g^{-1}$. The carbon loading was 2-3 mg per electrode and the geometric area was 4 x 4 mm to analogize the GDL electrode.

The amount of carbonate species in the discharged electrode was quantified by acid treatment measurements used before[30]. The cells with ^{13}C-carbon electrodes were cycled at a current density of 1 mA cm^{-2}_{areal} with a limited capacity of 2 mAh cm^{-2}_{areal}. Cells were stopped at the end of discharge and the ^{13}C-carbon electrode and separators were extracted, rinsed with dry DME, dried under vacuum and transferred into an empty vial connected to a mass spectrometer with a carrier gas of pure Ar. 1 ml min^{-1} of flow rate was applied. 0.3 mL of 2 M H_3PO_4 was injected into the glass vial and $^{13}CO_2$ was evolved from the reaction between $Li_2{}^{13}CO_3$ and the acid. The amount of $Li_2{}^{13}CO_3$ was calculated from the amount of $^{13}CO_2$ detected, and the results are shown in Fig. 5-11.

It shows that with DBBQ and TEMPO as dual mediators, conditions that promote carbon decomposition are avoided without the need of any modifications/coatings. In the absence of dual mediators, ~ 0.12 % of the carbon electrode decomposed each cycle and the cell can only sustain few cycles, similar to previous studies[3], while only ~ 0.008 % of the carbon electrode decomposed each cycle with DBBQ and TEMPO together, 15 times less than that without dual mediators. Thermodynamically Li_2O_2 in contact with carbon will react to form Li_2CO_3[3]. Moreover, when Li_2O_2 is in contact with carbon, the latter is oxidised on charge above 3.6 V, driving the voltage even higher, even in excess of 4 V, accelerating further carbon decomposition[3,30]. Therefore, the much lower carbon decomposition and the much

reduced effect on the performance of the Li-O_2 cell as seen in Fig. 5-4 (a) is attributed to the presence of dual mediators. The reduction mediator, DBBQ, ensures that Li_2O_2 forms remote from the carbon surface rather than as a thin film in contact with the carbon electrode[15]. The oxidation mediator, TEMPO, ensures that on charge, Li_2O_2 particles in solution are efficiently oxidised and without the voltage being driven up. In addition, the electron transfer reactions of the molecular mediators at the electrode are less affected by the presence of Li_2CO_3. This last factor is evident from the fact that the cell with dual mediators continues to cycle with amounts of Li_2CO_3 that have negative effects on non-mediated Li-O_2 cells. Comparing the 12th cycle with mediators and the 2nd cycle without mediators in Fig 5-11, both had similar carbon electrode decomposition, but the cell with dual mediators was much less affected and lasted much longer.

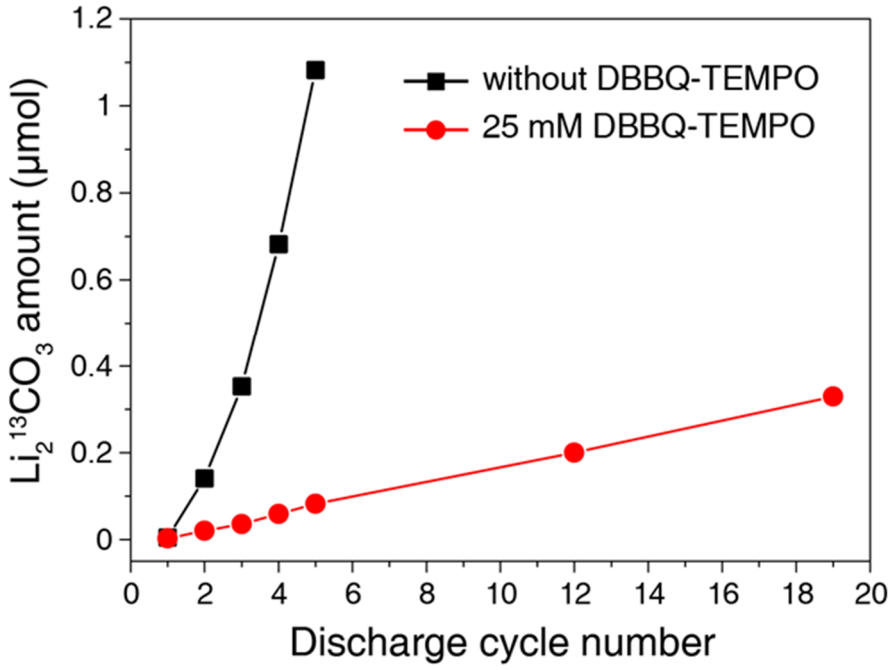


Figure 5-11. Amounts of $Li_2{}^{13}CO_3$ in the ^{13}C-carbon cathodes at the end of discharge on each cycle. Determined by subjecting the electrodes to acid to liberate $^{13}CO_2$ from $Li_2{}^{13}CO_3$. The electrolyte solution was 0.3 M $LiClO_4$ in DME without (black) and with (red) 25 mM DBBQ- 25 mM TEMPO mediators under 1 atm O_2.

Since experiments on ^{13}C-carbon have shown that dual mediators can minimise the carbon decomposition, and McCloskey *et al.* have demonstrated that the carbon decomposition is insensitive to the types of carbon[3], it is reasonable to expect the similar trend in the dual-mediator cells with GDL as the electrode. Besides, in this work, both GDL and ^{13}C-carbon were heated in 5 % H_2 in Ar before use to promote similar surface chemistries[30]. While it is not certain about the trend in side reactions in the long term, from the data shown in Fig. 5-11, $Li_2{}^{13}CO_3$ formation seems approximately linear. Assuming a constant rate of decomposition and if the decomposition happening on the carbon surface scales with surface area, then the GDL based porous carbon electrode would exhibit 0.1 % decomposition after 1500 cycles, as its surface area is 150 fold lower than the ^{13}C-carbon electrode for the same geometrical area of cathode. Carbon is the most attractive choice for the cathode in Li-O_2 cells, due to its low mass, low cost and high conductivity[10]. The suppression of carbon decomposition when using dual mediators is an important advance, as it may herald the use of carbon as a cathode for Li-O_2 batteries without the need for any carbon modification or surface coatings or non-carbon materials, as has been widely suggested. If carbon can truly be used as the cathode in Li-O_2 cells, it would remove one of the major barriers to the progress of Li-O_2 batteries.

5.6.2 Electrolyte solution stability

Given that the amount of carbon decomposition is very small, the major contributions to the side reactions, and hence the large amount of Li_2CO_3 seen in FTIR in Fig. 5-7, are very likely to come from reactions between the reduced oxygen species and the electrolyte solutions. This is confirmed by analysing the amounts of $Li_2{}^{12}CO_3$ formed in the ^{13}C-carbon experiments, as $Li_2{}^{12}CO_3$ rise only from electrolyte decomposition. The results are shown in Fig. 5-12, where the $Li_2{}^{12}CO_3$ is significantly greater than the $Li_2{}^{13}CO_3$ shown in Fig. 5-

11 in both cases with and without mediators. Both the carbon electrode and the electrolyte solution decomposition with mediators appeared to be linear with cycling, but the data is insufficient to make such conclusions in the long term. It is obvious that the electrolyte decomposition is suppressed with dual mediators as well, less than 1/3 of that in the cells without mediators, which is also seen by previous studies with addition of LiBr as the charge mediator[54].

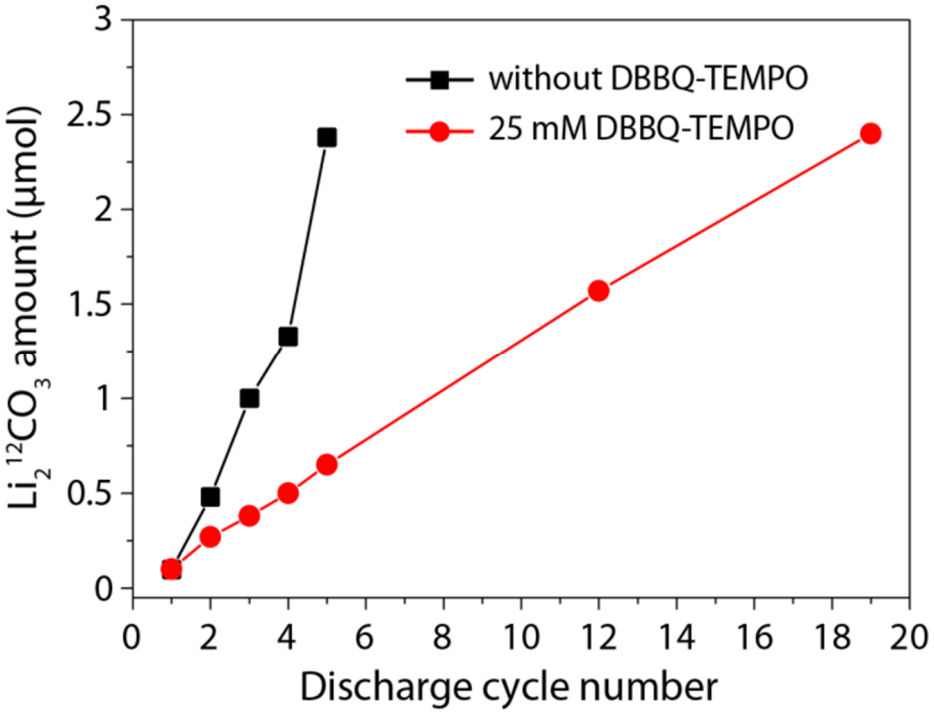


Figure 5-12. Amounts of $Li_2{}^{12}CO_3$ in the ^{13}C-carbon cathodes at the end of discharge on each cycle demonstrating the electrolyte decomposition with and without dual mediators. Determined by subjecting the carbon electrodes based on ^{13}C-carbon to acid to liberate $^{12}CO_2$ from $Li_2{}^{12}CO_3$. The electrolyte solution was 0.3 M $LiClO_4$ in DME without (black) and with (red) 25 mM DBBQ- 25 mM TEMPO mediators under 1 atm O_2.

It is noted that the H_2 and CO coming from electrolyte degradation were suppressed using LiBr, but the quantity of CO_2, arising from the oxidation of carbon was actually the same with and without LiBr within the experiment errors. In other words, there was no evidence

that LiBr suppressed carbon decomposition, only electrolyte decomposition, which was not surprising. In the studies with merely the charge mediators in ethers, Li_2O_2 formed on the carbon surface on discharge. There was still direct oxidation of Li_2O_2 at the carbon surface together with chemically oxidation of Li_2O_2 on charge. The direct oxidation of Li_2O_2 still promoted the carbon decomposition to form Li_2CO_3. In contrast, with DBBQ as the discharge mediator, Li_2O_2 grows away from the carbon surface, and therefore it is not in contact with the electrode and this mitigates carbon decomposition. In other words, it is the use of dual mediators, not just an oxidation mediator that is important in avoiding the carbon decomposition.

Comparing the amount of different types of Li_2CO_3, the moles of $Li_2{}^{12}CO_3$ is 8 times bigger than $Li_2{}^{13}CO_3$ with dual mediators, suggesting that the main factor now limiting reversibility is the electrolyte solution decomposition, emphasising the importance of addressing the stability issues and finding more stable electrolyte solutions for reversible, extended cycling in future work.

5.7 Practical dual-mediator cell with Li metal as the anode

$LiFePO_4$ is used as the anode in the laboratory, avoiding the use of reactive lithium metal[14,15,28]. However, such cells with $LiFePO_4$ would not lead to practical use, and instead lithium as the anode is required to provide a viable cell potential. Considering the reactivity of lithium with cell components and redox mediators, it needs to be protected by a Li^+-conducting solid electrolyte[10,55,56].

A lithium super ionic conductor disc (LISICON, Ohara) was applied in the cell to separate the GDL cathode and the Li anode. 25 mM DBBQ-25 mM TEMPO-300 mM $LiClO_4$ in DME served as catholyte and 0.3 M $LiClO_4$ in TEGDME served as anolyte due to its low vitality. The cell performance is shown in Fig. 5-13.

The resistance of LISICON was measured by impedance spectroscopy in a symmetric cell with Au as the working and counter electrode, then applying V = iR, to obtain the ohmic overpotential to compensate for the significant resistance of LISICON disc. The cell performance shown in Fig. 5-13 is after subtracting the ohmic overpotential in the load curves, recognising that higher conducting membranes would be required for practical cells. The results are very similar to that with $LiFePO_4$ as the anode. The yield of Li_2O_2 in the protected lithium anode cell was 87 % (± 2 %), close to the figure of 88 % from the cell with $LiFePO_4$, confirming the similar behaviour of the two cells.

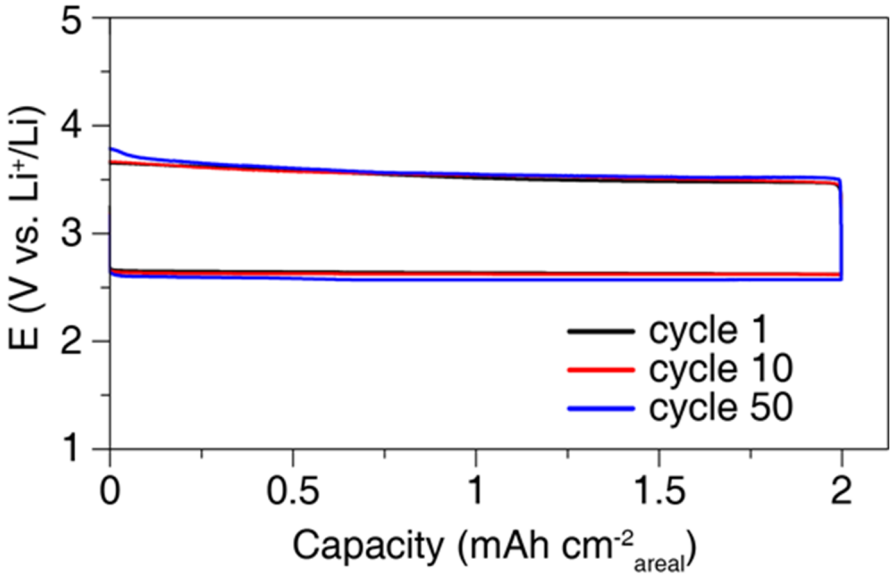


Figure 5-13. Cycling profile of a dual-mediator Li-O_2 cell with a Li metal anode protected with LISICON glass: 25 mM DBBQ-25 mM TEMPO-0.3 M $LiClO_4$ in DME used as catholyte and 0.3 M $LiClO_4$ in tetraglyme used as anolyte. The cell was cycled under 1 atm O_2 at an areal current density of 1 mA cm^{-2}. The data have been corrected for the iR drop associated with the Ohara glass membrane.

5.8 Mechanism

The promising performance of the dual-mediator Li-O_2 cell emphasizes the importance of understanding mechanisms of the solution pathways for future improvements and better

designs of mediators. The dual-mediator cell described here decouples the process of charge storage (Li_2O_2 formation and decomposition from solution) from the surface electrochemistry. This is represented schematically in Fig. 5-14.

On discharge, DBBQ is reduced to LiDBBQ on the cathode surface. LiDBBQ then diffuses into solution and reacts with O_2 to form $LiDBBQO_2$ intermediate, which can either disproportionate or undergo a second reduction to form Li_2O_2 and regenerate DBBQ. On charge, TEMPO is first oxidised at the cathode to $TEMPO^+$, which in turn oxidises Li_2O_2 particles in solution and in doing so regenerates TEMPO.

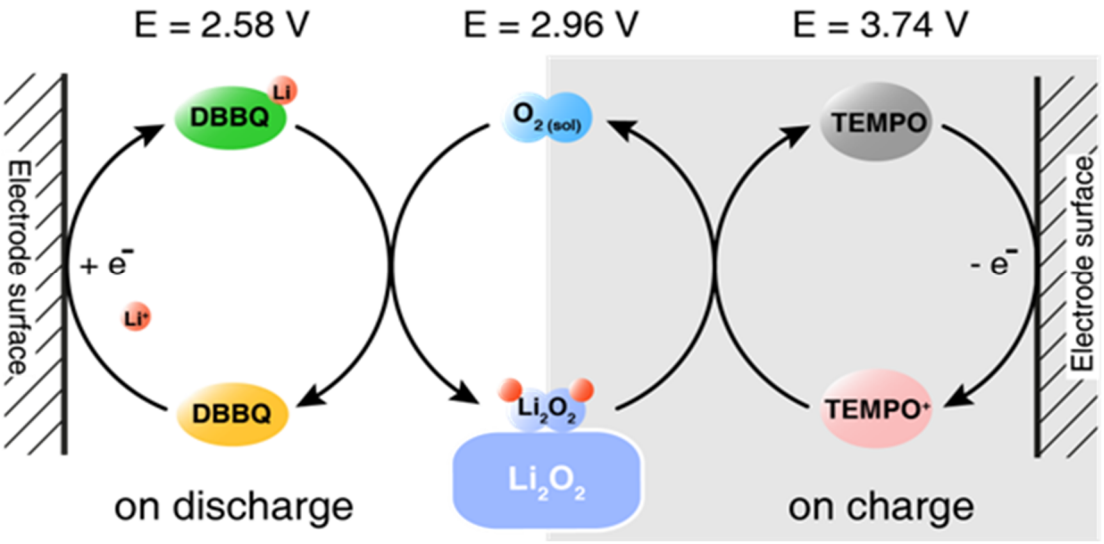


Figure 5-14. Schematics of positive electrode reactions on discharge and charge in the presence of DBBQ and TEMPO. On discharge (clear area), DBBQ is reduced to LiDBBQ, reacting with O_2 dissolved in solution (noted as $O_{2\ (sol)}$), forming Li_2O_2 away from electrode surface. On charge (shaded area), TEMPO is oxidised to $TEMPO^+$, which oxidises Li_2O_2 in solution, evolving O_2. Standard formation potentials for the redox couples DBBQ/LiDBBQ, $TEMPO^+$/TEMPO and O_2/Li_2O_2 are 2.58 V, 3.74 V and 2.96 V (vs. Li^+/Li), respectively.

The sequenced of the proposed reactions at the cathode in a Li-O_2 cell with DBBQ and TEMPO as dual mediators is summarised in following equations (5.1) to (5.5):

On discharge: $DBBQ_{(sol)} + Li^{+}_{(sol)} + e^{-} \rightarrow LiDBBQ_{(sol)}$ (5.1)

$LiDBBQ_{(sol)} + O_{2(sol)} \rightleftharpoons LiDBBQO_{2(sol)}$ (5.2)

$2\ LiDBBQO_{2(sol)} \rightarrow Li_2O_{2(s)} + O_{2(sol)} + 2\ DBBQ_{(sol)}$ (5.3a)

$LiDBBQ_{(sol)} + LiDBBQO_{2(sol)} \rightarrow Li_2O_{2(s)} + 2\ DBBQ_{(sol)}$ (5.3b)

On charge: $TEMPO_{(sol)} - e^{-} \rightarrow TEMPO^{+}_{(sol)}$ (5.4)

$2\ TEMPO^{+}_{(sol)} + Li_2O_{2(s)} \rightarrow 2\ Li^{+} + O_2 + 2\ TEMPO_{(sol)}$ (5.5)

5.9 Conclusions

The work represents a “proof of concept” for dual mediators in Li-O_2 cells with porous carbon cathodes, showing that dual mediators can deliver the combination of relatively high discharge and charge rates and capacities with low polarisation. In detail, a Li-O_2 cell using dual mediators has been cycled with capacities of 2 mAh cm^{-2}_{areal} at a rate of 1 mA cm^{-2}_{areal} and discharge/charge potentials of 2.7 and 3.6 V, respectively. By decoupling the electrochemical reactions at the cathode surface from the energy storage (formation/decomposition of Li_2O_2 from solution) using DBBQ and TEMPO as dual mediators, the Li-O_2 cell performance is no longer limited by the insulating and insoluble nature of Li_2O_2, and Li_2O_2 now only serves as the charge storage mediate. Instead, the O_2 mass transport and associated pore clogging at the electrode/gas interface is the factor limiting the cell performance. The results imply that combining dual mediator with a true gas diffusion electrode, where O_2 can be evenly distributed through the electrode, could deliver an encouraging capacity of 40 mAh cm^{-2}_{areal} with much higher rates and meet the goal for a practical cell with 500-600 Wh kg^{-1}. Future work should focus, in part, on the design of gas diffusion electrodes that deliver facile mass transport, as for fuel cell electrodes.

Carbon is by far the most attractive material for Li-O_2 cell cathode due to its low cost, high conductivity and low mass, but it is unstable in contact with Li_2O_2, especially at charging voltages over 4 V, degrading to Li_2CO_3. However, the carbon cathode is significantly more stable in the presence of dual mediators, exhibiting less than 0.008 % decomposition per cycle, and it does not have a deleterious effect on the cell performance, unlike the situation in the absence of mediators. This may be attributed to Li_2O_2 formation/decomposition no longer taking place at the carbon surface, charging occurring at 3.6 V rather than 4 V, and the electron transfer reactions associated with the mediators at the carbon surface being much less sensitive to the presence of Li_2CO_3. Coupled with dual mediators, it might be possible to use carbon directly as the cathode without any modification or coating, and if so remove one of the major barriers to progress of Li-O_2.

The results also show that now, the major source of side reactions and hence limitation of cycling and reversibility arises from reactions with electrolyte solution. The stability of mediators are not considered in this project. This emphasises that future research should focus on the search for more stable solvents and mediators, with the latter including searching for stable mediators resistant to reactive oxygen species in the cell and investigation of oxidation mediators able to operate at lower overpotentials with higher kinetics to further reduce the charging voltage. Using mediators on both discharge and charge can reduce one of the important sources of side reactions, i.e. carbon instability, and can mitigate another barrier to cell performance, namely the limitations on rate and capacity imposed if Li_2O_2 is formed and decomposed as a film on the cathode surface. If stable electrolyte solutions and appropriate mediators can be found, then the results in this project suggest a Li-O_2 cell with mediation at the cathode can sustain cycling with high capacities and rates, satisfying the market needs.

5.10 References

1 Khetan, A., Luntz, A. & Viswanathan, V. Trade-offs in capacity and rechargeability in nonaqueous Li–O_2 batteries: Solution-driven growth versus nucleophilic stability. *J. Phys. Chem. Lett.* **6**, 1254-1259 (2015).

2 Johnson, L. *et al.* The role of LiO_2 solubility in O_2 reduction in aprotic solvents and its consequences for Li–O_2 batteries. *Nat. Chem.* **6**, 1091-1099 (2014).

3 McCloskey, B. D. *et al.* Twin problems of interfacial carbonate formation in nonaqueous Li–O_2 batteries. *J. Phys. Chem. Lett.* **3**, 997-1001 (2012).

4 Grande, L. *et al.* The lithium/air battery: still an emerging system or a practical reality? *Adv. Mater.* **27**, 784-800 (2015).

5 Feng, N., He, P. & Zhou, H. Critical challenges in rechargeable aprotic Li-O_2 batteries. *Adv. Energy Mater.* **6**, 1502303 (2016).

6 Lu, J. *et al.* Aprotic and aqueous Li-O_2 batteries. *Chem. Rev.* **114**, 5611-5640 (2014).

7 Lu, Y. C. *et al.* Lithium-oxygen batteries: bridging mechanistic understanding and battery performance. *Energy Environ. Sci.* **6**, 750-768 (2013).

8 Black, R., Adams, B. & Nazar, L. F. Non-aqueous and hybrid Li-O_2 batteries. *Adv. Energy Mater.* **2**, 801-815 (2012).

9 Choi, J. W. & Aurbach, D. Promise and reality of post-lithium-ion batteries with high energy densities. *Nat. Rev. Mater.* **1**, 16013 (2016).

10 Aurbach, D., McCloskey, B. D., Nazar, L. F. & Bruce, P. G. Advances in understanding mechanisms underpinning lithium–air batteries. *Nat. Energy* **1**, 16128 (2016).

11 Luntz, A. C. & McCloskey, B. D. Nonaqueous Li-air batteries: a status report. *Chem. Rev.* **114**, 11721-11750 (2014).

12 Gallagher, K. G. *et al.* Quantifying the promise of lithium–air batteries for electric vehicles. *Energy Environ. Sci.* **7**, 1555 (2014).

13 Viswanathan, V. *et al.* Electrical conductivity in Li_2O_2 and its role in determining capacity limitations in non-aqueous Li-O_2 batteries. *J. Chem. Phys.* **135**, 214704 (2011).

14 Gao, X., Jovanov, Z. P., Chen, Y., Johnson, L. R. & Bruce, P. G. Phenol-catalyzed discharge in the aprotic lithium-oxygen battery. *Angew. Chem. Int. Ed.* **56**, 6539-6543 (2017).

15 Gao, X., Chen, Y., Johnson, L. & Bruce, P. G. Promoting solution phase discharge in Li-O_2 batteries containing weakly solvating electrolyte solutions. *Nat. Mater.* **15**, 882–888 (2016).

16 Bergner, B. J., Schurmann, A., Peppler, K., Garsuch, A. & Janek, J. TEMPO: a mobile catalyst for rechargeable Li-O_2 batteries. *J. Am. Chem. Soc.* **136**, 15054-15064 (2014).

17 Lim, H. D. *et al.* Superior rechargeability and efficiency of lithium-oxygen batteries: hierarchical air electrode architecture combined with a soluble catalyst. *Angew. Chem. Int. Ed.* **53**, 3926-3931 (2014).

18 Chen, Y., Freunberger, S. A., Peng, Z., Fontaine, O. & Bruce, P. G. Charging a Li–O_2 battery using a redox mediator. *Nat. Chem.* **5**, 489–494 (2013).

19 Lim, H.-D. *et al.* Rational design of redox mediators for advanced Li–O_2 batteries. *Nat. Energy* **1**, 16066 (2016).

20 Kwak, W.-J. *et al.* Li–O_2 cells with LiBr as an electrolyte and a redox mediator. *Energy Environ. Sci.* **9**, 2334-2345 (2016).

21 Bryantsev, V. S. *et al.* Predicting the electrochemical behavior of lithium nitrite in acetonitrile with quantum chemical methods. *J. Am. Chem. Soc.* **136**, 3087-3096 (2014).

22 Kwak, W.-J. *et al.* Understanding the behavior of Li-oxygen cells containing LiI. *J. Mater. Chem. A* **3**, 8855-8864 (2015).

23 Chase, G. V. *et al.* Soluble oxygen evolving catalysts for rechargeable metal-air batteries. US20120028137 A1 (2012).

24 Feng, N., He, P. & Zhou, H. Enabling catalytic oxidation of Li_2O_2 at the liquid-solid interface: the evolution of an aprotic Li-O_2 battery. *ChemSusChem* **8**, 600-602 (2015).

25 Li, Y. *et al.* Li-O_2 cell with LiI(3-hydroxypropionitrile)$_2$ as a redox mediator: Insight into the working mechanism of I^- during charge in anhydrous systems. *J. Phys. Chem. Lett.* **8**, 4218-4225 (2017).

26 Liu, Z. *et al.* Decomposing lithium carbonate with a mobile catalyst. *Nano Energy* **36**, 390-397 (2017).

27 Bergner, B. J. *et al.* Understanding the fundamentals of redox mediators in Li-O_2 batteries: a case study on nitroxides. *Phys. Chem. Chem. Phys.* **17**, 31769-31779 (2015).

28 Bergner, B. J. *et al.* How to improve capacity and cycling stability for next generation Li-O_2 batteries: approach with a solid electrolyte and elevated redox mediator concentrations. *ACS Appl. Mater. Interfaces* **8**, 7756-7765 (2016).

29 Veith, G. M., Nanda, J., Delmau, L. H. & Dudney, N. J. Influence of lithium salts on the discharge chemistry of Li–air cells. *J. Phys. Chem. Lett.* **3**, 1242-1247 (2012).

30 Ottakam Thotiyl, M. M., Freunberger, S. A., Peng, Z. & Bruce, P. G. The carbon electrode in nonaqueous Li-O_2 cells. *J. Am. Chem. Soc.* **135**, 494-500 (2013).

31 Grübl, D., Bergner, B., Schröder, D., Janek, J. & Bessler, W. G. Multistep reaction mechanisms in nonaqueous lithium–oxygen batteries with redox mediator: a model-based study. *J. Phys. Chem. C* **120**, 24623-24636 (2016).

32 Hojberg, J. *et al.* An electrochemical impedance spectroscopy investigation of the overpotentials in Li-O_2 batteries. *ACS Appl. Mater. Interfaces* **7**, 4039-4047 (2015).

33 Freunberger, S. A. *et al.* The lithium-oxygen battery with ether-based electrolytes. *Angew. Chem. Int. Ed.* **50**, 8609-8613 (2011).

34 Freunberger, S. A. *et al.* Reactions in the rechargeable lithium-O_2 battery with alkyl carbonate electrolytes. *J. Am. Chem. Soc.* **133**, 8040-8047 (2011).

35 Adams, B. D. *et al.* Towards a stable organic electrolyte for the Lithium oxygen battery. *Adv. Energy Mater.* **5**, 1400867 (2015).

36 Schwenke, K. U., Metzger, M., Restle, T., Piana, M. & Gasteiger, H. A. The influence of water and protons on Li_2O_2 crystal growth in aprotic Li-O_2 cells. *J. Electrochem. Soc.* **162**, A573-A584 (2015).

37 Hartmann, P. *et al.* A comprehensive study on the cell chemistry of the sodium superoxide (NaO_2) battery. *Phys. Chem. Chem. Phys.* **15**, 11661-11672 (2013).

38 McCloskey, B. D. *et al.* Combining accurate O_2 and Li_2O_2 assays to separate discharge and charge stability limitations in nonaqueous Li–O_2 batteries. *J. Phys. Chem. Lett.* **4**, 2989-2993 (2013).

39 Lepoivre, F., Grimaud, A., Larcher, D. & Tarascon, J.-M. Long-time and reliable gas monitoring in Li-O_2 batteries via a Swagelok derived electrochemical cell. *J. Electrochem. Soc.* **163**, A923-A929 (2016).

40 Li, Y., Wang, X., Dong, S., Chen, X. & Cui, G. Recent advances in non-aqueous electrolyte for rechargeable Li-O_2 batteries. *Adv. Energy Mater.* **6**, 1600751 (2016).

41 Bard, A. J. & Faulkner, L. R. *Electrochemical methods. Fundamentals and applications*. 2nd edn, (Wiley, 2000).

42 Imanishi, N., Luntz, A. C. & Bruce, P. G. *The lithium air battery: fundamentals*. (Springer, 2014).

43 Christensen, J. *et al.* A critical review of Li/air batteries. *J. Electrochem. Soc.* **159**, R1-R30 (2012).

44 Peng, Z., Freunberger, S. A., Chen, Y. & Bruce, P. G. A reversible and higher-rate Li-O_2 battery. *Science* **337**, 563-566 (2012).

45 Ottakam Thotiyl, M. M. *et al.* A stable cathode for the aprotic Li-O_2 battery. *Nat. Mater.* **12**, 1050-1056 (2013).

46 Kundu, D. *et al.* Nanostructured metal carbides for aprotic Li–O_2 batteries: New insights into interfacial reactions and cathode stability. *J. Phys. Chem. Lett.* **6**, 2252-2258 (2015).

47 Kundu, D., Black, R., Berg, E. J. & Nazar, L. F. A highly active nanostructured metallic oxide cathode for aprotic Li–O_2 batteries. *Energy Environ. Sci.* **8**, 1292-1298 (2015).

48 Qiu, F. *et al.* Ordered mesoporous TiC-C composites as cathode materials for Li-O_2 batteries. *Chem. Commun.* **52**, 2713-2716 (2016).

49 Liao, K. *et al.* Nanoporous Ru as a carbon- and binder-free cathode for Li-O_2 batteries. *ChemSusChem* **8**, 1429-1434 (2015).

50 Jian, Z. *et al.* Core–Shell-Structured CNT@RuO_2 composite as a high-performance cathode catalyst for rechargeable Li–O_2 batteries. *Angew. Chem. Int. Ed.* **53**, 442-446 (2014).

51 Wu, F. *et al.* Facile synthesis of boron-doped rGO as cathode material for high energy Li-O_2 batteries. *ACS Appl. Mater. Interfaces* **8**, 23635-23645 (2016).

52 Xue, H. *et al.* Hierarchical porous nickel cobaltate nanoneedle arrays as flexible carbon-protected cathodes for high-performance lithium-oxygen batteries. *ACS Appl. Mater. Interfaces* **8**, 8427-8435 (2016).

53 Li, F. *et al.* Performance-improved Li-O_2 battery with Ru nanoparticles supported on binder-free multi-walled carbon nanotube paper as cathode. *Energy Environ. Sci.* **7**, 1648-1652 (2014).

54 Liang, Z. & Lu, Y. C. Critical role of redox mediator in suppressing charging instabilities of lithium-oxygen batteries. *J. Am. Chem. Soc.* **138**, 7574-7583 (2016).

55 Ha, S. *et al.* Investigation on the stability of Li metal anode in the Li–O_2 batteries with a redox mediator. *J. Mater. Chem. A* **5**, 10609-10621 (2017).

56 Guo, Z., Li, C., Liu, J., Wang, Y. & Xia, Y. A long-life lithium-air battery in ambient air with a polymer electrolyte containing a redox mediator. *Angew. Chem. Int. Ed.* **56**, 7505-7509 (2017).

Chapter 6. Perspectives and future work

Previous studies have demonstrated the benefits of solution phase growth of Li_2O_2 in aprotic Li-O_2 batteries: large capacities and high rates. It is already known that the discharge pathways is determined by the solubility of LiO_2 intermediate, which is dependent on the strength of the cation and anion solvation. High DN solvents and high AN salts are shown to promote the solution phase formation of Li_2O_2. However, such electrolyte solutions are susceptible to nucleophilic attack or proton abstraction by the reactive O_2^- radical, leading to undesirable side reactions. Low DN solvents are relatively more stable, but they favour the surface mechanism, resulting in low capacities, low rates and early cell death. There were few good solutions to tackle the dilemma of achieving high capacity and stability. The stability problems of the O_2 electrode have not been solved over the past decade and present one of the greatest barriers to realising the transformational energy storage possible with the Li-O_2 battery.

In this project, several soluble catalysts were studied to promote solution phase discharge in low DN solvents. Phenol served as a protic phase transfer catalyst, protonating the discharge product to induce solubility and removing the proton of the conjugate base. Li_2O_2 is then recrystallized as large particles from solution. The addition of phenol results in a satisfying 35-fold increase in capacities, however, it does not change the formation of reactive superoxide intermediate and the equilibrium between solid Li_2O_2 and dissolved peroxide species limits the high rate performance. DBBQ was explored as a discharge mediator to change the discharge route that avoids the LiO_2 intermediate and at the same time, it promoted solution phase discharge in glycol ethers. The addition of DBBQ avoids the direct formation of Li_2O_2 thin film on the cathode, thus postponing cell death, increasing capacity 80-100 fold and facilitating discharge rates of > 1 mA cm^{-2}_{areal} for cathodes with

capacities of > 4 mAh cm^{-2}_{areal}. However, Li_2O_2 particles growing from solution is disconnected from the electrode surface and therefore electronically isolated during charging. TEMPO was therefore employed to oxidise Li_2O_2 on charge with DBBQ as the discharge mediator. Such a dual-mediator Li-O_2 cell can sustain over 50 cycles with capacities of 2 mAh cm^{-2}_{areal} at a rate of 1 mA cm^{-2}_{areal}.

The work described here has contributed to changing the understanding of aprotic Li-O_2 batteries. Li_2O_2 does not have to form and decompose on the electrode surface. The introduction of homogeneous catalysts can shift the formation/decomposition of Li_2O_2 into solution and decouple the electrochemical reactions at the cathode surface from the charge storage mediate, thus circumventing the problems encountered by formation/decomposition of Li_2O_2 on the carbon electrode surface. Carbon was previously considered to be unsuitable as the cathode in aprotic Li-O_2 batteries, because it is unstable in contact with Li_2O_2, especially at charging voltages over 4 V, degrading to Li_2CO_3. In this project, in contrast with the established view, the combination of dual mediators renders the carbon cathode stable by forming/decomposing Li_2O_2 away from the electrode surface and by doing so with a charging voltage of ~ 3.6 V.

Furthermore, this project show some of the future research focuses in aprotic Li-O_2 batteries. First, different morphologies of Li_2O_2 growing from solution are observed but the mechanism is poorly studied. It is important to understand the formation process fundamentally to compare the cell performance to study the relationship. *In situ* SEM or TEM during discharge and charge would be a good idea for this research. Besides, there is no need to search for high DN electrolytes to solvate LiO_2 intermediate and non-carbon materials or coating/modification of carbon material is becoming less attractive. The future work can focus on optimising the redox mediators. For example, charge mediators capable of operating at lower potentials with faster kinetics are preferable. Besides, the major source

of side reactions and hence limitation of cycling and reversibility of an aprotic Li-O_2 cell is now the decomposition of the electrolyte solutions. Future work should focus on searching for more stable electrolyte solvents, salts and mediators. For instance, alkanes should be stable and resistant to attack of superoxide species. However, it is challenging to find such proper lithium salts that can dissolve and dissociate in alkanes. In addition, true gas diffusion electrode is lacking, which causes the O_2 mass transport and associated pore clogging at the electrode/gas interface hindering the current cell performance. Future work can focus on the design of true gas diffusion electrodes that can deliver facile mass transport so that an encouraging capacity of 40 mAh cm^{-2}_{areal} with much higher rates and the goal for a practical cell with 500-600 Wh kg^{-1} is achievable, satisfying the market needs.